re-B

You have downloaded a document from RE-BUŚ repository of the University of Silesia in Katowice

Title: Simulated maturation by hydrous pyrolysis of bituminous coals and carbonaceous shales from the Upper Silesian and Lublin basins (Poland): Induced compositional variations in biomarkers, carbon isotopes and macerals

Author: Maciej J. Kotarba, Mirosław Słowakiewicz, Magdalena Misz-Kennan, Dariusz Więcław, Krzysztof Jurek, MartaWaliczek

Citation style: Kotarba Maciej J., Słowakiewicz Mirosław, Misz-Kennan Magdalena, Więcław Dariusz, Jurek Krzysztof, Waliczek Marta. (2021). Simulated maturation by hydrous pyrolysis of bituminous coals and carbonaceous shales from the Upper Silesian and Lublin basins (Poland): Induced compositional variations in biomarkers, carbon isotopes and macerals. „International Journal of Coal Geology" (Vol. 247, 2021, art. no. 103856, s. 1-27), DOI:10.1016/j.coal.2021.103856

Uznanie autorstwa - Użycie niekomercyjne - Bez utworów zależnych Polska - Licencja ta zezwala na rozpowszechnianie, przedstawianie i wykonywanie utworu jedynie w celach niekomercyjnych oraz pod warunkiem zachowania go w oryginalnej postaci (nie tworzenia utworów zależnych).

UNIWERSYTET ŚLĄSKI W KATOWICACH | Biblioteka Uniwersytetu Śląskiego | Ministerstwo Nauki i Szkolnictwa Wyższego

International Journal of Coal Geology 247 (2021) 103856

Contents lists available at ScienceDirect

International Journal of Coal Geology

journal homepage: www.elsevier.com/locate/coal

Simulated maturation by hydrous pyrolysis of bituminous coals and carbonaceous shales from the Upper Silesian and Lublin basins (Poland): Induced compositional variations in biomarkers, carbon isotopes and macerals

Maciej J. Kotarba [a,*], Mirosław Słowakiewicz [b], Magdalena Misz-Kennan [c], Dariusz Więcław [a], Krzysztof Jurek [a], Marta Waliczek [a]

[a] Faculty of Geology, Geophysics and Environmental Protection, AGH University of Science and Technology, Al. Mickiewicza 30, 30-059 Kraków, Poland
[b] Faculty of Geology, University of Warsaw, ul. Żwirki i Wigury 93, 02-089 Warszawa, Poland
[c] Faculty of Natural Sciences, University of Silesia, ul. Będzińska 60, 41-200 Sosnowiec, Poland

ARTICLE INFO

Keywords:
Biomarkers
Stable carbon isotopes
Macerals
Hydrous pyrolysis
Simulated maturation
Upper Silesian- and Lublin coal basins

ABSTRACT

Hydrous pyrolysis (HP) to simulate the maturation of organic matter (OM) and a variety of organic geochemical analyses and petrographic analyses of OM were performed to establish the origin and depositional environment in the Serpukhovian (Mississippian) and Pennsylvanian coals and carbonaceous shales from the Upper Silesian and Lublin coal basins. OM of coals and shales is dominated by vitrinite- with subordinate liptinite- and inertinite-group macerals, derived from C3 plants. The OM in both coals and shales is of humic origin, deposited in terrestrial, paralic and terrestrial, deltaic and lacustrine environments. The OM is rich in resins related to the presence of waxes derived from the coat of vascular plants. Shales were deposited in a more brackish-lacustrine environment than coals with algae and microbially reworked OM. Shales occurring above coal seams were deposited in more dynamic conditions than shales below seams. Coal sedimentation occurred in a stagnant setting reflected in the presence of paleosols and diverse plant groups. After heating at HP 330 °C and 360 °C, various new vitrinite forms appear, and semicoke, in the OM. The distributions of some biomarkers and polycyclic aromatic hydrocarbons are characteristic of specific macerals, and their ratios are controlled by OM type and thermal maturity related to the conditions of the HP experiments. This behaviour can be related to OM of type III and chemical reactions at two maturation stages. No significant geochemical or genetic differences in the OM of coals or shales from either basin are evident.

1. Introduction

The hydrous pyrolysis (HP) method better simulates natural maturation, and thus thermogenic petroleum generation processes, than does closed- and open-system anhydrous pyrolysis (e.g., Lewan, 1997; Lewan and Ruble, 2002; Kotarba and Lewan, 2004; Lewan et al., 2008; Lewan and Kotarba, 2014; Lohr and Hackley, 2020, 2021) as water is always present in geological settings (Lewan, 1993, 1997, 1998; Pan et al., 2009). Previously, dry pyrolysis was widely used for simulating natural thermogenic processes on a geological time scale (e.g., Higgs, 1986; Berner and Faber, 1996; Behar et al., 1997). However, the HP method provides the activation energies of hydrocarbon generation reactions more pertinent to natural conditions (e.g., Lewan and Ruble, 2002).

The main aim of this study was to determine the source- and depositional conditions of organic matter (OM) in coal seams or dispersed in carbonaceous shales in the Upper Silesian (USCB) and Lublin (LSB) coal basins in Poland. Data on extracted bitumen contents and fractions, carbon isotopes, maceral- and biomarker analyses of coal- and shale samples and HP simulations of two stages of OM maturity underpin the conclusions.

Biomarker, carbon isotope and maceral compositions of coals and carbonaceous shales from the USCB and LCB have already been published (Kotarba et al., 2002; Kotarba and Clayton, 2003). The innovative character of this paper lies in the application of the same analytical

* Corresponding author.
E-mail address: kotarba@agh.edu.pl (M.J. Kotarba).

https://doi.org/10.1016/j.coal.2021.103856
Received 14 July 2021; Received in revised form 16 September 2021; Accepted 19 September 2021
Available online 23 September 2021
0166-5162/© 2021 The Authors. Published by Elsevier B.V. This is an open access article under the CC BY-NC-ND license (http://creativecommons.org/licenses/by-nc-nd/4.0/).

methods to original coals and carbonaceous shales before and after HP at 330 °C and 360 °C for 72 h. The result should enable evaluation of the suitability of parameters, indices, biomarker ratios, and isotopic- and maceral compositions used for determining their origin and stages of maturation and allow comparison and an understanding of possible differences of these parameters, indices and ratios between coals and carbonaceous shales.

The published results of vitrinite reflectance (R_r) and Rock-Eval data from the same set of original coals and carbonaceous shales (Kotarba et al., 2021) and the results of earlier geochemical and petrological studies of coals and carbonaceous shales (Kotarba et al., 2002; Kotarba and Clayton, 2003) and on coals after HP at 360 °C (Kotarba and Lewan, 2004; Lewan and Kotarba, 2014) in the USCB and LCB (Fig. 1) contributed to the genetic interpretation. Gaseous products of the HP experiments were analysed and discussed in a paper by Kotarba et al. (2021).

2. Geological setting

The two study areas comprise the southern part of the USCB and the

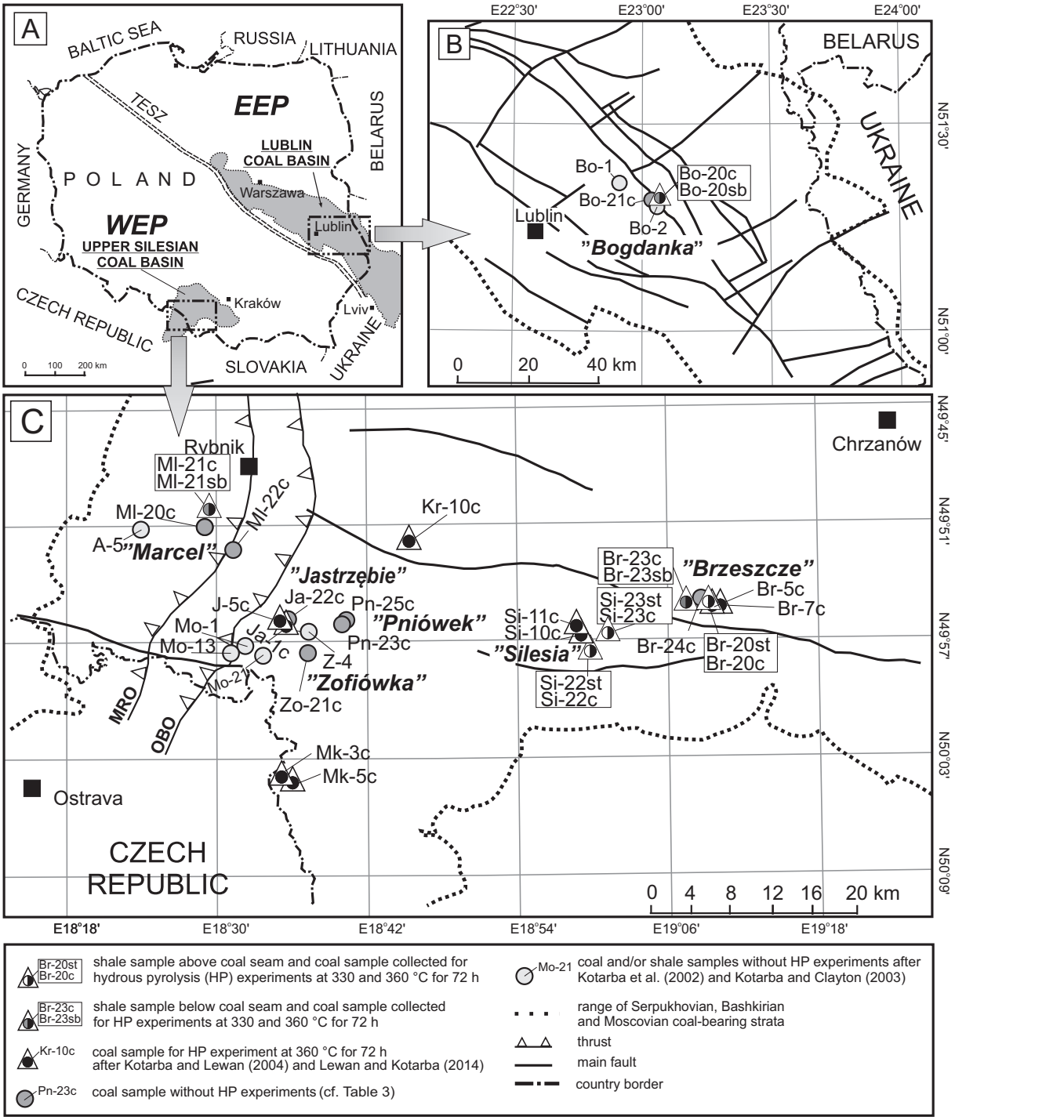

Fig. 1. (A) General sketch map of Poland, (B) Lublin Basin and (C) the southern part of the Upper Silesian Coal Basin and the western part of the Carpathian Foredeep showing the locations of sampling sites. WEP – West European Platform; EEP – East European Platform; MRO – Michálkovice-Rybnik Overthrust; OBO – Orlová-Boguszowice Overthrust.

"Bogdanka" Mine of the LCB (Fig. 1). The coals and carbonaceous shales of both basins (Table 1) occur in the Pennsylvanian- and Mississippian coal-bearing strata. The USCB, one of the major coal basins in the world, formed as a deep molasse basin of polygenetic origin, and coal-bearing strata comprise the lower part of the paralic Serpukhovian (Upper Mississippian) and the Bashkirian and Moscovian (Pennsylvanian) of continental deposition (e.g., Buła and Kotas, 1994; Kotas, 1994; Jureczka et al., 2005; Kędzior et al., 2007). The LCB is a molasse basin of polygenetic origin in which the lower part of the coal-bearing Upper Visean and Serpukhovian is marine-paralic, the middle part of the Bashkirian is paralic, and the upper part of the Moscovian is limnic-fluvial (e.g., Porzycki and Zdanowski, 1995; Zdanowski, 1999; Narkiewicz, 2007, 2020; Waksmundzka, 2010, 2013; Tomaszczyk and Jarosiński, 2017; Kufrasa et al., 2019; Kozłowska and Waksmundzka, 2020).

3. Sample description

Channel coal samples (labelled "c") were collected from eleven workings in six bituminous coal mines, namely ("Brzeszcze" [Br-20, Br-23 and Br-24], "Jastrzębie" [Ja-22], "Marcel" [Ml-20, Ml-21 and Ml-22], "Pniówek" [Pn-23], "Silesia" [Si-22 and Si-23] and "Zofiówka" [Zo-21]) in the the USCB and two workings in the "Bogdanka" Mine of the LCB. Block samples of carbonaceous shales (claystone and/or mudstone) were collected from above (labelled "st", "top shale") and below ("sb", "bottom shale") the seams sampled for coal was sampled. In the USCB, 10 carbonaceous shale samples (5 above and 5 below coal seams) were collected and, in the LCB, two coal samples and one carbonaceous shale sample (above coal seam). Locations of sampling sites are indicated in Table 1 and Fig. 1. Samples previously analysed are also shown in Fig. 1.

4. Methods

Hydrous pyrolysis experiments, organic geochemical and isotopic analyses and microscopic examinations of original samples were carried out at the AGH University of Science and Technology in Kraków. Microscopic examinations and microphotography of coal and shale samples obtained after HP at 330 °C and 360 °C were carried out at AGH University (as above) and at the University of Silesia in Katowice.

4.1. Hydrous pyrolysis: sample- and experimental procedures

The HP experiments were conducted in Hastelloy C-276 1-L reactors (Parr Instrument Co.). Rock samples placed in reactors were heated isothermally in electric heaters at 330 ± 0.4 °C and 360 ± 0.4 °C for 72.08 ± 0.04 h in the presence of liquid water. The water-to-rock proportion was based on calculations using steam tables and measured bulk rock densities to insure that the rock samples remained in contact with liquid water throughout the experiments (Lewan, 1993).

The bituminous coals and carbonaceous shales were crushed to gravel size (0.5–2.0 cm) with no prior extraction or drying before the experiments. In each experiment, 300 g of crushed bituminous coal or 500 g of shales were loaded into the reactor. The reactor was closed and evacuated for several minutes before 350 g of distilled water (for coals) or 380 g (for shales) was injected into the reactor. After loading, the reactors were sealed with a stainless steel 316 gasket and an eight-bolt split-ring head, pressurised to ~7 MPa of helium and checked for leaks using a Restek electronic leak detector. The helium pressure in the reactors was reduced to a pressure between 2.3 and 2.5 kPa. The helium pressures and the temperatures in the reactors were recorded. The duration of each HP experiment accounts for the time between when the required temperature was first reached to the time when temperature dropped below 0.4 °C of that temperature after heating was stopped. The reactor is weighed after cooling to room temperature to ascertain if any leakage had occurred. The gas from the reactor headspace was slowly bled into a gas inlet system of known volume (Kotarba et al., 2021). After each HP experiment, gaseous-, liquid- and solid products were collected.

4.2. Petrographic and geochemical analytical approach

Microscopic examinations of the coal- and shale samples were carried out on polished sections using a Carl Zeiss AxioImager A1m microscope equipped with a 50× oil immersion objective and HBO lamp. Macerals were identified in white reflected light (vitrinite and inertinite groups) and blue light (liptinite group), applying terminology recommended by the *International Committee for Coal and Organic Petrology* (ICCP, 1998, 2001), Kwiecińska and Petersen (2004), Pickel et al. (2017) and The Society for Organic Petrology/ICCP (Stasiuk et al., 2002).

Table 1
Location and information on sampling sites.

Sample code	Mine	Seam No. (Local division)	Chronostratigraphy		Surface (m above sea level)	Depth of seam bottom (m below sea level)	Depth of seam bottom (m below surface)	Sample		
			after Harland et al. (1982)	after Cohen et al. (2013)				Coal	Shale	
Upper Silesian Coal Basin (USCB)										
Br-20	Brzeszcze	610	Nam-A	Ser	253	856	1109	c	st	sb
Br-23	Brzeszcze	510	Nam-B	B	245	813	1058	c	st	sb
Br-24	Brzeszcze	364	Wes-A	B	250	734	984	c		
Ja-22	Jastrzębie	510/1łg	Nam-B	B	252	497	749	c		
Ml-20	Marcel	712/ 1–2 + 713/1	Nam-A	Ser	279	667	946	c		
Ml-21	Marcel	712/ 1–2 + 713/1	Nam-A	Ser	239	736	974	c	st	sb
Ml-22	Marcel	502/2	Nam-B	B	271	397	668	c		
Pn-23	Pniówek	404/1	Wes-A	B	274	579	853	c		
Si-22	Silesia	327	Wes-B	Mos	243	388	631	c		
Si-23	Silesia	315	Wes-B	Mos	260	528	788	c	st	sb
Zo-21	Zofiówka	505/1	Nam-B	B	258	694	952	c	st	sb
Lublin Coal Basin (LCB)										
Bo-20	Bogdanka	391	Wes-B	Mos	171	805	976	c		sb
Bo-21	Bogdanka	385	Wes-B	Mos	178	779	958	c		

Mos - Pennsylvanian-Moscovian (Łaziska beds = 201–215 seams and Orzesze beds = 301–327 seams in the USCB, and 381–391 seams in the LCB); B - Pennsylvanian-Bashkirian (Załęże beds = 328–406 seams, Ruda beds = 407–420 seams and Zabrze beds = 501–510 seams); Ser - Mississippian-Serpukhovian (Poruba beds = 601–630 seams and Jaklovec beds = 701–723 seams); Wes - Westphalian; Nam - Namurian; c - channel coal sample; st - block shale sample collected above coal seam; sb - block shale sample collected below coal seam.

Microscopic examinations of coal- and shale samples after HP at 330 °C and 360 °C were carried out on polished blocks using a Carl Zeiss AxioImager.A2m microscope equipped with a 50× oil objective and HBO lamp. The individual components were identified in reflected white light and fluorescence applying terminology modified after ICCP (1993), Taylor et al. (1998) and Kus et al. (2017). The components were quantified at 500 points randomly distributed on each sample using a PELCON point counter. All microphotographs of unaltered- and altered OM particles were taken using a digital AxioCamMRc 5 camera.

Pulverized (<0.2 mm) and homogenized coal and carbonaceous shale samples, both original and after HP at 330 °C and 360 °C for 72 h, were subjected to bitumen extraction using a Soxhlet apparatus with a mixture of dichloromethane and methanol (93:7, v/v) for 24 h. After filtering of the resulting solutions, the bitumen was concentrated by solvent evaporation to constant mass. The bitumen extracts were separated into four fractions: saturates, aromatics, resins and asphaltenes. The asphaltene fraction was separated from bitumen with petroleum ether (boiling range 40–60 °C). The composition of the resulting maltenes was determined using glass chromatographic columns (0.8 × 25 cm) filled with alumina/silica gel (2:1, v/v). Three fractions of maltenes (saturates, aromatics and resins) were eluted with petroleum ether, toluene and a mixture of toluene and methanol (1:1, v/v), respectively. The resulting solutions were concentrated by evaporation of solvents to constant mass.

The carbon isotope composition of extracted bitumen and the four separated fractions were analysed on-line using a Finnigan Delta Plus isotope-ratio mass spectrometer (IRMS) coupled to a Carlo Erba 1108 EA elemental analyser. Carbon dioxide produced during combustion was separated by chromatographic column from other products of combustion (water vapour, nitrogen oxides and sulphur dioxide) and introduced to the IRMS. The carbon isotope data are expressed in the δ-notation (δ^{13}C, ‰) relative to VPDB (Coplen, 2011). Three internal standards were used for isotopic normalization, which were calibrated by a dual inlet system method using international standards RM8563, NBS 22 and NBS 19. Analytical precision established as standard deviation from 10 measurements is estimated to be ±0.2‰.

After removing of bitumen and carbonates (boiling in 10% HCl for 30 min), kerogen samples from coals and carbonaceous shales were introduced to the elemental analyser where OM was combusted. The carbon isotope composition of kerogen was determined in the same way as extracted bitumen and their fractions relative to PDB standard.

The saturated- and aromatic hydrocarbon fractions were analysed by gas chromatography (GC), using a mass selective detector (MSD) for biomarker composition. The saturated fraction was diluted in isooctane spiked with 5β-cholane as an internal standard, and the aromatic fraction in toluene spiked with *o*-terphenyl as an internal standard. The analyses were carried out with an Agilent 7890A GC equipped with an Agilent 7683B automatic sampler, an on-column injection chamber and a fused silica capillary column (60 m × 0.25 mm i.d.) coated with a 95% methyl−/5% phenyl siloxane phase (DB-5MS, 0.25 μm film thickness). Helium was used as a carrier gas. The GC was coupled with an Agilent 5975C MSD operated with an ion-source temperature of 230 °C, an ionization energy of 70 eV and a cycle time of 1 s in the mass range from 45 to 500 Da. For the saturated hydrocarbon fraction, the GC oven was programmed from 40 to 300 °C at a rate of 3 °C/min. For the aromatic hydrocarbon fraction, the GC oven was first heated at 80 °C for 1 min, then to 120 °C at a rate of 20 °C/min., then to 300 °C at a rate of 3 °C/min with the final temperature held for 35 min. Compounds were identified by comparison of retention times and mass spectra in the literature. They were quantified using peak areas.

5. Results

5.1. Extracted bitumen, its fraction and stable carbon isotope compositions of original coals and carbonaceous shales and after HP, and expelled oil

Extracted bitumen yields of coals and carbonaceous shales after HP at 330 °C (62.7–137.0 mg/g TOC_o and 49.0–148.8 mg/g TOC_o, respectively) are higher than for original coals and shales (23.5–44.2 mg/g and 41.5–96.4 mg/g) and somewhat higher than for coals and shales after HP at 360 °C (35.9–98.1 mg/g and 46.1–124.9 mg/g) as shown in Table 2 and Figs. 2A–B and 3A–B. Bitumen determined by means of a chemical procedure is named as extracted bitumen in Table 2 and as bitumen when identified under the microscope (Table 3). In extracted bitumen, polar components (resins and asphaltenes) dominate in original coals (62–79 wt%) and carbonaceous shales (85–92 wt%) as shown in Table 2 and Fig. 4A–B with asphaltenes constituting, in coals, from 56 to 69 wt% and, in shales, from 77 to 89 wt% (Table 2). Similar patterns characterise bitumen extracted from coals and shales after HP at 330 °C and 360 °C (see Table 2; Fig. 4A–B).

Stable carbon isotope distributions for saturates, aromatics, resins and asphaltenes in bitumen extracted from original coals are always depleted in ^{12}C compared to bitumen extracted from coals after HP at 330 °C and 360 °C (Table 2; Fig. 5A–F). The same depletion almost always applies for original shales compared shales after HP at 330 °C and 360 °C (Table 2; Fig. 5G–L). The isotopic curves for coals are enriched in ^{13}C for all fractions compared to those for shales.

Immiscible oil was expelled from both coals and shales. However, quantities were insignificant (see Table 2; Fig. 3C–D).

5.2. Petrographic composition of organic matter

Maceral compositions of OM in original coals and shales and after HP at 330 °C and 360 °C is shown in Tables 3 and 4, Figs. 3E–F, 4C–G, 6 and 7A–H. The vitrinite maceral group usually dominates in the OM of original coals and carbonaceous shales; liptinite macerals are subordinate. Inertinite macerals commonly occur in smaller amounts compared to vitrinite macerals, though not so in samples Br-23c, Br-24c, Ml-22c, Ja-22c, and Br-23st (Tables 3 and 4; Fig. 4C).

Vitrinite group macerals dominate in the OM of the original coals (Figs. 3E and 6D, J) and carbonaceous shales (Figs. 3F and 6A, G) (38.4 to 82.2 vol% and 3.3 to 14.9 vol%; 41.0 to 90.2 vol% mmf (mmf – mineral matter free) and 35.7 to 89.4 vol% mmf, respectively with subordinate liptinite (Fig. 6D, J, G), (3.0 to 22.0 vol% and 0.0 to 5.1 vol %; 3.1 to 22.6 vol%, mmf and 0.0 to 30.0 vol% mmf, respectively) and inertinite (Fig. 6D, J, G), (1.9 to 45.0 vol% and 0.5 to 5.6 vol%; 2.1 to 45.9 vol% mmf and 8.9 to 39.2 vol% mmf, respectively) group macerals (Tables 3 and 4 and Fig. 4C–D). Four original coal samples (Br-24c, Ja-22c, Pn-23c, and Pn-25c) contain trace amounts of natural char which, in one sample (Ml-22c), amounts to 0.2 vol% and vol% mmf (Tables 3 and 4). Bitumen occurs only in original coal samples Pn-23c and Pn-25c (Tables 3 and 4) and in insignificant amount in Br-23c (Fig. 3G).

Coal- and carbonaceous shale samples altered at 330 °C and 360 °C contain paler vitrinite (Figs. 4G, 6E, H, and 7E), vitrinite with cracks (Figs. 4E, 6E and 7C–D), vitrinite with devolatilization pores (Figs. 4E–F and 6B, C, K, L), inertinite macerals, semicoke (Figs. 4G, 6F and 7A), bitumen, and natural char. In addition to being paler in colour, vitrinite reflectance is increased. These changes are more pronounced in samples altered at HP 360 °C. The content of paler vitrinite in coals heated to 330 °C is 21.8–61.4 vol% (21.9–65.2 vol% mmf) and heated to 360 °C is 2.0–66.2 vol% (2.1–66.9 vol% mmf) as shown on Tables 3 and 4 and Fig. 4G. For carbonaceous shales heated in the same temperatures, the content of paler vitrinite is 0.6–9.8 vol% (14.3–63.0 vol% mmf) and 0.8–4.6 vol% (26.7–100.0 vol% mmf).

The heating resulted in devolatilisation that mostly appears in coals as round or oval pores ranging in size from ~10-30 μm in samples after

Table 2
Extracted bitumen and expelled oil yields, bitumen fractions and their stable carbon isotope compositions of original coals and carbonaceous shales and samples after hydrous pyrolysis experiments at 330 and 360 °C for 72 h.

Sample code	HP temp. (°C)	TOC (wt%)	Ext. bitumen yield (mg/ g TOC_o)	Expelled oil yield (mg/g TOC_o)	Bitumen fractions (wt%)				Sat./ Aro.	Stable carbon isotopes (‰)						CV
					Sat.	Aro.	Res.	Asph.		Sat.	Ext. bit.	Aro.	Res.	Asph.	Ker.	
Upper Silesian Coal Basin																
Br-20st	Original	1.92	96.4		3	7	5	85	0.43	−28.2	−24.9	−25.1	−26.8	−24.7	−23.9	3.97
	330	1.48	101.5	28	6	13	13	68	0.46	−26.5	−24.7	−24.8	−25.8	−24.5	−23.8	0.35
	360	1.32	72.7	n.m.	2	16	26	56	0.13	−27.4	−25.4	−24.7	−25.9	−25.0	−23.7	2.93
Br-20c	Original	81.8	42.9		10	18	11	61	0.56	−27.5	−24.8	−25.2	−25.0	−24.5	−23.9	1.95
	330	78.1	77.4	26	14	18	16	52	0.78	−25.9	−24.1	−24.4	−24.0	−23.9	−23.9	−0.41
	360	69.6	35.9	34	8	27	19	46	0.30	−24.5	−23.7	−24.0	−23.6	−23.7	−23.9	−3.02
Br-23c	Original	76.1	23.5		9	20	12	59	0.45	−26.7	−24.6	−24.6	−24.8	−24.4	−23.5	1.25
	330	72.8	62.7	14	6	12	9	73	0.50	−26.2	−24.1	−24.2	−24.3	−24.0	−23.5	0.82
	360	69.8	57.7	29	8	20	18	54	0.40	−25.0	−23.7	−24.0	−23.7	−23.5	−23.6	−1.79
Br-23sb	Original	2.48	41.5		2	6	3	89	0.33	−28.4	−24.8	−24.6	−27.4	−24.5	−23.3	5.53
	330	1.55	49.0	9	5	17	11	67	0.29	−27.6	−24.7	−24.2	−26.9	−24.3	−23.2	4.36
	360	1.28	46.1	16	3	19	15	63	0.16	−27.5	−25.0	−23.3	−26.7	−24.7	−23.3	6.24
Ml-21c	Original	81.4	36.5		10	17	13	60	0.59	−27.7	−25.7	−25.8	−25.8	−25.5	−25.1	1.07
	330	76.9	80.2	25	7	16	12	65	0.44	−27.1	−24.9	−25.3	−24.7	−24.8	−24.9	0.53
	360	72.5	48.0	33	10	24	20	46	0.42	−25.6	−24.7	−25.0	−24.6	−24.6	−24.9	−2.50
Ml-21sb	Original	2.09	67.0		2	7	7	84	0.29	−28.5	−25.5	−25.8	−27.5	−25.4	−24.7	3.30
	330	1.88	63.3	21	4	9	10	77	0.44	−27.6	−25.4	−25.6	−26.4	−25.2	−24.6	1.49
	360	1.71	49.0	28	4	11	11	74	0.36	−27.3	−25.2	−25.3	−25.8	−25.0	−24.6	1.15
Si-22st	Original	2.00	58.2		4	6	5	85	0.67	−32.7	−26.7	−29.8	−28.5	−26.0	−24.9	5.04
	330	1.28	111.7	58	10	16	19	55	0.63	−30.2	−26.9	−27.1	−27.7	−25.7	−24.5	4.67
	360	0.94	66.2	96	8	12	12	68	0.67	−28.8	−25.8	−26.2	−26.7	−25.3	−24.3	3.19
Si-22c	Original	67.3	44.2		10	11	13	66	0.91	−29.6	−25.8	−26.3	−25.8	−25.2	−24.4	4.87
	330	64.9	137.0	33	7	10	10	73	0.70	−28.4	−24.9	−25.5	−24.8	−24.6	−24.4	3.67
	360	60.6	47.6	43	15	23	27	35	0.65	−25.9	−24.3	−24.6	−23.8	−24.2	−24.4	−0.81
Si-23st	Original	2.14	95.3		4	6	8	82	0.67	−28.4	−26.1	−26.3	−27.0	−25.4	−24.4	1.89
	330	2.09	148.8	74	7	11	17	65	0.64	−27.1	−25.1	−25.4	−25.5	−24.9	−24.3	0.57
	360	1.93	124.9	135	2	8	9	81	0.25	−26.3	−24.5	−25.0	−25.3	−24.6	−24.4	−0.61
Si-23c	Original	69.8	29.1		12	14	18	56	0.86	−27.5	−25.1	−25.5	−25.4	−24.8	−24.0	1.31
	330	67.4	108.1	41	7	11	11	71	0.64	−26.9	−24.1	−24.6	−24.1	−23.9	−23.9	1.84
	360	63.1	84.0	53	8	13	22	57	0.62	−25.0	−23.7	−24.2	−23.4	−23.7	−23.9	−2.29
Lublin Coal Basin																
Bo-20c	Original	73.4	35.6		7	16	8	69	0.44	−29.3	−25.3	−26.1	−25.6	−24.8	−23.8	4.73
	330	73.1	106.6	30	8	12	15	65	0.67	−26.8	−24.4	−25.2	−24.3	−24.1	−23.9	0.07
	360	68.6	98.1	n.m.	8	15	20	57	0.53	−25.8	−24.1	−24.5	−24.0	−24.0	−23.8	−0.76
Bo-20sb	Original	3.45	42.0		6	9	8	77	0.67	−28.3	−24.9	−25.3	−27.0	−24.4	−22.8	3.74
	330	2.34	88.5	n.m.	6	11	12	71	0.55	−26.8	−24.3	−24.3	−25.1	−23.9	−22.8	2.31
	360	2.74	67.5	35	6	13	15	66	0.46	−25.9	−23.8	−23.8	−24.5	−23.7	−22.7	0.92

TOC - total organic carbon of samples after Kotarba et al. (2021); TOCo - TOC of the original sample; HP temp. - hydrous pyrolysis temperature; Ext. - extracted; Sat. - saturates; Aro. - aromatics; Res. - resines; Asph. - asphaltenes; Ker. - kerogen; n.m. - not measured; c - channel coal sample; st - block shale sample collected above coal seam; sb - block shale sample collected below coal seam; CV (canonical variable) = $[-2.53*\delta^{13}C(Sat.)] + [2.22*\delta^{13}C(Aro.)]$ - 11.65 (Sofer, 1984).

HP at 330 °C. Pores are much larger, even >50 μm, after HP at 360 °C. Devolatilisation pores are also present in vitrinite (collotelinite and vitrodetrinite) in carbonaceous shales (Fig. 2B–C). The sizes of the pores depend on the size of the original vitrinite particles and range up to >10 μm. Devolatilisation pores are more common in coals after HP at 330 °C (0.8–47.6 vol%; 0.8–48.6 vol% mmf) than in coals after HP at 360 °C (7.0–35.8 vol%; 8.8–36.2 vol% mmf). Pores are present only in three shale samples and their content was <1.4 vol% (<15.6 vol% mmf) (Tables 3 and 4).

Notable features of heated samples are cracks. Though in some cases short and irregular, they are commonly circular and even occur in systems of cracks arranged in circles; such cracks are typical of samples after HP at 330 °C and 360 °C. The round cracks may form rose-like structures with one particle containing up to three systems of such cracks (Fig. 6E). These systems of cracks are not seen in heated carbonaceous shale samples. Vitrinite with cracks (<29.0 vol%) dominates in coal samples after HP at 330 °C (Fig. 6E), whereas after HP at 360 °C, it can comprise <4.0 vol% (Fig. 4E).

After HP at 360 °C, coals commonly contain semicoke showing fine (a few μm in size, rarely >5 μm) anisotropy (Tables 3 and 4 and Fig. 6). It is present in most altered coal samples and dominates samples heated to HP 360 °C (0.8–66.6 vol%; 0.8–68.5 vol% mmf). In coal samples after HP at 330 °C, semicoke is typically less common it is present in <15.4 vol% (<15.5 vol% mmf). Semicoke particles are rare in carbonaceous shales and, in some cases, occur only in traces.

Carbonaceous shales after HP also contain vitrinite that is very porous, has a spongy structure and very thin walls. This vitrinite has reacted strongly to the HP processes. Its content is <8.2 vol% (64.1 vol% mmf) and, in general, is higher in samples heated to 360 °C than to 330 °C (Tables 3 and 4 and Figs. 4G and 7G–H).

Heating the coal and carbonaceous shale samples generates bitumen with a strong yellow fluorescence. This mostly fills cracks. Its content is <2.9 vol%; 3.0 vol% mmf in coals and, in the carbonaceous shales, <1.0 vol% (23.8 vol% mmf).

Inertinite present in the HP altered samples is mostly represented by fusinite, semifusinite and inertodetrinite, funginite, macrinite and secretinite are rare. In general, the inertinite content in coal is 1.0–43.2 vol% (1.3–43.5 vol% mmf) and, in the shales is low (<2.4 vol%; 30.8 vol % mmf). The content of inertinite is always lower than the sum of altered vitrinite and semicoke (Tables 3 and 4).

Liptinite macerals, mostly altered during heating, are absent in the HP heated samples (Tables 3 and 4, and Fig. 4C–D). Some of these contain extremely rare liptinite particles but their optical properties have changed, i.e., their colour in reflected white light is paler, their

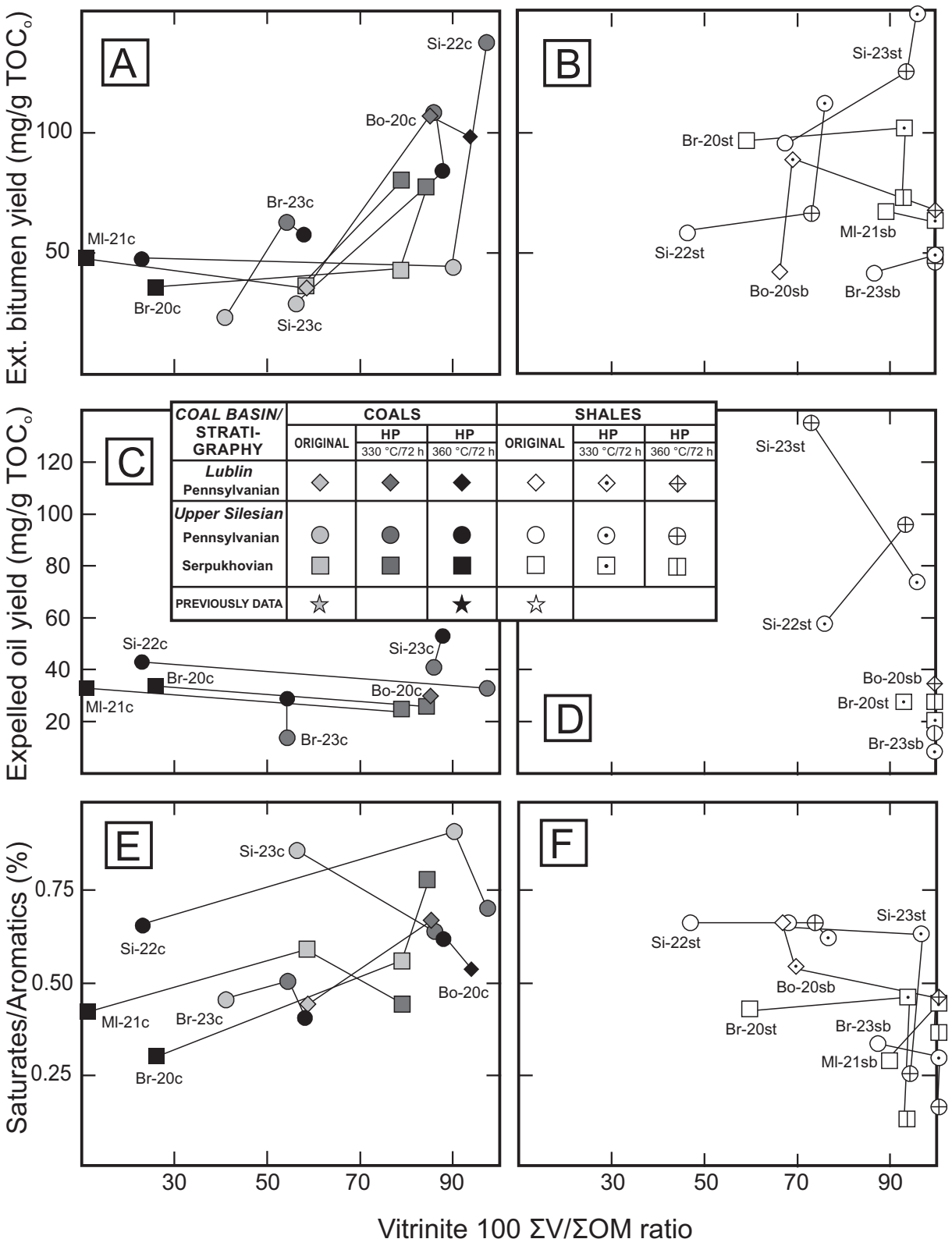

Fig. 2. (A and B) Extracted bitumen yield (mg/g TOC_o), (C and D) expelled oil yield (mg/g TOC_o) and (E and F) saturates/aromatics ratio versus 100 ΣV/ΣOM ratio of (A, C and E) coals and (B, D and F) carbonaceous shales of original samples and after HP at 330 °C and 360 °C for 72 h. Ext. – extracted, ΣOM – sum of components of OM = ΣV + ΣI + ΣL + Ch + Bit + Sem; ΣV – sum of vitrinite macerals, ΣI – sum of inertinite macerals, ΣL – sum of liptinite macerals; Ch – natural char; Bit – bitumen; Sem – semicoke.

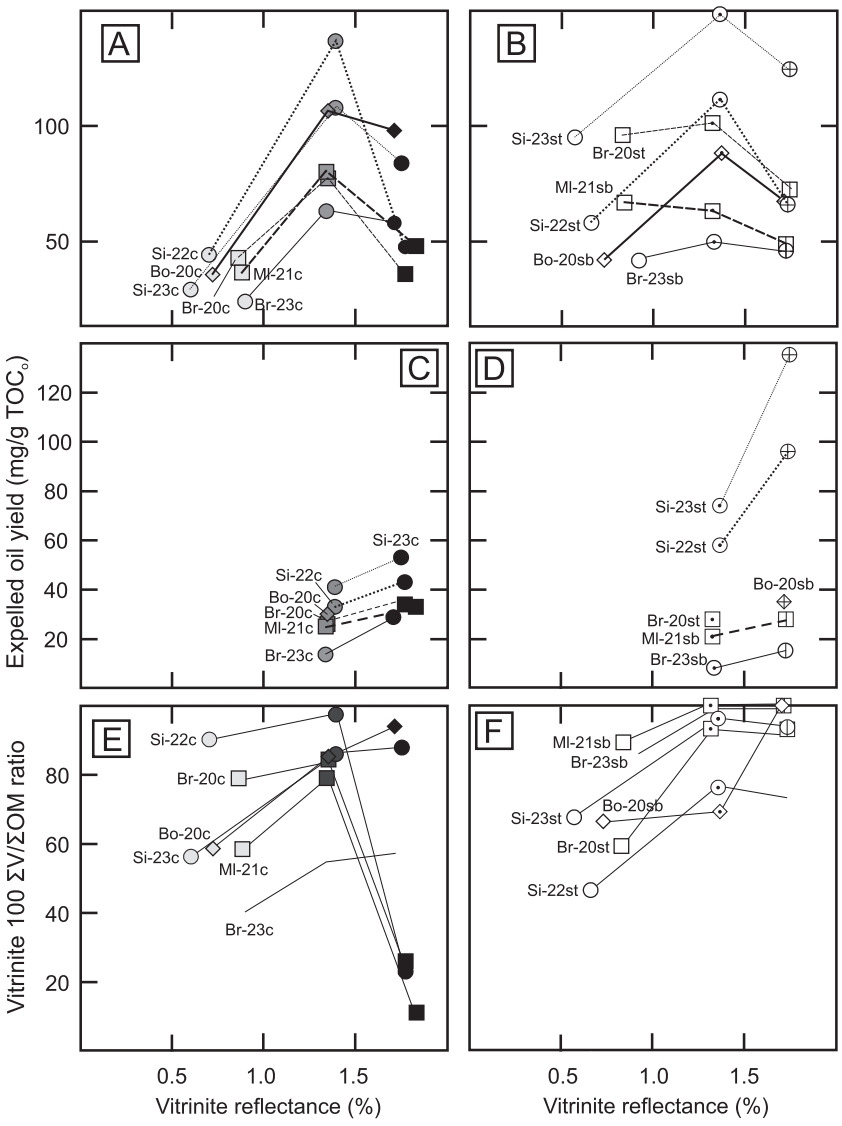

Fig. 3. (A and B) Extracted bitumen yield (mg/g TOC_o), (C and D) expelled oil yield (mg/g TOC_o), (E and F) 100 ΣV/ΣOM ratio and (G and H) 100 Bit/ΣOM ratio versus vitrinite reflectance of (A, C, E and G) coals and (B, D, F and H) carbonaceous shales of original samples and after HP at 330 °C and 360 °C for 72 h. See Fig. 2 for sample key and stratigraphy of currently analysed samples in this and following figures.
Ext. – Extracted; TOC_o – initial total organic carbon; ΣOM – sum of components of organic matter = ΣV + ΣI + ΣL + Ch + Bit + Sem; ΣV – sum of vitrinite macerals; ΣI – sum of inertinite macerals; ΣL – sum of liptinite macerals; Ch – natural char; Bit – bitumen; Sem – semicoke.

reflectance higher and their fluorescence considerably weaker.

5.3. Biomarker and non-biomarker signatures

Selected indices were calculated based on the distribution of *n*-alkanes, isoprenoids, steranes and terpanes in the saturated hydrocarbon fraction of the bitumen extracted from the coals and carbonaceous shales before and after HP. All abbreviations and ratios are given in Table 5). Similarly, non-biomarker indices of methylphenanthrene, phenanthrene (Phen), dibenzothiophene (DBT), methyldibenzothiophene, triaromatic steroids, as well as dibenzofuran (DBF) and fluorene (F) representing polycyclic aromatic hydrocarbons (PAHs) detected in the bitumen extracted from the coals and shales before and after HP were also calculated. All abbreviations and ratios are given in Table 6. Finally, biomarker and non-biomarker maturity indicators typically used for OM maturity assessment were also tested (Radke et al., 1982; Radke, 1988; Beach et al., 1989; Peters et al., 2005; Asif and Wenger, 2019).

The distribution of *n*-alkanes is characterized by low abundance of low molecular weight (LMW) *n*-alkanes (<C_{17}) in original samples and a subsequent increase of LMW and high molecular weight (HMW) *n*-alkane abundance after HP at 330 °C and a decrease in LMW and an increase of HMW *n*-alkanes after HP 360 °C in shale and coal samples from the USCB and LCB (Fig. 8). This trend, however, is different in the USCB shale samples with slight biodegradation (unresolved complex mixture [UCM] present) where at HP 330 °C and 360 °C, LMW (<C_{20}) and HMW ($C_{21–24}$) *n*-alkanes decrease in abundance compared to the original samples (Fig. 8).

In the case of isoprenoid, sterane and some hopane ratios, pristane/phytane (Pr/Ph), Pr/*n*-C_{17}, pH/*n*-C_{18}, %$C_{27–29}$ sterane, C_{29} norhopane/C_{30} 17α-hopane (C_{29}H/Hop), C_{35}S/C_{34}S hopane values are, in general, characterized by a significant decrease from original values to those at HP 330 and 360 °C for both coals and shales (Table 5). This decreasing trend is particularly evident in most Pr/Ph values which decrease from original values to those at HP 360 °C by 39–83%. In four USCB samples (Br-20c, Br-23cb, MI-21c and Si-22c), Pr/Ph values increase from those at HP 330 °C by at least ~60% on average.

Hopane and triterpenoid ratios decrease from original values after HP at 330 °C and increase after HP at 360 °C in most coal and shale samples (Table 5). In a few cases, sterane/terpane (S/T) and tricyclic/pentacyclic terpane (Tri/Pen) values (Table 5) could not be calculated, particularly at HP 360 °C due to coelution of tricyclic compounds with aromatic hydrocarbons, which did not wash out at the separation stage.

In the case of the aromatic hydrocarbon fraction, the aromatic compounds (DBF, DBT and F) and their ratios (DBT/Phen, triaromatic steroids) show no regularity although, in general, they increase from the

Table 3
Vitrinite reflectance and organic matter petrographic composition of original coal and shale samples and samples after hydrous pyrolysis at 330 and 360 °C for 72 h.

Sample code	HP temp. (°C)	*R_r (%)	Maceral composition (%)																						Ch (%)	Bit (%)	Sem (%)	Min. Mat. (%)	Petrographic ratios								
			Ct	Cd	Te	Vd	PaV	VPo	VCr	SRV	ΣV	Fu	Sf	Fg	Ma	Mi	Sec	Id	ΣI	Sp	Cu	Re	Ld	ΣL					100 ΣV/ΣOM	100 ΣI/ΣOM	100 ΣL/ΣOM	100 (Sem + VCr)/ΣOM	100 Ch/ΣOM	100 Bit/ΣOM	100 Sem/ΣOM	100 PaV/ΣOM	100 VCr/ΣOM	100 VPo/ΣOM	100 SRV/ΣOM
Upper Silesian Coal Basin																																					
Br-20st	Original	0.83	7.1	0.0	0.0	1.8	0.0	0.0	0.0	0.0	8.9	0.2	1.1	0.0	0.0	0.0	0.0	0.1	1.3	2.6	0.6	0.2	2.0	0.7	3.5	0.0	0.0	0.0	85.0	59.3	17.3	23.4	0.0	0.0	0.0	0.0	0.0	0.0	0.0	0.0
	330	1.32	0.0	0.0	0.0	0.0	2.0	0.0	0.0	0.8	2.8	0.0	0.0	0.0	0.0	0.0	0.0	0.0	0.0	0.0	0.0	0.0	0.0	0.0	0.0	0.0	0.2	0.0	97.0	93.3	0.0	0.0	0.0	0.0	6.7	0.0	66.7	0.0	0.0	26.7
	360	1.74	0.0	0.0	0.0	0.0	4.4	0.0	0.0	1.0	5.4	0.0	0.0	0.0	0.0	0.0	0.0	0.0	0.2	0.2	0.0	0.0	0.0	0.0	0.0	0.0	0.2	0.0	94.2	93.1	3.4	0.0	0.0	0.0	3.4	0.0	75.9	0.0	0.0	17.2
Br-20c	Original	0.86	62.0	13.2	0.0	0.2	0.0	0.0	0.0	0.0	75.4	2.1	5.0	0.3	0.5	0.0	0.3	0.2	11.1	6.0	2.2	0.7	0.1	9.0	0.0	0.0	0.0	4.5	79.0	11.6	9.4	0.0	0.0	0.0	0.0	0.0	0.0	0.0	0.0
	330	1.35	0.0	0.0	0.0	0.0	54.6	0.8	29.0	0.0	84.4	4.0	1.0	0.0	0.2	0.0	0.0	2.2	5.6	0.0	0.0	0.0	0.0	0.0	0.0	0.4	9.6	0.0	84.4	5.6	0.0	38.6	0.0	0.4	9.6	54.6	29.0	0.8	0.0
	360	1.77	0.0	0.0	0.0	0.0	15.8	9.0	1.2	0.0	26.0	6.4	0.8	0.0	0.2	0.0	0.0	0.6	8.0	0.0	0.0	0.0	0.0	0.0	0.0	0.0	0.0	66.0	0.0	26.0	8.0	0.0	67.2	0.0	0.0	66.0	15.8	1.2	9.0	0.0
Br-20sb	Original	0.83	4.7	0.0	0.0	0.9	0.0	0.0	0.0	0.0	5.6	1.1	2.5	0.0	0.2	0.0	0.0	0.4	4.2	0.8	0.1	0.1	0.3	1.3	3.0	0.0	0.0	0.0	88.9											
Br-23st	Original	0.86	3.3	0.0	0.0	1.8	0.0	0.0	0.0	0.0	5.1	1.2	2.2	0.0	0.3	0.0	0.0	1.9	5.6	1.6	0.7	0.4	0.9	3.6	0.0	0.0	0.0	85.7											
Br-23c	Original	0.90	24.8	14.5	0.3	0.2	0.0	0.0	0.0	0.0	39.8	5.7	22.2	0.7	6.8	1.3	0.6	7.7	43.4	9.8	3.4	0.8	0.0	14.0	0.0	0.0	0.0	2.8	40.9	44.7	14.4	0.0	0.0	0.0	0.0	0.0	0.0	0.0	0.0
	330	1.34	0.0	0.0	0.0	0.0	21.8	28.0	4.2	0.0	54.0	12.4	23.0	0.6	1.0	1.6	0.6	0.6	43.2	0.0	0.0	0.0	0.0	0.0	0.0	2.2	0.0	0.6	54.3	43.5	0.0	4.2	0.0	2.2	0.0	21.9	4.2	28.2	0.0
	360	1.71	0.0	0.0	0.0	0.0	25.4	30.0	1.2	0.0	56.6	15.2	7.8	0.0	3.0	0.0	0.2	0.8	28.8	0.0	0.0	0.0	0.0	0.0	0.0	0.6	11.6	2.4	58.0	29.5	0.0	13.1	0.0	0.6	11.9	26.0	1.2	30.7	0.0
Br-23sb	Original	0.92	1.9	0.0	0.0	1.4	0.0	0.0	0.0	0.0	3.3	0.1	0.2	0.0	0.0	0.0	0.0	0.2	0.5	0.0	0.0	0.0	0.0	0.0	0.0	0.0	0.0	96.2	86.8	13.2	0.0	0.0	0.0	0.0	0.0	0.0	0.0	0.0	0.0
	330	1.33	0.0	0.0	0.0	0.0	1.6	0.0	0.0	0.2	1.8	0.0	0.0	0.0	0.0	0.0	0.0	0.0	0.0	0.0	0.0	0.0	0.0	0.0	0.0	0.0	0.0	0.0	98.2	100.0	0.0	0.0	0.0	0.0	0.0	0.0	88.9	0.0	0.0	11.1
	360	1.70	0.0	0.0	0.0	0.0	0.8	0.0	0.0	0.0	0.8	0.0	0.0	0.0	0.0	0.0	0.0	0.0	0.0	0.0	0.0	0.0	0.0	0.0	0.0	0.0	0.0	0.0	99.2	100.0	0.0	0.0	0.0	0.0	0.0	0.0	100.0	0.0	0.0	0.0
Br-24c	Original	0.80	32.7	11.8	0.1	0.0	0.0	0.0	0.0	0.0	44.6	7.1	23.3	3.4	2.4	1.0	0.7	0.8	45.0	5.8	2.2	0.3	0.1	8.4	0.0	0.0	0.0	2.0											
Ja-22c	Original	1.12	36.9	6.1	0.3	0.0	0.0	0.0	0.0	0.0	43.3	6.1	27.1	1.3	1.0	1.9	0.6	0.1	43.5	7.0	0.0	2.0	0.0	9.0	0.0	0.0	0.0	4.2											
Si-22st	Original	0.66	6.1	0.0	0.0	1.8	0.0	0.0	0.0	0.0	7.9	0.3	2.4	0.0	0.0	0.0	0.0	0.1	3.3	4.0	3.6	0.2	0.0	1.3	5.1	0.0	0.0	0.0	83.0	46.5	23.5	30.0	0.0	0.0	0.0	0.0	0.0	0.0	0.0	0.0
	330	1.36	0.0	0.0	0.0	0.0	0.6	0.0	0.0	2.6	3.2	0.0	0.0	0.0	0.0	0.0	0.0	0.0	0.0	0.0	0.0	0.0	0.0	0.0	0.0	0.0	1.0	0.0	95.8	76.2	0.0	0.0	0.0	0.0	23.8	0.0	14.3	0.0	0.0	61.9
	360	1.73	0.0	0.0	0.0	0.0	0.8	0.0	0.0	1.4	2.2	0.0	0.0	0.0	0.0	0.0	0.0	0.0	0.0	0.0	0.0	0.0	0.0	0.0	0.0	0.0	0.2	0.0	97.0	73.3	0.0	0.0	0.0	20.0	6.7	0.0	26.7	0.0	0.0	46.7
Si-22c	Original	0.70	61.5	20.7	0.0	0.0	0.0	0.0	0.0	0.0	82.2	0.1	0.9	0.4	0.5	0.0	0.0	0.0	1.9	4.4	1.7	0.1	0.8	7.0	0.0	0.0	0.0	8.9	90.2	2.1	7.7	0.0	0.0	0.0	0.0	0.0	0.0	0.0	0.0
	330	1.39	0.0	0.0	0.0	0.0	61.4	8.4	22.0	0.0	91.8	1.2	0.0	0.0	0.0	1.0	0.0	2.0	2.4	0.0	0.0	0.0	0.0	0.0	0.0	0.0	0.0	5.8	97.5	2.5	0.0	23.4	0.0	0.0	0.0	65.2	23.4	8.9	0.0
	360	1.77	0.0	0.0	0.0	0.0	10.2	7.0	0.0	0.0	17.2	0.0	0.8	0.0	0.0	0.0	0.0	0.0	2.0	1.0	0.0	0.0	0.0	0.0	0.0	0.0	0.0	56.6	25.2	23.0	1.3	0.0	75.7	0.0	0.0	75.7	13.6	0.0	9.4	0.0
Si-22sb	Original	0.68	3.7	0.0	0.0	2.6	0.0	0.0	0.0	0.0	6.3	0.4	1.0	0.0	0.0	0.0	0.0	0.1	2.5	0.6	0.3	0.0	0.3	1.2	0.0	0.0	0.0	90.0											
Si-23st	Original	0.57	11	0.0	0.7	3.2	0.0	0.0	0.0	0.0	14.9	0.4	1.7	0.0	0.0	0.0	0.0	0.7	2.8	1.8	1.1	0.4	1.0	4.3	0.0	0.0	0.0	78.0	67.6	12.9	19.5	0.0	0.0	0.0	0.0	0.0	0.0	0.0	0.0
	330	1.36	0.0	0.0	0.0	0.0	9.8	1.2	0.0	4.2	15.2	0.0	0.0	0.0	0.0	0.0	0.0	0.0	0.0	0.0	0.0	0.0	0.0	0.0	0.0	0.0	0.6	0.0	84.2	96.2	0.0	0.0	0.0	0.0	3.8	0.0	62.0	0.0	7.6	26.6
	360	1.74	0.0	0.0	0.0	0.0	3.6	0.2	0.0	8.2	12.0	0.0	0.0	0.0	0.0	0.0	0.0	0.0	0.0	0.0	0.0	0.0	0.0	0.0	0.0	0.0	0.8	0.0	87.2	93.8	0.0	0.0	0.0	0.0	6.3	0.0	28.1	0.0	1.6	64.1
Si-23c	Original	0.60	35.3	18.8	0.1	0.1	0.0	0.0	0.0	0.0	54.3	4.9	11.1	0.3	1.6	0.0	0.6	0.9	24.8	13.2	2.9	0.9	0.3	17.3	**0.0**	0.0	3.6	56.3	25.7	17.9	0.0	0.0	0.0	0.0	0.0	0.0	0.0	0.0	0.0
	330	1.39	0.0	0.0	0.0	0.0	36.2	47.6	1.0	0.0	84.8	5.6	1.8	0.0	0.6	3.4	0.1	0.4	12.8	0.0	0.0	0.0	0.0	0.0	0.0	1.0	0.0	1.4	86.0	13.0	0.0	1.0	0.0	1.0	0.0	36.7	1.0	48.3	0.0
	360	1.75	0.0	0.0	0.0	0.0	47.2	35.8	4.0	0.0	87.0	4.8	3.2	0.0	0.0	0.0	0.0	1.0	9.0	0.0	0.0	0.0	0.0	0.0	0.0	1.2	1.8	1.0	87.9	9.1	0.0	5.9	0.0	1.2	1.8	47.7	4.0	36.2	0.0
Si-23sb	Original	0.59	9.6	0.0	0.0	3.5	0.0	0.0	0.0	0.0	13.1	0.5	2.0	0.0	0.0	0.0	0.0	0.1	3.6	1.9	0.4	0.1	0.9	3.3	0.0	0.0	0.0	80.0											
Pn-23c	Original	1.57	43.7	16.4	0.0	0.0	0.0	0.0	0.0	0.0	60.1	5.3	9.7	0.0	1.3	4.1	0.8	0.5	28.9	5.3	0.0	0.0	0.0	5.3	0.0	2.9	0.0	2.8											
Pn-25c	Original	1.06	46.1	14.4	0.0	0.3	0.0	0.0	0.0	0.0	60.8	3.7	11.6	0.2	0.3	1.3	0.4	0.2	21.3	4.3	0.5	0.0	0.0	4.8	0.0	2.3	0.0	10.8											
Ml-20c	Original	0.70	39.1	17.7	0.1	0.8	0.0	0.0	0.0	0.0	57.7	5.2	9.1	0.3	2.0	0.0	0.6	0.2	22.8	9.3	3.0	0.0	0.7	13.0	0.0	0.0	0.0	6.5											
Ml-21st	Original	0.87	7.7	0.0	0.3	0.8	0.0	0.0	0.0	0.0	8.8	0.1	0.6	0.1	0.0	0.0	0.0	0.2	1.0	0.9	0.1	0.1	0.3	1.4	0.0	0.0	0.0	88.8											
Ml-21c	Original	0.88	44.7	11.8	0.0	0.2	0.0	0.0	0.0	0.0	56.7	11.8	12.8	0.9	0.7	0.0	0.2	0.3	28.5	8.2	2.1	0.6	0.9	11.8	0.0	0.0	0.0	3.0	58.5	29.4	12.2	0.0	0.0	0.0	0.0	0.0	0.0	0.0	0.0
	330	1.34	0.0	0.0	0.0	0.0	53.0	6.6	8.8	0.0	78.4	3.4	0.8	0.0	0.2	0.0	0.0	0.8	5.2	0.0	0.0	0.0	0.0	0.0	0.0	0.2	15.4	0.8	79.0	5.2	0.0	34.5	0.0	0.2	15.5	53.4	19.0	6.7	0.0
	360	1.83	0.0	0.0	0.0	0.0	2.0	8.6	0.2	0.0	10.8	7.2	4.8	0.2	1.0	0.0	0.6	0.6	19.8	0.0	0.0	0.0	0.0	0.0	0.0	0.0	66.6	2.8	11.1	20.4	0.0	68.7	0.0	0.0	68.5	2.1	0.2	8.8	0.0
Ml-21sb	Original	0.84	3.7	0.0	0.0	0.5	0.0	0.0	0.0	0.0	4.2	0.1	0.3	0.0	0.0	0.0	0.0	0.1	0.5	0.0	0.0	0.0	0.0	0.0	0.0	0.0	0.0	95.3	89.4	10.6	0.0	0.0	0.0	0.0	0.0	0.0	0.0	0.0	0.0
	330	1.32	0.0	0.0	0.0	0.0	3.4	0.0	0.0	2.0	5.4	0.0	0.0	0.0	0.0	0.0	0.0	0.0	0.0	0.0	0.0	0.0	0.0	0.0	0.0	0.0	0.0	94.6	100.0	0.0	0.0	0.0	0.0	0.0	0.0	63.0	0.0	0.0	37.0
	360	1.72	0.0	0.0	0.0	0.0	4.6	1.4	0.0	3.0	9.0	0.0	0.0	0.0	0.0	0.0	0.0	0.0	0.0	0.0	0.0	0.0	0.0	0.0	0.0	0.0	0.0	91.0	100.0	0.0	0.0	0.0	0.0	0.0	0.0	51.1	0.0	15.6	33.3
Ml-22c	Original	0.72	19.0	19.2	0.1	0.1	0.0	0.0	0.0	0.0	38.4	2.4	24.5	0.0	1.7	2.4	0.8	0.3	39.3	6.7	3.9	0.0	0.1	0.1	0.0	0.0	0.0	11.4											
Zo-21c	Original	1.06	32.9	23.1	0.0	0.0	0.0	0.0	0.0	0.0	56.0	0.4	20.9	0.6	1.7	3.8	0.9	0.8	37.2	2.9	0.1	0.0	0.0	0.0	0.0	0.0	0.0	3.8											
Lublin Coal Basin																																					
Bo-20c	Original	0.72	46.0	11.5	0.0	0.0	0.0	0.0	0.0	0.0	57.5	4.2	11.6	0.0	2.4	1.8	0.7	0.9	27.9	12.0	0.7	0.0	0.0	12.7	**0.0**	0.0	1.9	58.6	28.4	12.9	0.0	0.0	0.0	0.0	0.0	0.0	0.0	0.0	0.0
	330	1.35	0.0	0.0	0.0	0.0	55.4	24.2	4.8	0.0	84.4	9.4	2.4	0.0	0.0	0.8	0.2	0.0	14.6	0.0	0.0	0.0	0.0	0.0	0.0	0.0	0.0	1.0	85.3	14.7	0.0	4.8	0.0	0.0	0.0	56.0	4.8	24.4	0.0
	360	1.71	0.0	0.0	0.0	0.0	66.2	25.2	1.6	0.0	93.0	3.4	0.8	0.0	0.0	0.0	0.2	0.0	0.6	5.0	0.0	0.0	0.0	0.0	0.0	0.2	0.0	0.8	1.0	93.9	5.1	0.0	2.4	2.0	0.0	0.8	66.9	1.6	25.5	0.0
Bo-20sb	Original	0.73	6.7	0.0	0.0	1.4	0.0	0.0	0.0	0.0	8.1	0.1	1.7	0.0	0.0	0.0	0.0	0.1	2.8	0.9	0.1	0.1	0.2	1.3	0.0	0.0	0.0	87.8	66.4	23.0	10.7	0.0	0.0	0.0	0.0	0.0	0.0	0.0	0.0
	330	1.37	0.0	0.0	0.0	0.0	2.8	0.4	0.0	2.2	5.4	0.8	0.2	0.0	0.0	0.0	0.0	0.1	2.4	0.0	0.0	0.0	0.0	0.0	0.0	0.0	0.0	92.2	69.2	30.8	0.0	0.0	0.0	0.0	0.0	35.9	0.0	5.1	28.2
	360	1.71	0.0	0.0	0.0	0.0	3.2	0.8	0.0	5.0	9.0	0.0	0.0	0.0	0.0	0.0	0.0	0.0	0.0	0.0	0.0	0.0	0.0	0.0	0.0	0.0	0.0	91.0	100.0	0.0	0.0	0.0	0.0	0.0	0.0	35.6	0.0	8.9	55.6
Bo-21c	Original	0.62	45.9	9.4	0.0	0.0	0.0	0.0	0.0	0.0	55.3	1.9	9.4	0.0	1.3	0.0	0.7	0.6	20.2	19.0	2.0	1.0	0.0	22.0	**0.0**	0.0	2.5												

*R_r - mean vitrinite reflectance value after Kotarba et al. (2021); ΣOM - sum of components of organic matter = ΣV + ΣI + ΣL + Ch + Bit + Sem; ΣV - sum of vitrinite macerals; ΣI - sum of inertinite macerals; ΣL - sum of liptinite macerals; Ct - collotelinite; Cd - collodetrinite; Te - telinite; Vd - vitrodetrinite; PaV - paler vitrinite; VPo - vitrinite with pores; VCr - vitrinite with cracks; SRV - strongly reacted vitrinite; Fu - fusinite; Sf - semifusinite; Ma - macrinite; Mi - micrinite; Fg - funginite; Sec - secretinite; Id - inertodetrinite; Sp - sporinite; Cu - cutinite; Re - resinite; Ld - liptodetrinite; Ch - natural char; Bit - bitumen; Sem - semicoke; Min. Mat. - mineral matter; c - channel coal sample; st - block shale sample collected above coal seam; sb - block shale sample collected below coal seam. Petrographic ratios were calculated for coal and shale samples selected for hydrous pyrolysis.

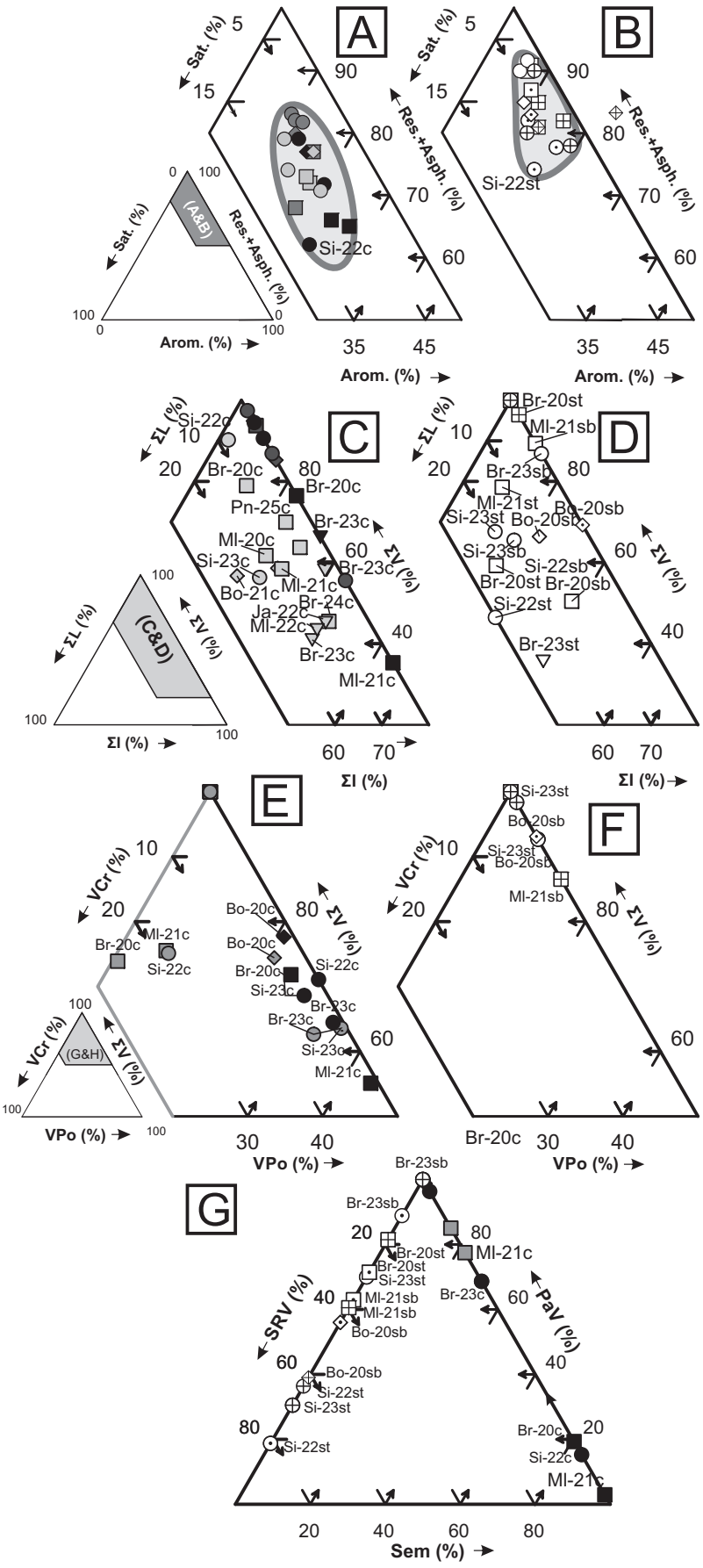

Fig. 4. Ternary diagrams for (A, C and E) coals and (B, D and F) carbonaceous shales of original samples and after HP at 330 °C and 360 °C for 72 h for (A and B) fraction composition of extracted bitumen, (C and D) maceral group composition, (E and F) vitrinite with cracks (VCr) – vitrinite with pores (VPo) – sum of vitrinite macerals (ΣV). (G) Ternary diagram of semicoke (Sem) – strongly reacted vitrinite (SRV) – paler vitrinite (PaV) for coals and carbonaceous shales.
For data, see Tables 2 and 3. Sat. – Saturates, Aro. – Aromatics, Res. – Resins, Asph. – Asphaltenes, ΣV – sum of vitrinite macerals, ΣI – sum of inertinite macerals, ΣL – sum of liptinite macerals.

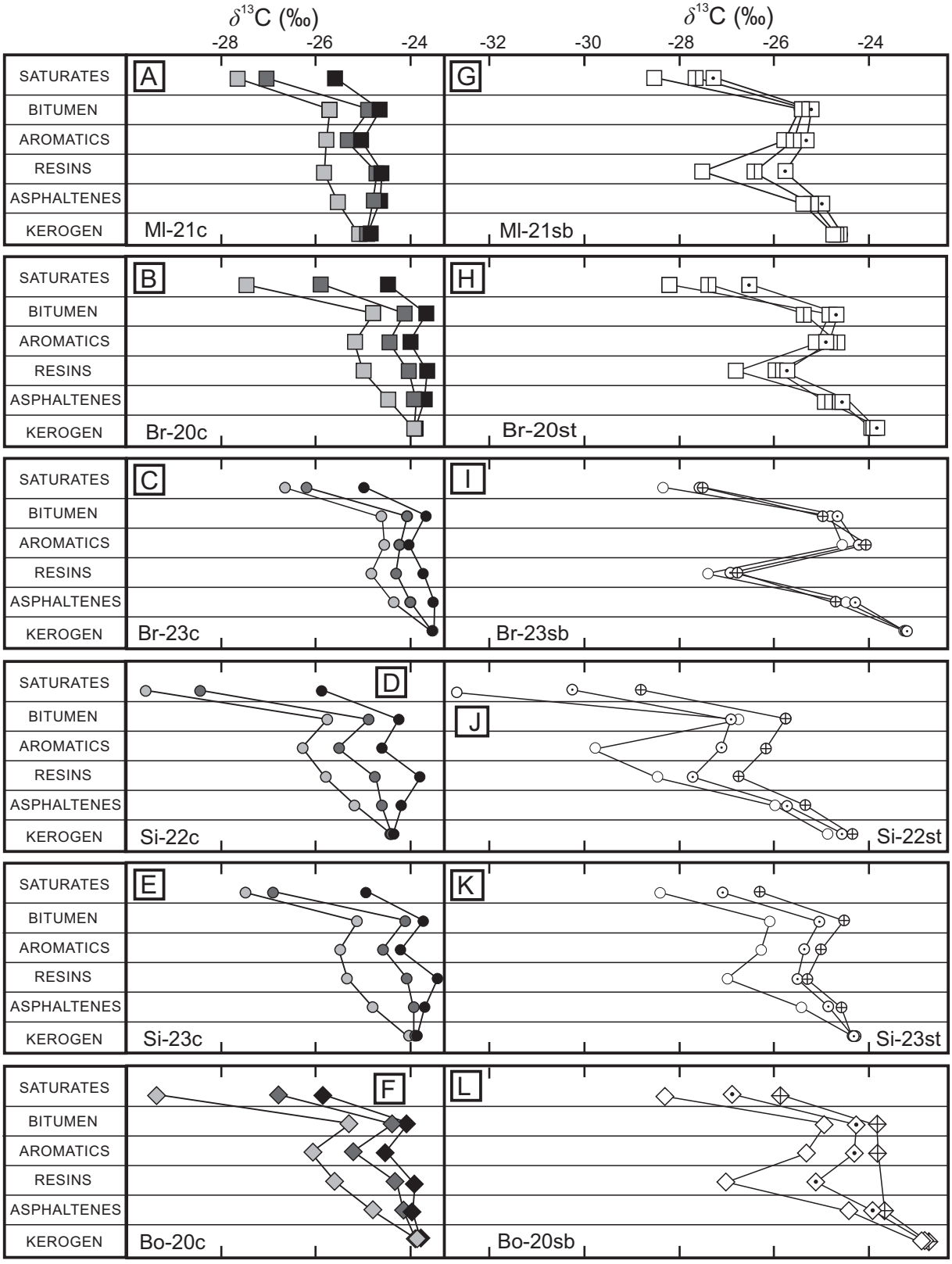

Fig. 5. Stable carbon isotope curves for saturated hydrocarbons, extracted bitumen, aromatic hydrocarbons, resins, asphaltenes and kerogen of analysed original coals (A to F) and carbonaceous shales (G to L) and after HP at 330 °C and 360 °C for 72 h of Sepukhovian (A and G) Ml-21c and Ml-21sb, (B and H) Br-20c and Br-20st, Pennsylvanian (C and I) Br-23c and Br-23sb, (D and J) Si-22c and Si-22st, (E and K) Si-23c and Si-23st samples from the USCB, and Pennsylvanian (F and L) Bo-20c and Bo-20sb samples from the LCB. See Fig. 2 for sample key and stratigraphy of analysed samples.

Table 4
Organic matter petrographic composition of original coal and shale samples and samples after hydrous pyrolysis at 330 and 360 °C for 72 h calculated into mineral matter free base (mmf).

Sample code	HP temp. (°C)	Maceral composition (%)																						Ch (%)	Bit (%)	Sem (%)
		Ct	Cd	Te	Vd	PaV	VPo	VCr	SRV	∑V	Fu	Sf	Fg	Ma	Mi	Sec	Id	∑I	Sp	Cu	Re	Ld	∑L			
Upper Silesian Coal Basin																										
Br-20st	Original	47.3	0.0	0.0	12.0	0.0	0.0	0.0	0.0	59.3	1.3	7.3	0.0	0.0	0.0	0.0	8.7	17.3	4.0	1.3	13.3	4.8	23.4	0.0	0.0	0.0
	330	0.0	0.0	0.0	0.0	66.7	0.0	0.0	26.7	93.3	0.0	0.0	0.0	0.0	0.0	0.0	0.0	0.0	0.0	0.0	0.0	0.0	0.0	0.0	6.7	0.0
	360	0.0	0.0	0.0	0.0	75.9	0.0	0.0	17.2	93.1	0.0	0.0	0.0	0.0	0.0	0.0	3.4	3.4	0.0	0.0	0.0	0.0	0.0	0.0	3.4	0.0
Br-20c	Original	64.9	13.8	0.0	0.2	0.0	0.0	0.0	0.0	79.0	2.2	5.2	0.3	0.5	0.0	0.0	3.4	11.6	6.3	2.3	0.7	0.1	9.4	0.0	0.0	0.0
	330	0.0	0.0	0.0	0.0	54.6	0.8	29.0	0.0	84.4	4.0	1.0	0.0	0.2	0.0	0.2	0.2	5.6	0.0	0.0	0.0	0.0	0.0	0.0	0.4	9.6
	360	0.0	0.0	0.0	0.0	15.8	9.0	1.2	0.0	26.0	6.4	0.8	0.0	0.2	0.0	0.0	0.6	8.0	0.0	0.0	0.0	0.0	0.0	0.0	0.0	66.0
Br-20sb	Original	42.3	0.0	0.0	8.1	0.0	0.0	0.0	0.0	50.5	9.9	22.5	0.0	1.8	0.0	0.0	3.6	37.8	7.2	0.9	0.9	2.7	11.7	0.0	0.0	0.0
Br-23st	Original	23.1	0.0	0.0	12.6	0.0	0.0	0.0	0.0	35.7	8.4	15.4	0.0	2.1	0.0	0.0	13.3	39.2	11.2	4.9	2.8	6.3	25.2	0.0	0.0	0.0
Br-23c	Original	25.5	14.9	0.3	0.2	0.0	0.0	0.0	0.0	40.9	5.9	22.8	0.7	7.0	1.3	0.0	6.9	44.7	10.1	3.5	0.8	0.0	14.4	0.0	0.0	0.0
	330	0.0	0.0	0.0	0.0	21.9	28.2	4.2	0.0	54.3	12.5	23.1	0.6	1.0	1.6	0.0	4.6	43.5	0.0	0.0	0.0	0.0	0.0	0.0	2.2	0.0
	360	0.0	0.0	0.0	0.0	26.0	30.7	1.2	0.0	58.0	15.6	8.0	0.0	3.1	0.0	0.0	2.9	29.5	0.0	0.0	0.0	0.0	0.0	0.0	0.6	11.9
Br-23sb	Original	50.0	0.0	0.0	36.8	0.0	0.0	0.0	0.0	86.8	2.6	5.3	0.0	0.0	0.0	0.0	5.3	13.2	0.0	0.0	0.0	0.0	0.0	0.0	0.0	0.0
	330	0.0	0.0	0.0	0.0	88.9	0.0	0.0	11.1	100.0	0.0	0.0	0.0	0.0	0.0	0.0	0.0	0.0	0.0	0.0	0.0	0.0	0.0	0.0	0.0	0.0
	360	0.0	0.0	0.0	0.0	100.0	0.0	0.0	0.0	100.0	0.0	0.0	0.0	0.0	0.0	0.0	0.0	0.0	0.0	0.0	0.0	0.0	0.0	0.0	0.0	0.0
Br-24c	Original	33.4	12.0	0.1	0.0	0.0	0.0	0.0	0.0	45.5	7.2	23.8	3.5	2.4	1.0	0.0	8.0	45.9	5.9	2.2	0.3	0.1	8.6	0.0	0.0	0.0
Ja-22c	Original	38.5	6.4	0.3	0.0	0.0	0.0	0.0	0.0	45.2	6.4	28.3	1.4	1.0	2.0	0.0	6.4	45.4	7.3	0.0	2.1	0.0	9.4	0.0	0.0	0.0
Si-22st	Original	35.9	0.0	0.0	10.6	0.0	0.0	0.0	0.0	46.5	1.8	14.1	0.0	0.0	0.0	0.0	7.6	23.5	21.2	1.2	0.0	7.6	30.0	0.0	0.0	0.0
	330	0.0	0.0	0.0	0.0	14.3	0.0	0.0	61.9	76.2	0.0	0.0	0.0	0.0	0.0	0.0	0.0	0.0	0.0	0.0	0.0	0.0	0.0	0.0	23.8	0.0
	360	0.0	0.0	0.0	0.0	26.7	0.0	0.0	46.7	73.3	0.0	0.0	0.0	0.0	0.0	0.0	0.0	0.0	0.0	0.0	0.0	0.0	0.0	20.0	6.7	0.0
Si-22c	Original	67.5	22.7	0.0	0.0	0.0	0.0	0.0	0.0	90.2	0.1	1.0	0.4	0.5	0.0	0.0	0.0	2.1	4.8	1.9	0.1	0.9	7.7	0.0	0.0	0.0
	330	0.0	0.0	0.0	0.0	65.2	8.9	23.4	0.0	97.5	1.3	0.0	0.0	0.0	1.1	0.2	0.0	2.5	0.0	0.0	0.0	0.0	0.0	0.0	0.0	0.0
	360	0.0	0.0	0.0	0.0	13.6	9.4	0.0	0.0	23.0	0.0	1.1	0.0	0.0	0.0	0.0	0.3	1.3	0.0	0.0	0.0	0.0	0.0	0.0	0.0	75.7
Si-22sb	Original	37.0	0.0	0.0	26.0	0.0	0.0	0.0	0.0	63.0	4.0	10.0	0.0	0.0	0.0	0.0	11.0	25.0	6.0	3.0	0.0	3.0	12.0	0.0	0.0	0.0
Si-23st	Original	49.9	0.0	3.2	14.5	0.0	0.0	0.0	0.0	67.6	2.0	7.7	0.0	0.0	0.0	0.0	3.2	12.9	8.2	5.0	1.8	4.5	19.5	0.0	0.0	0.0
	330	0.0	0.0	0.0	0.0	62.0	7.6	0.0	26.6	96.2	0.0	0.0	0.0	0.0	0.0	0.0	0.0	0.0	0.0	0.0	0.0	0.0	0.0	0.0	3.8	0.0
	360	0.0	0.0	0.0	0.0	28.1	1.6	0.0	64.1	93.8	0.0	0.0	0.0	0.0	0.0	0.0	0.0	0.0	0.0	0.0	0.0	0.0	0.0	0.0	6.3	0.0
Si-23c	Original	36.6	19.5	0.1	0.1	0.0	0.0	0.0	0.0	56.3	5.1	11.5	0.3	1.7	0.0	0.0	7.2	25.7	13.7	3.0	0.9	0.3	17.9	0.0	0.0	0.0
	330	0.0	0.0	0.0	0.0	36.7	48.3	1.0	0.0	86.0	5.7	1.8	0.0	0.6	3.4	0.0	1.4	13.0	0.0	0.0	0.0	0.0	0.0	0.0	1.0	0.0
	360	0.0	0.0	0.0	0.0	47.7	36.2	4.0	0.0	87.9	4.8	3.2	0.0	0.0	0.0	0.0	1.0	9.1	0.0	0.0	0.0	0.0	0.0	0.0	1.2	1.8
Si-23sb	Original	48.0	0.0	0.0	17.5	0.0	0.0	0.0	0.0	65.5	2.5	10.0	0.0	0.0	0.0	0.0	5.5	18.0	9.5	2.0	0.5	4.5	16.5	0.0	0.0	0.0
Pn-23c	Original	45.0	16.9	0.0	0.0	0.0	0.0	0.0	0.0	61.8	5.5	10.0	0.0	1.3	4.2	0.0	8.7	29.7	5.5	0.0	0.0	0.0	5.5	0.0	3.0	0.0
Pn-25c	Original	51.7	16.1	0.0	0.3	0.0	0.0	0.0	0.0	68.2	4.1	13.0	0.2	0.3	1.5	0.0	4.7	23.9	4.8	0.6	0.0	0.0	5.4	0.0	2.6	0.0
Ml-20c	Original	41.8	18.9	0.1	0.9	0.0	0.0	0.0	0.0	61.7	5.6	9.7	0.3	2.1	0.0	0.0	6.6	24.4	9.9	3.2	0.0	0.7	13.9	0.0	0.0	0.0
Ml-21st	Original	68.8	0.0	2.7	7.1	0.0	0.0	0.0	0.0	78.6	0.9	5.4	0.9	0.0	0.0	0.0	1.8	8.9	8.0	0.9	0.9	2.7	12.5	0.0	0.0	0.0
Ml-21c	Original	46.1	12.2	0.0	0.2	0.0	0.0	0.0	0.0	58.5	12.2	13.2	0.9	0.7	0.0	0.0	2.4	29.4	8.5	2.2	0.6	0.9	12.2	0.0	0.0	0.0
	330	0.0	0.0	0.0	0.0	53.4	6.7	19.0	0.0	79.0	3.4	0.8	0.0	0.2	0.0	0.0	0.8	5.2	0.0	0.0	0.0	0.0	0.0	0.0	0.2	15.5
	360	0.0	0.0	0.0	0.0	2.1	8.8	0.2	0.0	11.1	7.4	4.9	0.2	1.0	0.0	0.0	6.8	20.4	0.0	0.0	0.0	0.0	0.0	0.0	0.0	68.5
Ml-21sb	Original	78.7	0.0	0.0	10.6	0.0	0.0	0.0	0.0	89.4	2.1	6.4	0.0	0.0	0.0	0.0	2.1	10.6	0.0	0.0	0.0	0.0	0.0	0.0	0.0	0.0
	330	0.0	0.0	0.0	0.0	63.0	0.0	0.0	37.0	100.0	0.0	0.0	0.0	0.0	0.0	0.0	0.0	0.0	0.0	0.0	0.0	0.0	0.0	0.0	0.0	0.0
	360	0.0	0.0	0.0	0.0	51.1	15.6	0.0	33.3	100.0	0.0	0.0	0.0	0.0	0.0	0.0	0.0	0.0	0.0	0.0	0.0	0.0	0.0	0.0	0.0	0.0
Ml-22c	Original	21.4	21.7	0.1	0.1	0.0	0.0	0.0	0.0	43.3	2.7	27.7	0.0	1.9	2.7	0.0	9.4	44.4	7.6	4.4	0.0	0.1	12.1	0.2	0.0	0.0
Zo-21c	Original	34.2	24.0	0.0	0.0	0.0	0.0	0.0	0.0	58.2	0.4	21.7	0.6	1.8	4.0	0.0	10.2	38.7	3.0	0.1	0.0	0.0	3.1	0.0	0.0	0.0
Lublin Coal Basin																										
Bo-20c	Original	46.9	11.7	0.0	0.0	0.0	0.0	0.0	0.0	58.6	4.3	11.8	0.0	2.4	1.8	0.0	8.1	28.4	12.2	0.7	0.0	0.0	12.9	0.0	0.0	0.0
	330	0.0	0.0	0.0	0.0	56.0	24.4	4.8	0.0	85.3	9.5	2.4	0.0	0.0	0.8	0.0	2.0	14.7	0.0	0.0	0.0	0.0	0.0	0.0	0.0	0.0
	360	0.0	0.0	0.0	0.0	66.9	25.5	1.6	0.0	93.9	3.4	0.8	0.0	0.0	0.2	0.0	0.6	5.1	0.0	0.0	0.0	0.0	0.0	0.2	0.0	0.8
Bo-20sb	Original	54.9	0.0	0.0	11.5	0.0	0.0	0.0	0.0	66.4	0.8	13.9	0.0	0.0	0.0	0.0	8.2	23.0	7.4	0.8	0.8	1.6	10.7	0.0	0.0	0.0
	330	0.0	0.0	0.0	0.0	35.9	5.1	0.0	28.2	69.2	10.3	2.6	0.0	0.0	0.0	0.0	17.9	30.8	0.0	0.0	0.0	0.0	0.0	0.0	0.0	0.0
	360	0.0	0.0	0.0	0.0	35.6	8.9	0.0	55.6	100.0	0.0	0.0	0.0	0.0	0.0	0.0	0.0	0.0	0.0	0.0	0.0	0.0	0.0	0.0	0.0	0.0
Bo-21c	Original	47.1	9.6	0.0	0.0	0.0	0.0	0.0	0.0	56.7	1.9	9.6	0.0	1.3	0.0	0.0	7.8	20.7	19.5	2.1	1.0	0.0	22.6	0.0	0.0	0.0

ΣV - sum of vitrinite macerals; ΣI - sum of inertinite macerals; ΣL - sum of liptinite macerals; Ct - collotelinite; Cd - collodetrinite; Te - telinite; Vd - vitrodetrinite; PaV - paler vitrinite; VPo - vitrinite with pores; VCr - vitrinite with cracks; SRV - strongly reacted vitrinite; Fu - fusinite; Sf - semifusinite; Ma - macrinite; Mi - micrinite; Fg - funginite; Sec - secretinite; Id - inertodetrinite; Sp - sporinite; Cu - cutinite; Re - resinite; Ld - liptodetrinite; Ch - natural char; Bit - bitumen; Sem - semicoke; c - channel coal sample; st - block shale sample collected above coal seam; sb - block shale sample collected below coal seam.

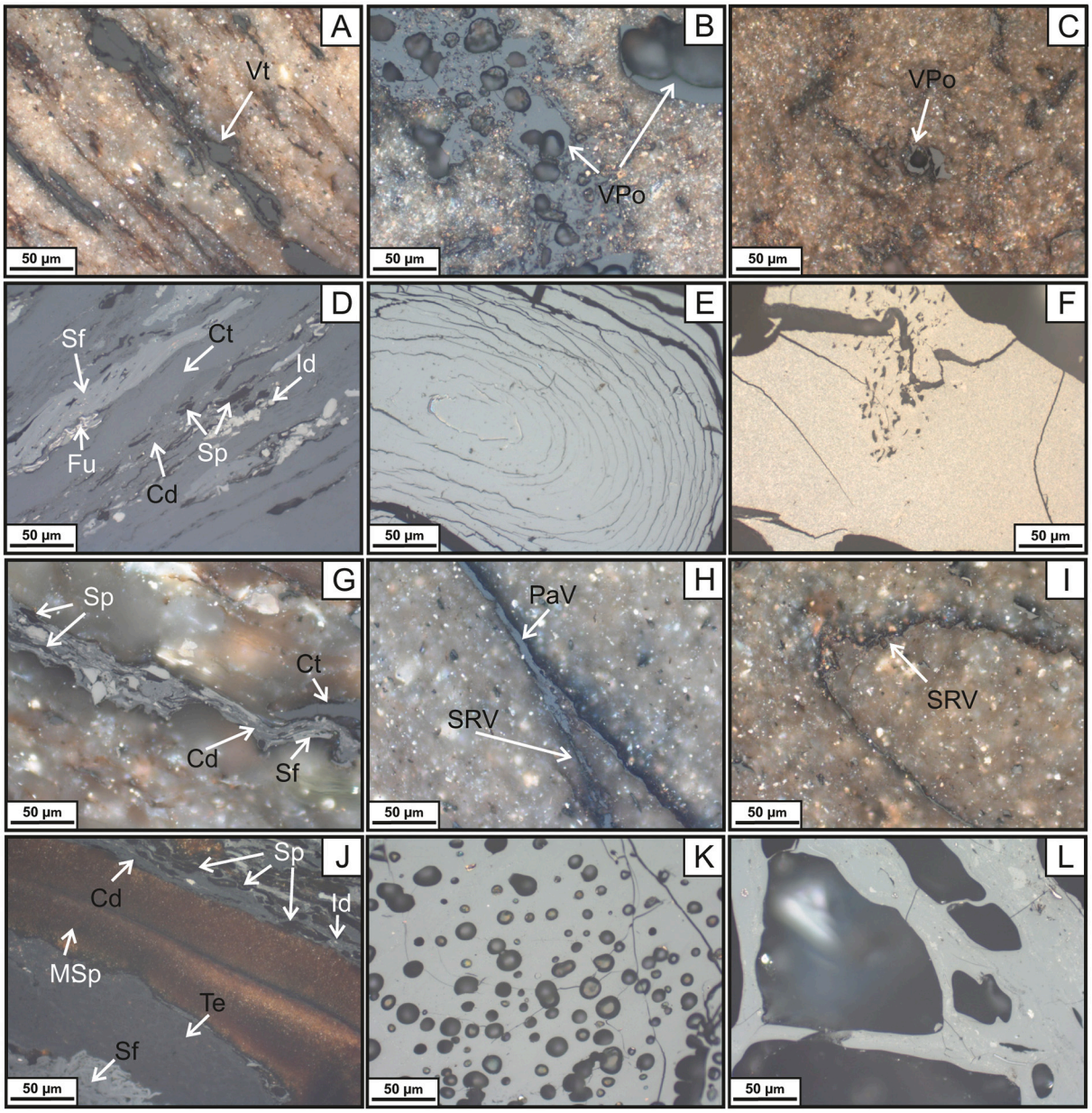

Fig. 6. Photomicrographs of macerals, reflected white light, oil immersion. (A) vitrinite (Vt) dispersed in original shale sample Si-23st; (B) and (C) vitrinite with devolatisation pores (VPo) in shale sample Si-23st after HP at 330 and 360 °C, respectively; (D) collotelinite (Ct), collodetrinite (Cd), semifusinite (Sf), fusinite (Fu), inertodetrinite (Id), sporinite (Sp) in original coal sample Br-20c; (E) paler vitrinite with round cracks in sample Br-20c after HP at 330 °C; (F) semicoke in sample Br-20c after HP at 360 °C; (G) collotelinite (Ct), collodetrinite (Cd), semifusinite (Sf), sporinite (Sp) dispersed in original shale sample Br-20st; (H) paler vitrinite (PaV) and strongly reacted vitrinite (SRV) in shale sample Br-20st after HP at 330 °C; (I) strongly reacted vitrinite (SRV) in shale sample Br-20st after HP at 360 °C; (J) telinite (Te), collodetrinite (Cd), inertodetrinite (Id), sporinite (Sp) mega-sporinite (MSp) in original coal sample Si-23c; (K) and (L) vitrinite with devolatisation pores (VPo) in coal sample Si-23c after HP at 330 and 360 °C, respectively.

original conditions to HP 330 °C and decrease at HP 360 °C (Table 6). A decreasing trend in DBT with temperature is only seen in LCB samples.

The aromatic compounds detected are those commonly used for thermal maturity estimation (Table 6). The temperature-increasing trend from original conditions to HP 360 °C is well recorded by MPI 1 and the triaromatic steroid ratio for all samples except MPI 1 in the LCB. MPR and MDR used for calculating the equivalent of vitrinite reflectance ($R_{cal\ (MDR)}$) show discrepancies and are irrelevant. Similarly, ββ/(αα + ββ) C_{29} sterane values show an increasing trend with temperature in almost all samples but 20S/(20 S + 20 R) C_{29} values are inconclusive except for samples from the LCB where they also increase with temperature (Table 5).

6. Discussion

In this section we discuss questions of the origin and depositional environment of OM in coals and carbonaceous shales from the Serpukhovian and Pennsylvanian coal-bearing strata of the USCB and LCB and their transformation during increasing maturity as simulated by the HP experiments.

6.1. Origin and depositional environment of bituminous coals and carbonaceous shales

Carbon isotope signatures ($\delta^{13}C_{VPDB}$) of the C_{15+} saturated- and aromatic hydrocarbon fractions and canonical variable (Sofer, 1984) are

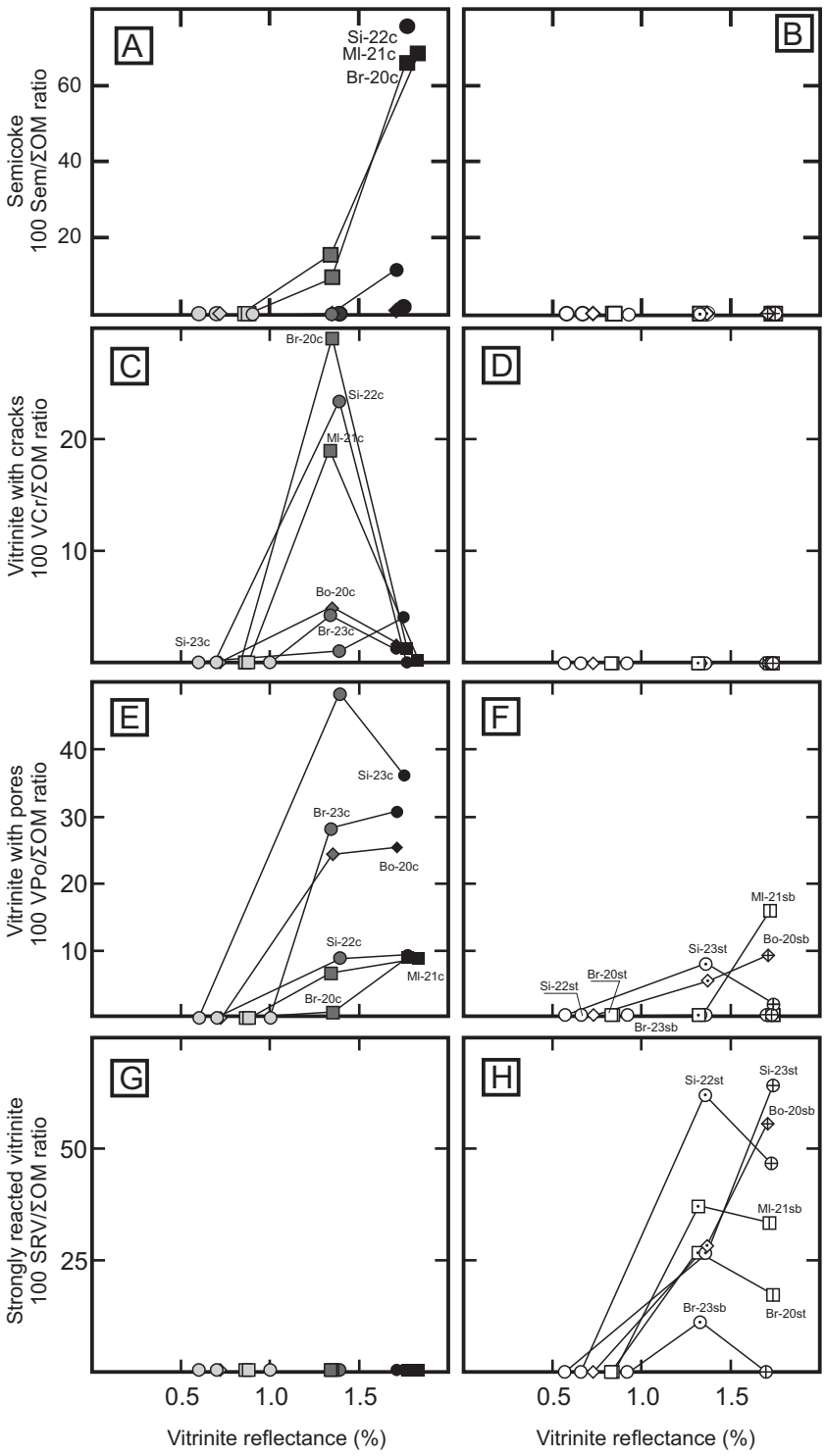

Fig. 7. (A and B) Semicoke 100 Sem/ΣOM ratio, (C and D) vitrinite with cracks 100 VCr/ΣOM ratio, (E and F) vitrinite with pores 100 VPo/ΣOM ratio, and (G and H) strongly reacted vitrinite 100 SRV/ΣOM ratio versus vitrinite reflectance of (A, C, E and G) coals and (B, D, F and H) carbonaceous shales of original samples and after HP at 330 °C and 360 °C for 72 h. ΣOM – sum of components of OM = ΣV + ΣI + ΣL + Ch + Bit + Sem; ΣV – vitrinite maceral group; ΣI – inertinite maceral group; ΣL – liptinite maceral group; Ch – natural char; Bit – bitumen; VPO – vitrinite with pores; Sem – semicoke; VCr – vitrinite with cracks; SRV – strongly reacted vitrinite; PaV – paler vitrinite.

frequently used to decipher the origin of crude oils and hence their OM marine- or terrestrial source environments. Here, shale-sample values that vary between −32.7 and −26.7‰, and between −29.8 and −24.6‰, respectively, and coal-sample values that vary between −29.3 and −28.3‰, and between −26.1 and −25.3‰, respectively, are indicative of OM from a chiefly terrigenous source (Figs. 5, 9 and 10). δ^{13}C values of original kerogen of both USCB and LCB varies from −25.1 to −23.5‰ for coals and from −24.9 to −22.8‰ for shales and no diversity for coals and shales after HP experiments (Table 2, Fig. 5). These values are very similar for original coals of these basins from Kotarba and Clayton (2003). δ^{13}C values of C3 and C4 plants vary from −35 to −23‰ (median of about −27‰) and from −23 to −6‰ (median of about −14‰), respectively (Schidlowski, 1988; Marshall et al., 2007; Kohn, 2010) therefore kerogen of our coals and shales can have originated from C3 plants.

The maceral distribution in the original coal and shale samples from the USCB and LCB shows a predominance of the vitrinite macerals with subordinate liptinite group and inertinite maceral groups. Nevertheless, the richness in vitrinite macerals is typical of humic coals occurring in the northern hemisphere (Bertrand et al., 1986), including Poland

Table 5
Selected indices calculated based on GC–MS (saturated hydrocarbon fraction) analyses of samples of original coals and carbonaceous shales and samples after hydrous pyrolysis at 330 and 360 °C for 72 h.

Sample code	HP temp. (°C)	$CPI_{(Total)}$	$CPI_{(17-23)}$	$CPI_{(25-31)}$	Pr/Ph	Pr/n-C_{17}	Ph/n-C_{18}	S/T	Tri/Pen	Hopane/Sterane	$C_{27}C_{28}C_{29}$ Sum = 100%	C_{27}Dia/(Dia + Reg)	$C_{29}\beta\beta$/($\beta\beta + \alpha\alpha$)	C_{29}S/(S+R)	C_{22}t/C_{21}t	C_{24}t/C_{23}t	C_{26}t/C_{24}t	C_{29}H/Hop	C_{29}Ts/(C_{29}Ts + C_{29}H)	H_{31}R/C_{30}H	GI	C_{35}S/C_{34}S	Ts/(Ts + Tm)	H_{31}S/(S + R)
Upper Silesian Coal Basin																								
Br-20c	Original	1.05	1.01	1.14	6.00	5.90	0.67	0.04	0.05	27.8	10 39 51	0.21	0.36	0.59	1.01	0.97	0.97	0.90	0.09	0.38	12.0	0.08	0.02	0.57
	330	0.99	0.98	1.01	1.53	0.27	0.17	0.04	0.14	36.0	16 42 42	0.37	0.37	0.62	0.38	1.57	0.60	0.91	0.06	0.27	7.8	0.25	0.07	0.56
	360	1.00	0.98	1.03	2.09	0.15	0.05	n.a.	n.a.	6.5	34 33 33	0.48	0.50	0.42	n.a.	n.a.	0.71	1.05	0.10	0.33	16.1	0.81	0.19	0.54
Br-20st	Original	1.12	1.08	1.24	3.85	2.59	0.68	0.23	0.05	5.0	21 14 65	0.15	0.36	0.51	0.25	0.99	1.51	1.14	0.15	0.38	13.0	0.15	0.02	0.57
	330	1.01	0.92	1.16	1.90	0.46	0.19	0.14	0.11	8.2	15 23 62	0.30	0.28	0.48	0.09	1.02	1.06	1.07	0.11	0.32	11.6	0.32	0.03	0.55
	360	1.02	0.95	1.12	0.85	0.33	0.16	0.25	0.12	7.7	31 31 38	0.45	0.47	0.58	0.35	0.67	0.89	1.16	0.16	0.34	9.8	0.66	0.17	0.56
Br-23c	Original	1.01	1.01	1.03	4.79	3.75	0.48	0.06	0.05	21.0	11 37 52	0.26	0.36	0.54	0.11	1.75	1.41	0.70	0.12	0.38	21.0	0.10	0.03	0.57
	330	1.01	1.00	1.03	1.62	0.38	0.20	0.08	0.10	37.3	12 41 48	0.36	0.42	0.50	0.40	0.93	0.90	0.74	0.03	0.25	15.2	0.23	0.04	0.56
	360	0.99	0.99	1.01	0.78	0.25	0.06	n.a.	n.a.	4.9	34 35 31	0.55	0.53	0.53	n.a.	n.a.	0.84	1.14	0.15	0.25	10.9	0.52	0.15	0.56
Br-23sb	Original	0.99	0.89	1.24	3.12	1.35	0.19	0.06	0.10	24.9	27 33 40	0.33	0.34	0.58	0.20	1.30	1.80	0.69	0.14	0.28	9.0	0.14	0.03	0.57
	330	1.10	0.94	1.31	1.33	0.36	0.19	n.a.	n.a.	22.7	27 33 40	0.36	0.46	0.51	n.a.	n.a.	0.74	0.77	0.08	0.27	8.4	0.23	0.07	0.54
	360	1.14	1.09	1.25	2.14	0.52	0.19	0.18	0.07	9.3	37 28 35	0.43	0.54	0.61	0.50	1.03	0.94	0.90	0.20	0.31	10.7	0.61	0.15	0.56
Ml-21c	Original	1.17	1.21	1.15	4.44	1.74	0.58	0.10	0.06	10.1	20 28 52	0.10	0.31	0.48	0.34	0.58	1.11	0.82	0.08	0.45	19.0	0.07	0.03	0.58
	330	1.01	1.00	1.05	1.29	0.27	0.19	0.09	0.13	15.8	15 37 48	0.34	0.38	0.60	0.57	1.39	1.24	0.74	0.17	0.32	12.7	0.27	0.08	0.55
	360	1.00	0.99	1.04	2.07	0.21	0.08	n.a.	n.a.	9.1	28 29 43	0.50	0.54	0.56	n.a.	n.a.	0.86	1.21	0.10	0.30	9.9	0.62	0.18	0.57
Ml-21sb	Original	1.04	0.92	1.29	5.46	1.60	0.22	0.14	0.08	10.4	17 38 45	0.22	0.35	0.53	0.28	0.79	1.39	0.64	0.23	0.40	17.0	0.20	0.04	0.57
	330	1.06	0.89	1.31	1.80	0.63	0.23	0.15	0.13	14.7	29 27 44	0.34	0.42	0.50	0.16	0.67	0.88	0.87	0.06	0.39	18.8	0.29	0.10	0.54
	360	1.17	1.11	1.27	1.17	0.62	0.28	0.09	0.15	11.7	29 32 39	0.42	0.45	0.51	0.35	0.69	0.88	1.04	0.17	0.35	11.5	0.70	0.12	0.57
Si-22c	Original	1.61	1.43	1.95	7.10	5.17	1.24	n.a.	n.a.	7.0	4 40 56	0.25	0.24	0.33	n.a.	n.a.	2.16	0.99	0.09	0.47	28.0	l.i.	0.02	0.55
	330	1.08	1.11	1.07	1.87	1.61	0.40	0.04	0.11	50.1	11 30 59	0.36	0.33	0.53	0.61	1.10	1.11	1.13	0.10	0.29	14.8	0.37	0.05	0.54
	360	1.05	1.04	1.07	3.23	0.57	0.13	n.a.	n.a.	8.6	30 34 36	0.46	0.50	0.51	n.a.	n.a.	0.71	0.92	0.11	0.38	9.9	0.66	0.19	0.58
Si-22st	Original	1.23	1.06	1.32	1.85	1.48	0.40	0.09	0.05	16.7	18 32 50	0.27	0.29	0.37	0.71	1.28	2.22	0.61	0.10	0.27	4.0	0.12	0.06	0.54
	330	1.03	0.99	1.08	1.33	0.36	0.17	0.06	0.06	26.8	29 22 50	0.28	0.33	0.42	0.31	0.93	1.20	1.12	0.06	0.31	13.7	0.30	0.04	0.51
	360	1.05	1.02	1.11	1.10	0.43	0.11	0.08	0.04	22.9	29 30 41	0.33	0.41	0.45	0.45	1.15	0.94	1.04	0.14	0.30	13.8	0.58	0.07	0.52
Si-23c	Original	1.35	1.25	1.57	7.66	4.83	0.76	0.08	0.04	10.4	6 38 56	0.24	0.30	0.29	0.88	1.28	1.82	0.69	0.02	0.48	30.0	l.i.	0.01	0.55
	330	1.04	1.01	1.10	2.48	0.95	0.24	0.04	0.10	37.7	2 41 57	0.43	0.35	0.47	n.a.	n.a.	0.94	0.96	0.03	0.28	15.1	0.30	0.04	0.54
	360	1.03	1.01	1.08	2.34	0.43	0.14	n.a.	n.a.	7.0	34 40 25	0.64	0.56	0.48	n.a.	n.a.	0.17	1.42	0.10	0.28	12.8	0.81	0.17	0.56
Si-23st	Original	1.27	1.14	1.50	3.64	13.37	1.03	0.27	0.05	1.9	5 21 74	0.24	0.21	0.21	0.83	1.77	2.48	0.63	0.08	0.41	24.0	0.10	0.01	0.51
	330	1.06	1.00	1.15	1.69	0.95	0.33	0.14	0.07	4.0	8 18 75	0.28	0.21	0.29	0.27	1.04	1.07	1.08	0.03	0.38	26.1	0.32	0.03	0.50
	360	1.05	1.02	1.11	1.34	0.31	0.15	n.a.	n.a.	12.2	19 33 48	0.39	0.35	0.44	n.a.	n.a.	0.42	1.31	0.07	0.33	18.9	0.55	0.03	0.53
Lublin Coal Basin																								
Bo-20c	Original	1.24	1.24	1.28	6.87	7.66	1.44	0.07	0.05	11.6	6 37 57	0.29	0.22	0.44	n.a.	n.a.	1.22	0.93	0.08	0.49	24.0	0.07	0.01	0.57
	330	1.04	1.01	1.07	3.03	1.34	0.34	0.03	0.08	48.9	2 34 64	0.43	0.32	0.60	0.70	0.73	0.97	0.82	0.11	0.25	9.8	0.23	0.03	0.55
	360	1.02	1.01	1.04	2.76	0.54	0.15	n.a.	n.a.	6.4	31 44 25	0.48	0.53	0.63	n.a.	n.a.	0.08	1.25	0.08	0.23	11.7	0.57	0.10	0.57
Bo-20sb	Original	1.19	1.01	1.52	3.20	2.37	0.55	0.09	0.07	9.5	10 38 52	0.26	0.27	0.41	n.a.	n.a.	1.83	0.99	0.06	0.39	20.0	0.05	0.02	0.57
	330	1.02	0.95	1.06	1.67	0.64	0.25	0.09	0.11	17.0	20 26 54	0.34	0.34	0.42	n.a.	n.a.	1.08	1.17	0.07	0.30	12.7	0.41	0.04	0.51
	360	1.05	1.01	1.14	1.33	0.25	0.11	n.a.	n.a.	16.0	35 30 35	0.43	0.54	0.60	n.a.	n.a.	0.90	1.36	0.15	0.29	12.8	0.57	0.11	0.55

HP temp. - hydrous pyrolysis temperature; $CPI_{(Total)} = [(C_{17} + C_{19} + \ldots + C_{27} + C_{29}) + (C_{19} + C_{21} + \ldots + C_{29} + C_{31})]/[2*(C_{18} + C_{20} + \ldots + C_{28} + C_{30})]$; $CPI_{(17-23)} = [(C_{17} + C_{19} + C_{21}) + (C_{19} + C_{21} + C_{23})]/[2*(C_{18} + C_{20} + C_{22})]$; $CPI_{(25-31)} = [(C_{25} + C_{27} + C_{29}) + (C_{27} + C_{29} + C_{31})]/[2*(C_{26} + C_{28} + C_{30})]$; Pr/Ph = pristane/phytane; Pr/n-C_{17} = pristane/heptadecane; Ph/n-C_{18} = phytane/octadecane; S/T = steranes/terpanes; steranes - all regular steranes and diasteranes identified at $m/z = 217$; terpanes - all tri-, tetra- and pentacyclic terpanes identified at $m/z = 191$; Tri/Pen = tricyclic/pentacyclic terpanes; tricyclic terpanes - all C_{19}-C_{30} tricyclic terpanes; pentacyclic terpanes - all C_{28} - C_{35} pentacyclic terpanes; Hopane/sterane: calculated using highest peak from hopanes (ion 191) and steranes (ion 217) after Isaksen (1991). $C_{27} = C_{27}\alpha\alpha\alpha$20R sterane/($C_{27} + C_{28} + C_{29}$)ααα20R steranes*100; $C_{28} = C_{28}\alpha\alpha\alpha$20R sterane/($C_{27} + C_{28} + C_{29}$)ααα20R steranes*100; $C_{29} = C_{29}\alpha\alpha\alpha$20R sterane/($C_{27} + C_{28} + C_{29}$)ααα20R steranes*100; C_{27} Dia/(Dia + Reg) = C_{27} βα 20(S + R) diasteranes/(C_{27} βα 20(S + R) diasteranes+ΣC_{27} regular steranes); $C_{29}\beta\beta/(\beta\beta + \alpha\alpha)$ = ββ-epimers and sum ββ- and αα-epimers of C_{29} regular steranes ratio; C_{29}S/(S + R) = 20S/(20S + 20R) of C_{29} regular steranes ratio; t - tricyclic terpane; C_{29}H/Hop = C_{29} norhopane/17α hopane; C_{29}Ts/(C_{29}Ts + C_{29}H) = C_{29} Ts 18α(H)-norneohopane/(C_{29} Ts 18α(H)-norneohopane+C_{29} Tm 17α(H)21β(H)-norhopane); HC_{31}R/Hop = C_{31}R homohopane/17α hopane; GI = gammacerane/17α hopane*100; C_{35}S/C_{34}S = C_{35}(22S) homohopane/C_{34}(22S) homohopane; Ts/(Ts + Tm) = C_{27} 18α trisnorhopane/(C_{27} 18α trisnorhopane+C_{27} 17α trisnorhopane); H_{31}S/(S + R) = C_{31} homohopanes 22S/(22S + 22R) ratio; l.i. - low intensity; c - channel coal sample; st - block shale sample collected above coal seam; sb - block shale sample collected below coal seam; n.a. - not analysed.

Table 6
Indices calculated based on GC–MS (aromatic hydrocarbon fraction) analyses of original samples of coals and shales and samples after hydrous pyrolysis at 330 and 360 °C for 72 h.

Sample code	HP temp. (°C)	MPR	MPI1	R_{cal} (MPI1) (%)	MDR	R_{cal} (MDR) (%)	DBT/ Phen	TA(I)/ TA (I + II)	TA C_{20}/ ($C_{20} + C_{27}$)	TA C_{21}/ ($C_{21} + C_{28}$)	TA C_{28}/ C_{26} 20S	TA C_{28}/ C_{27} 20R	%TA C_{26}	%TA C_{27}	%TA C_{28}	%TA C_{29}	DBT (%)	DBF (%)	F (%)
Upper Silesian Coal Basin																			
Br-20c	Original	0.93	0.62	0.77	1.07	0.59	0.03	0.23	0.28	0.22	9.40	0.92	3.1	43.4	49.0	4.4	33.7	10.3	55.9
	330	0.65	0.75	0.85	1.33	0.61	0.02	1.00	1.00	1.00	l.i.	l.i.	l.i.	l.i.	l.i.	l.i.	29.8	2.1	68.0
	360	1.87	1.11	1.06	1.43	0.61	0.06	1.00	1.00	1.00	l.i.	l.i.	l.i.	l.i.	l.i.	l.i.	15.6	37.3	47.1
Br-20st	Original	1.13	0.92	0.95	0.68	0.56	0.03	0.08	0.15	0.05	20.28	2.27	2.0	25.4	70.6	2.0	77.1	3.1	19.8
	330	0.73	0.97	0.98	0.21	0.53	0.01	0.55	0.77	0.45	29.37	3.42	1.3	18.8	72.5	7.5	14.5	6.8	78.7
	360	1.23	1.12	1.07	0.71	0.56	0.05	1.00	1.00	1.00	l.i.	l.i.	l.i.	l.i.	l.i.	l.i.	96.7	0.2	3.1
Br-23c	Original	1.03	0.73	0.84	1.23	0.60	0.02	0.29	0.33	0.29	11.04	0.84	2.7	44.4	48.0	4.9	29.4	4.7	65.9
	330	0.75	0.74	0.84	0.84	0.57	0.02	0.82	0.87	0.83	8.17	1.16	4.0	37.0	44.3	14.7	23.3	2.2	74.5
	360	1.70	0.89	0.93	1.48	0.62	0.03	1.00	1.00	1.00	l.i.	l.i.	l.i.	l.i.	l.i.	l.i.	7.7	24.4	67.9
Br-23sb	Original	1.16	0.60	0.76	1.93	0.65	0.07	0.44	0.52	0.40	5.31	1.14	5.7	42.1	47.6	4.6	88.6	1.0	10.4
	330	0.98	0.96	0.98	0.90	0.58	0.01	1.00	1.00	1.00	l.i.	l.i.	l.i.	l.i.	l.i.	l.i.	17.0	3.4	79.6
	360	1.70	0.89	0.93	1.48	0.62	0.03	1.00	1.00	1.00	l.i.	l.i.	l.i.	l.i.	l.i.	l.i.	100.0	l.i.	l.i.
Ml-21c	Original	0.83	0.57	0.74	0.70	0.56	0.01	0.09	0.06	0.19	13.05	0.23	0.9	75.3	20.7	3.1	27.4	4.9	67.7
	330	0.80	0.77	0.86	1.18	0.60	0.03	0.45	0.39	0.73	5.65	0.08	1.3	86.4	10.2	2.2	30.7	18.6	50.7
	360	2.24	0.98	0.99	1.45	0.62	0.03	1.00	1.00	1.00	l.i.	l.i.	l.i.	l.i.	l.i.	l.i.	9.3	40.9	49.8
Ml-21sb	Original	0.90	0.69	0.81	1.21	0.60	0.02	0.37	0.41	0.36	8.19	0.95	3.7	45.4	48.7	2.2	58.7	13.3	28.0
	330	0.61	0.73	0.84	0.59	0.55	0.01	0.70	0.70	0.72	7.59	1.16	3.4	46.4	47.2	3.0	31.5	19.3	49.2
	360	1.03	1.04	1.02	0.77	0.57	0.03	1.00	1.00	1.00	l.i.	l.i.	l.i.	l.i.	l.i.	l.i.	97.3	0.8	2.0
Si-22c	Original	0.61	0.60	0.76	0.29	0.53	0.04	0.09	0.12	0.07	7.99	1.43	3.5	37.6	55.9	3.0	60.2	5.2	34.6
	330	0.44	0.63	0.78	0.59	0.55	0.07	0.81	0.90	0.65	4.40	1.31	7.0	37.0	49.8	6.3	72.3	6.0	21.7
	360	2.01	0.89	0.93	0.67	0.56	0.09	1.00	1.00	1.00	l.i.	l.i.	l.i.	l.i.	l.i.	l.i.	27.5	22.6	50.0
Si-22st	Original	0.79	0.54	0.72	0.78	0.57	0.04	0.05	0.08	0.03	4.50	1.89	6.8	33.7	57.5	2.0	70.8	6.0	23.2
	330	0.47	0.56	0.74	0.50	0.55	0.01	0.51	0.67	0.44	4.12	2.15	7.0	27.4	61.6	4.0	9.5	1.7	88.7
	360	0.87	0.92	0.95	0.54	0.55	0.04	1.00	1.00	1.00	l.i.	l.i.	l.i.	l.i.	l.i.	l.i.	96.9	1.6	1.4
Si-23c	Original	0.55	0.48	0.69	0.41	0.54	0.03	0.07	0.12	0.05	7.28	1.52	4.1	35.4	56.5	4.0	44.2	6.5	49.2
	330	0.48	0.64	0.78	0.48	0.54	0.04	0.72	0.83	0.63	5.53	1.36	5.9	35.2	54.0	4.8	69.5	3.5	26.9
	360	1.48	0.69	0.81	0.67	0.56	0.05	1.00	1.00	1.00	l.i.	l.i.	l.i.	l.i.	l.i.	l.i.	13.3	24.0	62.7
Si-23st	Original	0.91	0.62	0.77	0.65	0.56	0.02	0.07	0.14	0.03	8.65	1.76	3.8	32.0	59.4	4.8	76.5	3.7	19.8
	330	0.37	0.55	0.73	0.53	0.55	0.01	0.44	0.58	0.38	7.25	2.48	4.3	28.2	62.7	4.8	22.1	37.3	40.7
	360	1.42	0.65	0.79	0.39	0.54	0.04	1.00	1.00	1.00	l.i.	l.i.	l.i.	l.i.	l.i.	l.i.	12.1	5.7	82.1
Lublin Coal Basin																			
Bo-20c	Original	0.64	0.74	0.84	0.31	0.53	0.10	0.09	0.12	0.07	7.36	1.38	4.1	37.2	54.9	3.8	72.3	6.4	21.3
	330	0.42	0.65	0.79	0.53	0.55	0.03	0.71	0.85	0.54	11.36	0.93	28.0	32.4	51.0	13.9	32.0	3.9	64.1
	360	1.29	1.17	1.10	1.58	0.63	0.02	1.00	1.00	1.00	l.i.	l.i.	l.i.	l.i.	l.i.	l.i.	14.9	9.1	76.0
Bo-20sb	Original	0.90	0.70	0.82	0.63	0.56	0.04	0.12	0.17	0.09	9.25	1.55	3.4	37.6	56.9	2.0	62.6	7.6	29.8
	330	0.43	0.73	0.84	0.42	0.54	0.01	0.78	0.91	0.53	18.54	2.31	1.4	28.6	60.2	9.8	25.8	9.6	64.6
	360	1.39	0.69	0.82	0.76	0.57	0.08	1.00	1.00	1.00	l.i.	l.i.	l.i.	l.i.	l.i.	l.i.	18.3	11.7	70.0

HP temp. - hydrous pyrolysis temperature; MPR = (2MP)/(1MP) (Radke et al., 1982); MP - methylphenanthrene; MPI1 = 1.5(2MP + 3MP)/(Phen+1MP + 9MP) (Radke et al., 1982); $R_{cal(MPI1)} = 0.6(MPI1) + 0.4$ (for MPR < 2.65) (Radke and Welte, 1983); MDR = 4-MDBT/1-MDBT (Radke et al., 1986); MDBT - methyldibenzothiophene; $R_{cal(MDR)} = 0.073MDR + 0.51$ (Radke, 1988); DBT - dibenzothiophene; Phen - phenanthrene; TA (I) = ($C_{20} + C_{21}$) triaromatic steroids, TA(II) = ($C_{26} + C_{27} + C_{28}$) triaromatic steroids (Beach et al., 1989); % DBF, DBT, F: 100% normalized from peak areas of corresponding ions i.e. DBF - dibenzofuran (*m/z* 168), DBT - dibenzothiophene (*m/z* 184) and F - fluorene (m/z 166) (Asif and Wenger, 2019); l.i. - low intensity; c - channel coal sample; st - block shale sample collected above coal seam; sb - block shale sample collected below coal seam.

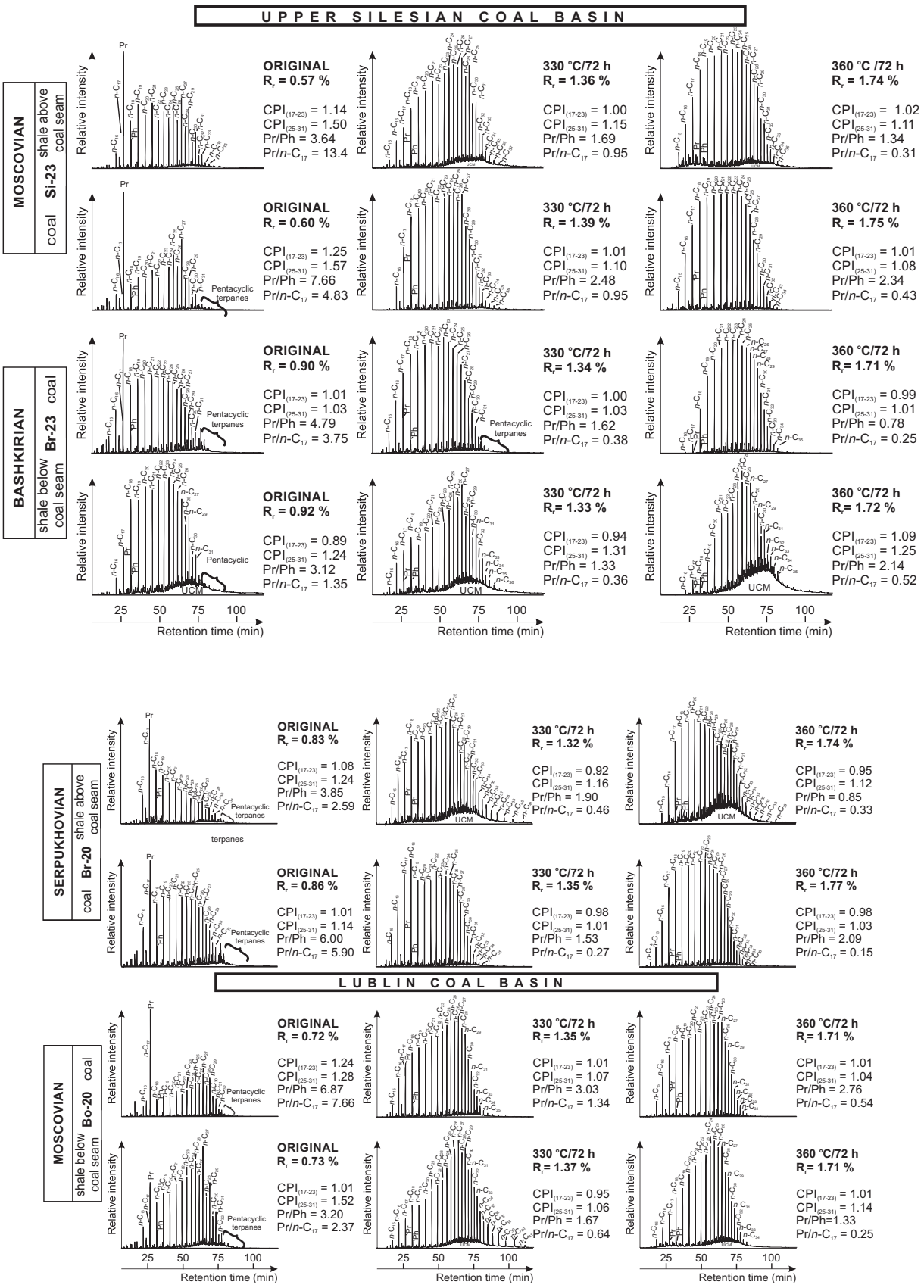

Fig. 8. Examples of *n*-alkane and isoprenoid distributions representing original coals and carbonaceous shales from the USCB (samples Si-23, Br-23 and Br-20) and LCB (sample Bo-20) and after HP at 330 °C and 360 °C for 72 h.

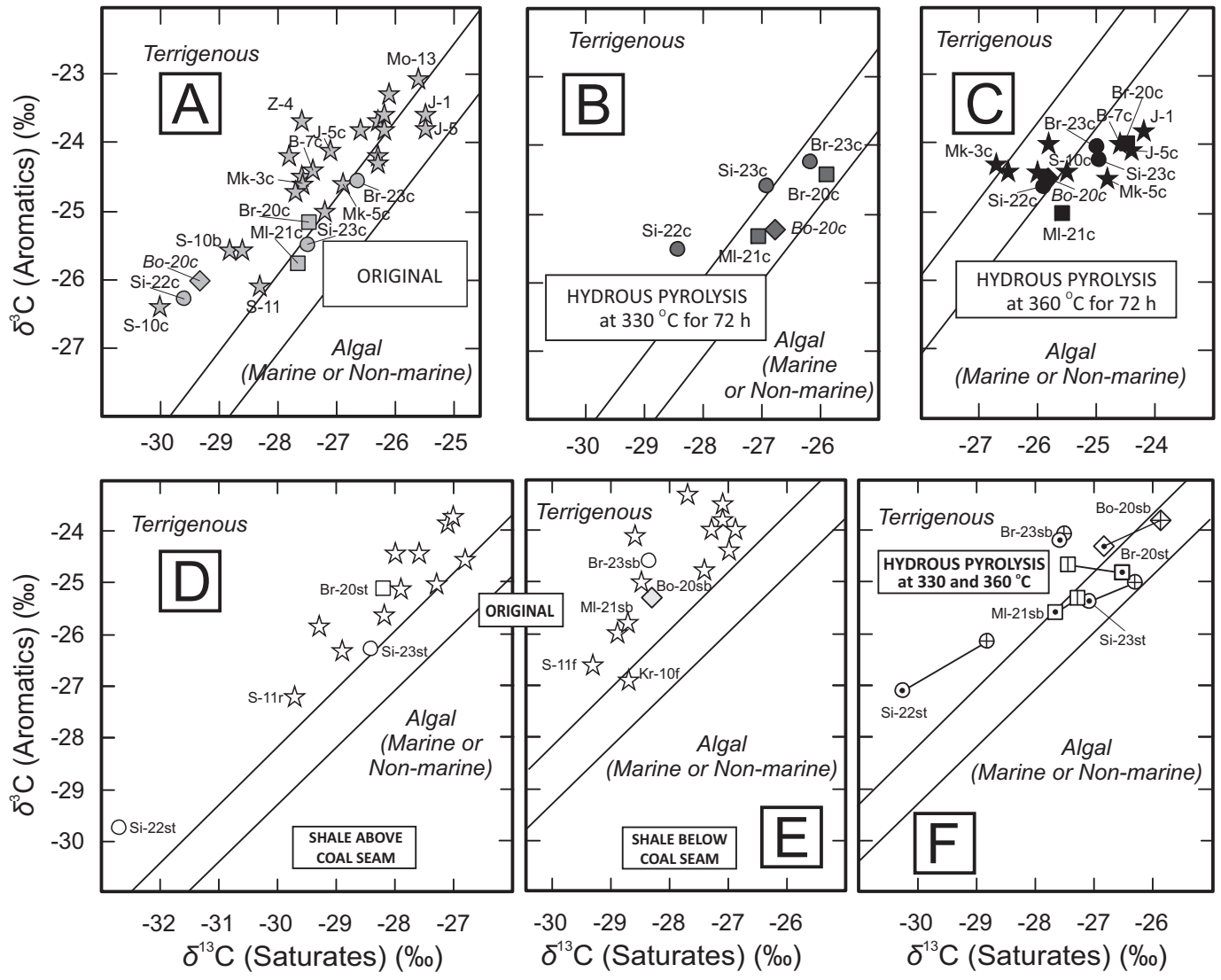

Fig. 9. Stable carbon isotope composition of aromatic hydrocarbons versus saturated hydrocarbons of original (A) coal samples and after hydrous pyrolysis at (B) 330 °C and (C) 360 °C for 72 h, and original carbonaceous shale samples collected (D) above and (E) below coal seams, and (F) carbonaceous shale samples after HP at 330 °C and 360 °C for 72 h. Genetic fields after Sofer (1984). Isotopic data from Table 2 and previously published data from Kotarba and Clayton (2003).

(Kotarba and Clayton, 2003) originally deposited in a paralic-terrestrial environment (Buła and Kotas, 1994; Jurczak-Drabek, 1996).

In the concept of organofacies proposed by Pepper and Corvi (1995) and Petersen (2017) OM in the analysed samples is represented by organofacies of type D/E or F. The type D/E is characteristic of terrigenous non-marine kerogen type III with dominant macerals: vitrinite, sporinite, cutinite, resinite, and minor alginite which is observed in most analysed shales. Type F is associated with humic coal kerogen type III, rarely IV, containing mainly maceral vitrinite, inertinite and liptinite less than 12 vol%. This organofacies type is characteristic of the analysed coals.

Both coals and shales have CPI values >1 (Table 5; Fig. 8), consistent with the terrestrial origin of precursor OM. In shales, the tendency for higher values of $CPI_{(25–31)}$ than $CPI_{(17–23)}$ (Table 5; Fig. 8) is probably related to the presence of waxes derived from the coats of vascular plants. Waxes in the sedimentary environment which contain HMW *n*-alkanes in the range C_{23}-C_{33} with a predominance of odd *n*-alkanes (McSween et al., 2003) may be the cause of the high $CPI_{(25–31)}$ values. LMW *n*-alkanes, a product of the degradation of HMW *n*-alkanes, have lower $CPI_{(17–23)}$ values. Similarly, values of the tricyclic terpane ratios ($C_{22}t/C_{21}t$ and $C_{24}t/C_{23}t$) also suggest coal/resin rich OM and/or a lacustrine environment (Peters et al., 2005). Likewise, values (>1.1 in general) of the original coals and carbonaceous shales calculated for the $C_{26}t/C_{25}t$ versus $H_{31}R/C_{30}H$ plot (Fig. 11) also suggest lacustrine setting of OM accumulation (Peters et al., 2005).

In all coals and shales, typically high (>2.0) Pr/Ph values (Table 5) and the Pr/*n*-C_{17} and Ph/*n*-C_{18} values (Table 5) suggest terrigenous OM input deposited under oxic conditions (Shanmugam, 1985; Peters et al., 2005). These biomarker data are similar to those reported by Kotarba and Clayton (2003). Pr/Ph in coal samples is higher than that in shales and is typical of a non-marine or deltaic environment (Powell and McKirdy, 1973; Hughes et al., 1995). Based on the classification of Hughes et al. (1995), the correlation of DBT/Phen and Pr/Ph for shales (Tables 5 and 6; Fig. 12A) indicates that coal and shale in both basins were deposited in a lacustrine- and fluvio-deltaic environment. Locally, lacustrine sulphate-poor clastic sediments (sample Si-22st) may have been deposited in the USCB; low Pr/Ph values such as in the Si-22st shale have also been reported from non-marine Permian-Jurassic sediments of northern Perth, Australia and from the Galilee Basin, Queensland (Permian) containing immature OM derived from higher plants (Powell and McKirdy, 1973).

Even though the DBT/Phen versus Pr/Ph plot (Fig. 12A) suggests a

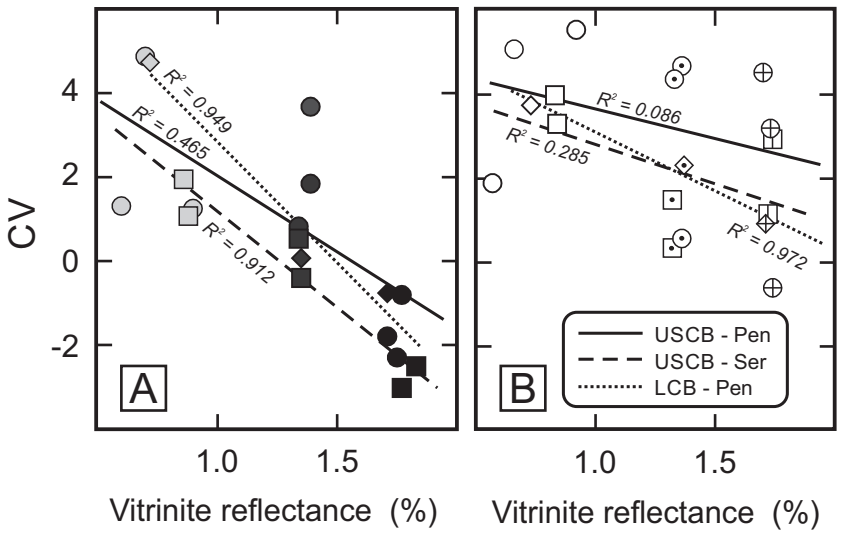

Fig. 10. Canonical variable (CV) versus vitrinite reflectance of (A) coals and (B) carbonaceous shales of original samples and after HP at 330 °C and 360 °C for 72 h. Calculation of CV after Sofer (1984). USCB – Upper Silesian Coal Basin, LCB – Lublin Coal Basin, Pen – Pennsylvanian, Ser – Serpukhovian.

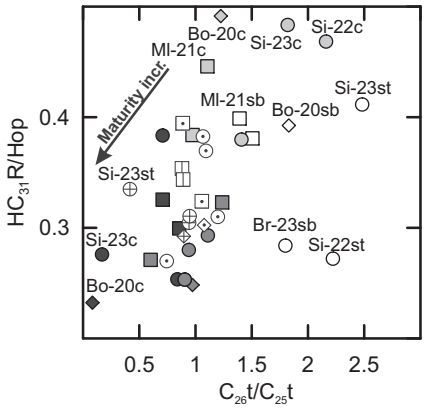

Fig. 11. $C_{26}t/C_{25}t$ versus $H_{31}R/C_{30}H$ for original samples of coals and carbonaceous shales and samples after HP at 330 °C and 360 °C for 72 h.

sulphate-poor depositional environment for both coals and shales, the gammacerane index (GI) versus Pr/Ph plot (Fig. 12B) shows an increasing trend in water salinity, which results in higher GI values, with the increasing Pr/Ph likely indicating lacustrine environment (see below). This increasing GI versus Pr/Ph trend contradicts Peters et al.'s (2005) interpretation that higher salinity results in lower Pr/Ph. In addition, gammacerane is often found in sediments deposited under hypersaline conditions but this compound is not necessarily restricted to such deposits. Lacustrine deposits may contain abundant gammacerane since most lakes in the temperate climatic zones are stratified during summer (Sinninghe Damsté et al., 1995).

Low values of tricyclic/pentacyclic terpanes (Tri/Pen) and high (> 1) hopane/sterane values (Table 5) suggest a significant proportion by prokaryotes (bacteria and archaea) in the total OM. The Tri/Pen values are similar in all samples but the hopane/sterane values are more variable. The highest hopane/sterane values characterise the Br-20c and Br-23c coals and Br-23sb shales (Table 5). Moreover, in the bottom shales the hopane/sterane value is much higher than in the top shales (Table 5). High values of this ratio indicates terrigenous- and microbially-reworked OM (Tissot and Welte, 1984). Lower values, especially that of Si-23st, may reflect (i) the role of planktonic- or benthic algae (Moldowan et al., 1985), (ii) anoxic conditions in the sedimentary basin impeding bacterial growth and later OM reworking (Connan et al., 1986; Mouro et al., 2017) and (iii) a higher contribution of terrigenous OM than usual with more OM preserved in its original form. However, Pr/Ph of >1.1 in Si-23st and the low $C_{35}S/C_{34}S < 0.6$ are indicative of oxic/suboxic conditions typical of coal/resin depositional environments (Peters et al., 2005). Similarly, the $C_{35}S/C_{34}S$ versus $C_{29}H/Hop$ plot (Fig. 13A; Table 5), used to identify the source of OM (Peters et al., 2005), also suggests a coal/resin and lacustrine environment.

The regular sterane distribution of all coals and shales, is dominated by C_{29} steranes (Table 5; Fig. 14) suggests vascular plants as the main source of OM (Huang and Meinschein, 1979). The low concentration of C_{27} steranes (Table 5) clearly favours terrestrial- rather than marine sedimentation (Huang and Meinschein, 1979). A similar distribution of C_{27}-C_{29} steranes was reported in C_{27}-C_{29} sterols of freshwater green algae, e.g., Chlorophyceae, Trebouxiophyceae (Kodner et al., 2008). There is a minor difference in the C_{28} sterane contribution; shales above coal seams contain less C_{28} steranes than shales occurring below seams. Considering that a higher vascular plant contribution leads to an increase in the C_{29} sterane concentration and the lower concentrations of other components related to green algae, the C_{28} steranes are indicative of more plant detritus in the total OM; sedimentation above coal seams appears to be dynamic compared to more stagnant sedimentation elsewhere. This phenomenon can likely be connected with the significant presence of paleosols with shales occurring below seams (Kędzior, 2016; Opluštil et al., 2019) or the diversity of plant groups between seams and shales (Gmur and Kwiecińska, 2002) in the Pennsylvanian limnic coal-bearing strata of the USCB. According to Sheldon and Tabor (2009) and Tabor and Myers (2015), paleosols could modify depositional environments through secondary processes.

Relative concentrations of DBT, DBF and F depend on the proportion of S-species, O-species and methylene-species in organic material (Asif and Wenger, 2019). Thus, coals containing higher concentrations of O-species should be enriched in DBF. However, the analysed coals and shales have low DBF. The coals are dominated by F and DBT (Table 6; Fig. 15) with F usually more abundant than DBT. Dominance of F suggests sedimentation in a lacustrine, freshwater environment, with algae and microbially-reworked OM (Asif and Wenger, 2019). Increasing DBT values suggest higher salinity and a more freshwater-brackish environment (Asif and Wenger, 2019) as also reflected in GI values (Table 5) which are clearly higher in Carboniferous shale samples (except Si-22st above coal seam) than in other shales. The shales are characterized by a much higher abundance of DBT suggesting a more brackish-lacustrine environment. Their composition is similar to that of marine shales

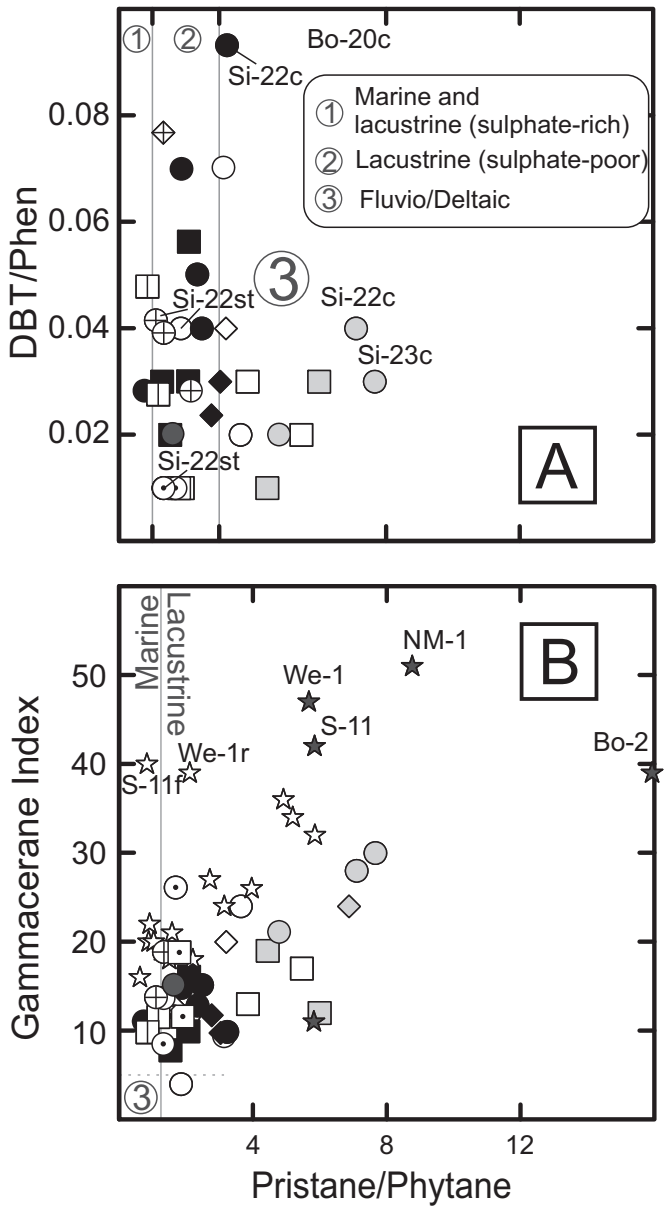

Fig. 12. (A) Dibenzothiophene/phenanthrene versus pristane/phytane ratio and (B) gammacerane index (100 x gammacerane/17α hopane) versus pristane/phytane ratio for original coals and carbonaceous shales and after HP at 330 °C and 360 °C for 72 h.

containing terrigenous OM (Asif and Wenger, 2019) or to shales deposited in more anoxic conditions.

6.2. *Thermal influence of two maturation stages of OM in the coals and shales on maceral-, fraction-, biomarker- and isotope compositions*

The R_r of the original coals and carbonaceous shales selected for HP ranges from 0.60–0.90% and 0.57–0.92%, respectively. This parameter increased from 1.34–1.39% and from 1.32–1.37%, respectively, after HP at 330 °C and from 1.71–1.83% and from 1.71–1.74% after HP at 360 °C (Table 3; Kotarba et al., 2021). A similar trend was observed by Duan et al. (2011) for Chinese Pennsylvanian and Lower Permian coals and recent peat.

Except for higher reflectance, the colour of vitrinite particles changed in a comparable way as reflectance, i.e., the paler the higher the experiment temperature. The impact of HP heating at a moderate rate was also seen in irregular- or round cracks in vitrinite particles, mostly collotelinite, and more frequently in coal, probably due to larger OM components. In shales, they occur (<0.2 vol%) in larger particles. Their greater abundance in coals after HP at 330 °C than at 360 °C confirms the findings by e.g., Su et al. (2020).

Devolatisation of vitrinite particles during heating is expressed by small round- or oval pores, especially common in samples heated at 360 °C. Pores in samples heated at higher temperature are also larger, confirming the observations by Su et al. (2020). Such pores in vitrinite also indicate the release of volatiles from liptinite macerals. Pores in vitrinite particles in shales tend to be relatively small due as the organic particles are small. Strongly reacted vitrinite in shales is very porous. Longer heating times would lead to its complete destruction.

Extended heating of vitrinite- or trimacerite particles results in formation of semicoke commonly showing fine anisotropy. More resistant inertinite macerals (fusinite, semifusinite, inertodetrinite) remain within the semicoke. Large pores in semicoke are related to vitrinite plasticity during longer heating. Large irregular cracks are occasionally present also. Semicoke is rarely observed. If present, rare particles in heated carbonaceous shales are irregular and several μm in size at most. Semicoke contents are always higher after heating to 360 °C (Fig. 4E, F).

During HP at 330 °C, contents of liptinite macerals decreased in most samples; trace contents (<0.2 vol%) remain in only a few. They devolatilised, changed into different components or they simply could not be recognised. At ~330 °C, the R_r of ~1.3% lies on the limit for distinguishing liptinite macerals (Pickel et al., 2017). In fact, liptinite macerals were likely essentially destroyed during coalification (Tables 3 and 4).

The ^{13}C isotope depletion of saturated hydrocarbons in bitumen extracted from shales, in contrast to coals, can be due to the catalytic influence of clay minerals in the original shales and to thermal reactions at HP 330 °C and 360 °C (Figs. 5, 9 and 10). Unlike their kerogen, asphaltenes in original coals and shales, and in shales at 330 °C and 360 °C, are always enriched in ^{12}C but, at the same time, asphaltenes and kerogen in coals at HP 330 °C and 360 °C are isotopically more similar (Fig. 5). This isotope distribution shows that asphaltenes and extracted bitumen are co-genetic with their corresponding kerogen of both coals and shales. As isotope differentiation between coals and shales can result from the catalytic influence of clay minerals in shales during thermal reactions, stable carbon isotope distributions in saturates, aromatics, resins and asphaltenes of oils or extracted bitumen and kerogen (e.g., Galimov, 1986, 2006; Kotarba et al., 2013, 2014) and in individual hydrocarbons (e.g., Curiale and Sperry, 2000; Curiale, 2008) are used for oil-source rock correlations. Although the $\delta^{13}C$ values of the saturates and aromatics were plotted using Sofer's (1984) approach, the diagrams for coals (Fig. 9A) and shales (Fig. 9D-E) show a significant depletion in ^{13}C, i.e., for $\delta^{13}C_{[Saturates]}$ from −29.6 to −26.7‰ for coals and from −32.7‰ to −24.8‰ for shales, and for $\delta^{13}C_{[Aromatics]}$ from −26.3 to −24.6‰ for coals and from −29.8 to −24.6‰ for shales (Table 2). They are isotopically heaviest at 360 °C, i.e., for $\delta^{13}C_{[Saturates]}$ from −25.9 to −24.5‰ for coals and from −28.8 to −25.9‰ for shales, and for $\delta^{13}C_{[Aromatics]}$ from −25.0 to −24.0‰ for coals and from −26.2 to −23.8‰ for shales (Table 2). Isotopic shifts and enrichment of saturated hydrocarbons in bitumen extracted from both coals and shales after HP 330 °C and 360 °C (Fig. 9B–C and F) compared to original samples (Fig. 9A and D–E) reflect kinetic effects during the HP heating experiments. Hence, the canonical variable (CV) values are shifted from the initially terrigenous OM field (CV >0.47) to the algal OM field, especially for coals subjected to heating at HP 360 °C (Fig. 10). The regular decrease of the CV values is evident for coals. OM dispersed in shales also shows a slight decrease in CV values but, even in shales with the highest maturity, values typically >0.47 suggest that terrigenous material was predominant (Fig. 10). Such behaviour of stable isotope compositions for coals from the USCB and LCB was also reported by Kotarba and Clayton (2003).

Sofer's (1984) genetic lines were constructed based on the analyses of isotopic composition of oils generated from dispersed OM, not from

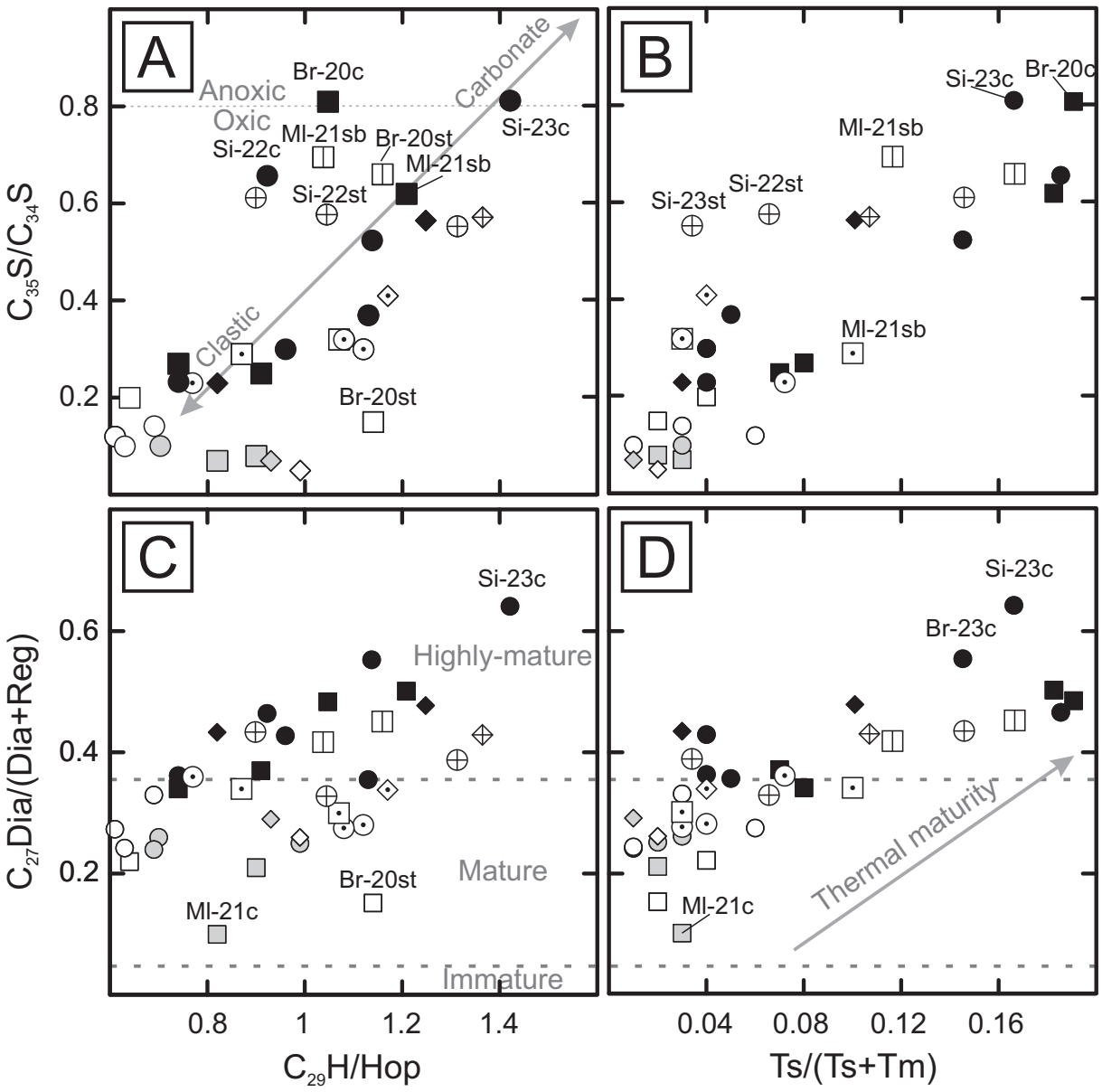

Fig. 13. $C_{35}S/C_{34}S$ versus (A) $C_{29}H/Hop$ and (B) Ts/(Ts + Tm), and $C_{27}Dia/(Dia + Reg)$ versus (C) $C_{29}H/Hop$ and (D) Ts/(Ts + Tm) for original coals and carbonaceous shales and after HP at 330 °C and 360 °C for 72 h.

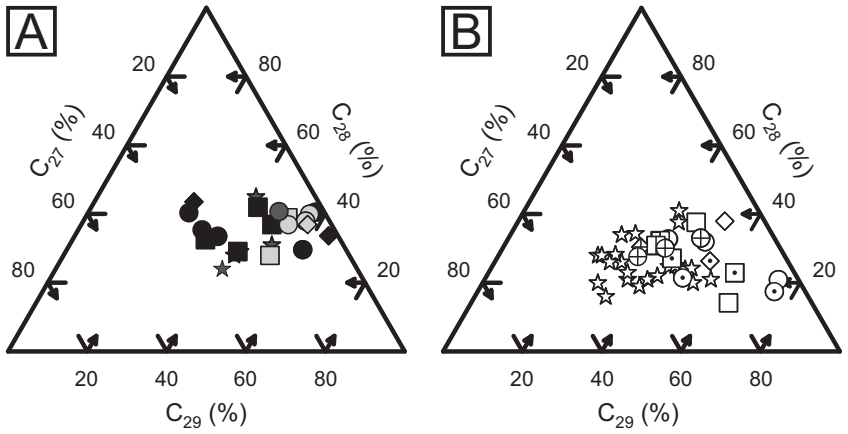

Fig. 14. Ternary diagram of C_{27}, C_{28} and C_{29} regular sterane composition in extracted bitumen from (A) coals and (B) carbonaceous shales of original samples and after HP at 330 °C and 360 °C for 72 h.

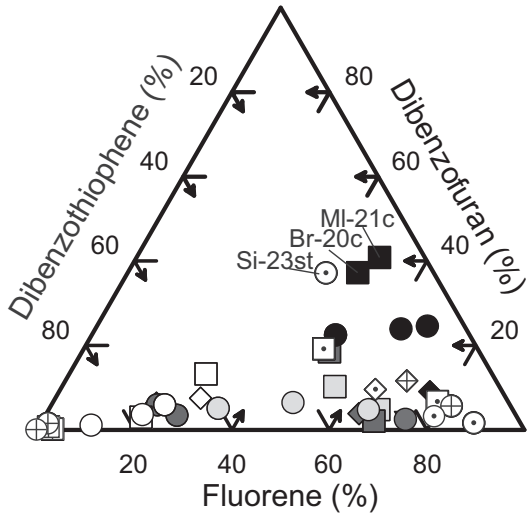

Fig. 15. Ternary diagram of the dibenzothiophene (DBT), dibenzofuran (DBF) and fluorene (F) composition in extracted bitumen from original coals and carbonaceous shales and after HP at 330 °C and 360 °C for 72 h.

bitumen extracted from it. Our isotopic data (Table 2), and the data of Kotarba and Clayton (2003), reveal that the Sofer's graph is not totally applicable to the genetic characterization of extracted bitumen.

The isomerisation of steranes indicates that sample maturity is variable though it generally increases from initial temperature to 360 °C (Table 5; Figs. 16 and 17A). The Pennsylvanian LCB original samples are early-mature/mature, and those from the USCB are in the early stage of catagenesis. The least mature shales selected for HP are two samples from above coal seams (Si-23st and Si-22st) containing immature OM. The most mature samples are Br-20c and Br-23c (Table 3). These observations are confirmed by other maturity indices, e.g., C_{27}Dia/(Dia + Reg), and Ts/(Ts + Tm) the values of which gradually increase to HP at 360 °C (Table 5; Figs. 13C–D, 16A and 17C). Based on the C_{31} homohopane isomerisation ratio (Table 5; Fig. 17B), only samples Si-22 and Si-23 do not achieve homohopane equilibrium of 0.57 at 360 °C (Peters et al., 2005). The general gradual increase of aromatic maturity parameters (Table 6) has been similarly interpreted (Radke et al., 1984; Beach et al., 1989; Peters et al., 1990).

Individual biomarkers and their ratios in all samples behave differently during the gradual temperature increase to 360 °C. Notably, *n*-alkanes in initial samples have bimodal- or unimodal distributions dependent on the maturity level, which changes at HP 330 °C and 360 °C (Fig. 8). In general, LMW *n*-alkanes are reduced and HMW *n*-alkanes start to dominate with increasing temperature; this may result from the parent OM, i.e., terrigenous OM, in the biomarker distributions. Similar observations in a microbial mat have been made by Franco et al. (2016). In addition, a slightly biodegraded shale sample with unresolved complex mixture (UCM) present shows that at the higher HP temperature, the UCM extends its area likely at the expense of HMW *n*-alkanes (*n*-$C_{31–36}$; Fig. 8).

Significant decreases in the Pr/Ph, Pr/*n*-C_{17} and Ph/*n*-C_{18} values from the initial temperature to 360 °C confirm that these parameters are sensitive to thermal maturity changes and the source of OM (Connan, 1974; Albrecht et al., 1976; Radke et al., 1980; Shanmugam, 1985; Wei et al., 2007; Spigolon et al., 2015). Similarly, thermal control on biomarker ratios is clearly evident in the C_{29}H/Hop values which, in almost all samples, increases with HP temperature (Table 5). The behaviour of this ratio is dictated by thermal changes and can be related to hopane demethylation (Philip and Gilbert, 1984; Van Graas, 1986) as the C_{29} hopane is thermally more stable and the C_{30} hopane less so (Peters et al., 2005). Therefore, this ratio can be a useful maturity indicator for coals and shales (Liang et al., 2015; this study). Likewise, the C_{35}S/C_{34}S homohopane ratio commonly used as an indicator of marine redox conditions (Peters and Moldowan, 1991) increases with HP temperature (Table 5), and could be also used as a maturity indicator. The observed increase of the C_{35}S/C_{34}S homohopane ratio with maturity could be the result of the C_{35} homologue releasing from kerogen due to the thermal stress since content of hopanes in the kerogen-bound biomarkers is relatively high because hopanoid precursors (e.g., C_{35} bacteriohopanepolyol) are generally bound into kerogen via relatively large number of binding sites (Love et al., 1997; Bishop et al., 1998). This would, however, question validity of this ratio as a redox-recording biomarker during diagenesis. Finally, the increasing temperature also appears in the Tri/Pen ratio (Table 5) which is regulated by the thermal maturity and depends on the type of rock matrix (shales preferred; Peters et al., 2005) and faster release of tricylic terpanes than 17α-hopanes from kerogen (Aquino Neto et al., 1983; Zhusheng et al., 1988).

Regular steranes (Table 5) do not show any regularity, except for C_{29} steranes which are thermal maturity indicators dependent on the thermal degradation of different C_{29} sterane isomers and increase in their concentration (Farrimond et al., 1998). C_{27} and C_{28} steranes either increase or decrease at 330 °C and 360 °C, likely dictated by isomerisation processes controlled by thermal stress, duration and presence of an acidic clay catalyst (Peters et al., 2005).

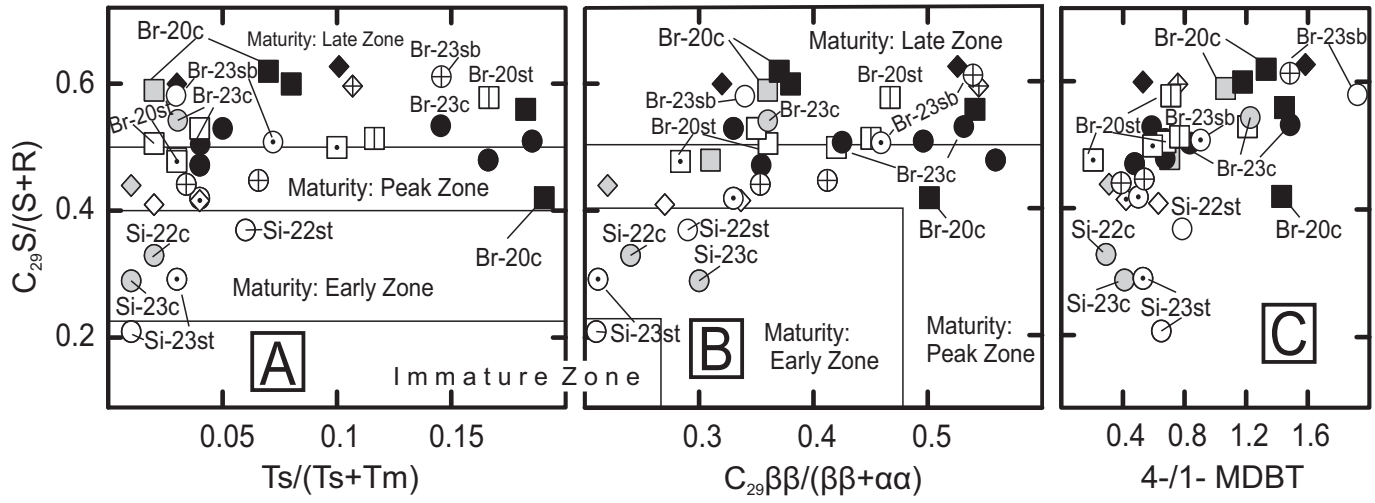

Fig. 16. C_{29}20S/(20S + 20R) sterane ratio versus (A) Ts/(Ts + Tm), (B) C_{29}ββ/(ββ + αα) and (C) 4−/1-MDBT ratios for original coals and carbonaceous shales and after HP at 330 °C and 360 °C for 72 h. Maturity fields after Peters and Moldowan (1993).

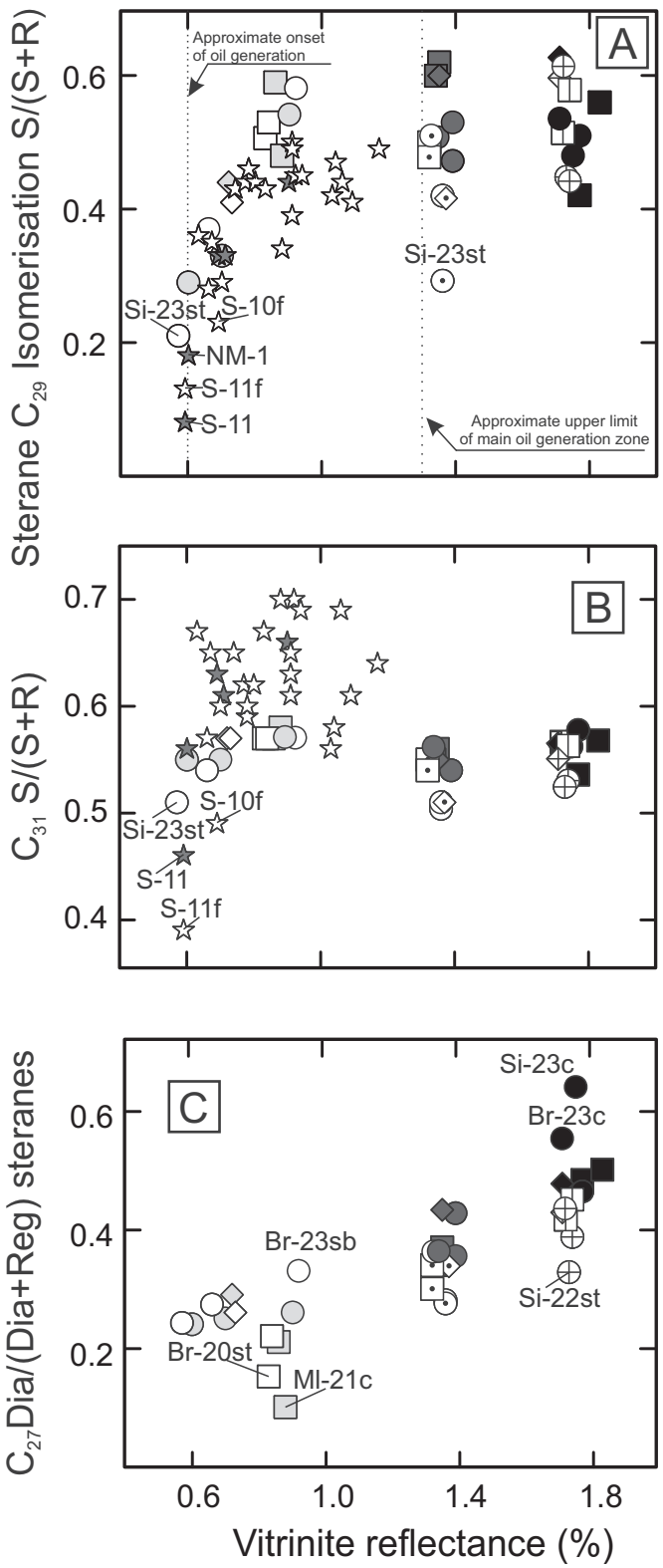

Fig. 17. (A) 14α(H)17(H) C_{29} sterane [20S/(20S + 20R)], (B) C_{31} 17α(H)21β(H)homohopane [22S/(22S + 22R) and (C) C_{27} diasteranes/(diasteranes+regular steranes) ratios versus vitrinite reflectance for original coals and bituminous coals and after HP at 330 °C and 360 °C for 72 h. Previously published data after Kotarba and Clayton (2003).

However, other biomarker ratios ($C_{24}t/C_{23}t$, $C_{29}Ts/[C_{29}Ts + C_{29}H]$, H_{31} S/[S + R]) are generally characterized by a significant decreases from the initial conditions to HP 330 °C and subsequent increases at 360 °C. This behaviour can be related to the original source of OM, the fact that almost all samples represent mainly type III kerogen and to chemical reactions at the maturation stage. For example, tricyclic terpanes ($C_{19–30}$) were suggested to be probable degradation products of a regular C_{30} isoprenoid (tricyclohexaprenol) produced by prokaryote membranes (Aquino Neto et al., 1982) and thermally generated by thermal cleavage (Liang et al., 2015). Furthermore, C_{29}Ts and C_{31} homohopanes, which can be used as maturity indicators (Peters et al., 2005; Seifert and Moldowan, 1980), do not increase at HP 330 °C in most coal and shale samples; this questions their reliability as maturity-related biomarkers. However, these ratios increase from HP 330 °C to 360 °C almost reaching their equilibrium (in the case of C_{31} homohopanes ~0.6; for C_{29}Ts unspecified; Peters et al., 2005) which suggests that both indicators are likely controlled by source of OM during thermal stress.

Aromatic-base components (DBT, DBF and F), which have similar skeleton structure, and which have been suggested to originate from biphenyl (Asif et al., 2010), also do not show any regularity at HP temperatures (Table 6). Only the DBT and F values in coal samples from the LCB decrease with temperature; can be a signal of thermal stress. In fact, DBT is used to calculate well-known maturity indices (Radke et al., 1982) and is particularly abundant in coaly-sourced oils (Asif and Wenger, 2019). Likewise, the F content which decreases with HP temperature in the coal samples can also result from thermal influence and is abundant in lacustrine source rocks (Asif and Wenger, 2019). In all other cases including DBT/Phen (except Si-22c and Si-23c), the DBT, DBF and F values may or may not decrease at 330 °C and increase at 360 °C. These fluctuations can be related to the type III kerogen catalysis mechanism producing DBT, DBF and F at 360 °C in the shales and DBF in the coals by reaction with S-, O- or methylene species present in the kerogen structure.

6.3. *Variations of petrographic- and geochemical compositions of organic matter under HP heating*

The main problem with correlating petrographic- and biomarker indices of samples subjected to heating is the fact that most biomarkers (Peters et al., 2005) and liptinite macerals (Pickel et al., 2017) are stable up to maturity referring to peak- or final stage of the "oil window" whereas at such maturities, new petrographic particles are recorded. HP heating at 330 °C resulted in $R_r > 1.3\%$ and at 360 °C is >1.7% R_r (Table 3). As only reduced organic molecules are resistant to such conditions and usually occur in low concentrations, calculated ratios may be subject to a higher inaccuracy than that for the original samples.

Undoubtedly, the most obvious impact of the temperature increases during the HP experiments are increasing contents of semicoke, paler vitrinite, and vitrinite with pores, especially in samples subjected to heating at 360 °C (Tables 3 and 4). Strongly reacted vitrinite was also recorded in all shales subjected to HP heating though its contents decreased with increasing temperature (Table 3, Fig. 7). Thus, it is crucial to decipher their possible organic precursors and the processes leading to their formation during HP heating to 360 °C. Semicoke (expressed as 100 Sem/[ΣOM]; Table 3) has a good correlation with relative concentration of DBF (DBT + DBF + F = 100%), $R^2 = 0.65$ (Fig. 18A) and MPR value ($R^2 = 0.66$; Fig. 18B) only in coals whereas the concentration of the sum of vitrinites in OM (Table 3) correlates poorly with relative concentrations of C_{27} diasteranes in C_{27} steranes ($R^2 = 0.42$) and C_{29}ββ steranes in ββ and αα C_{29} steranes ($R^2 = 0.28$) only in shales (Fig. 18C-D). Concentration of vitrinite with pores in OM (Table 3) can be correlated with the Pr/Ph ($R^2 = 0.30$; Fig. 19A) and with C_{27} Dia/(Dia + Reg) ($R^2 = 0.46$; Fig. 19B) in coals whereas concentration of paler vitrinite in OM (Table 3) is negatively correlated with the Pr/Ph in coals ($R^2 = 0.42$; Fig. 19C) and shales ($R^2 = 0.33$; Fig. 19E),

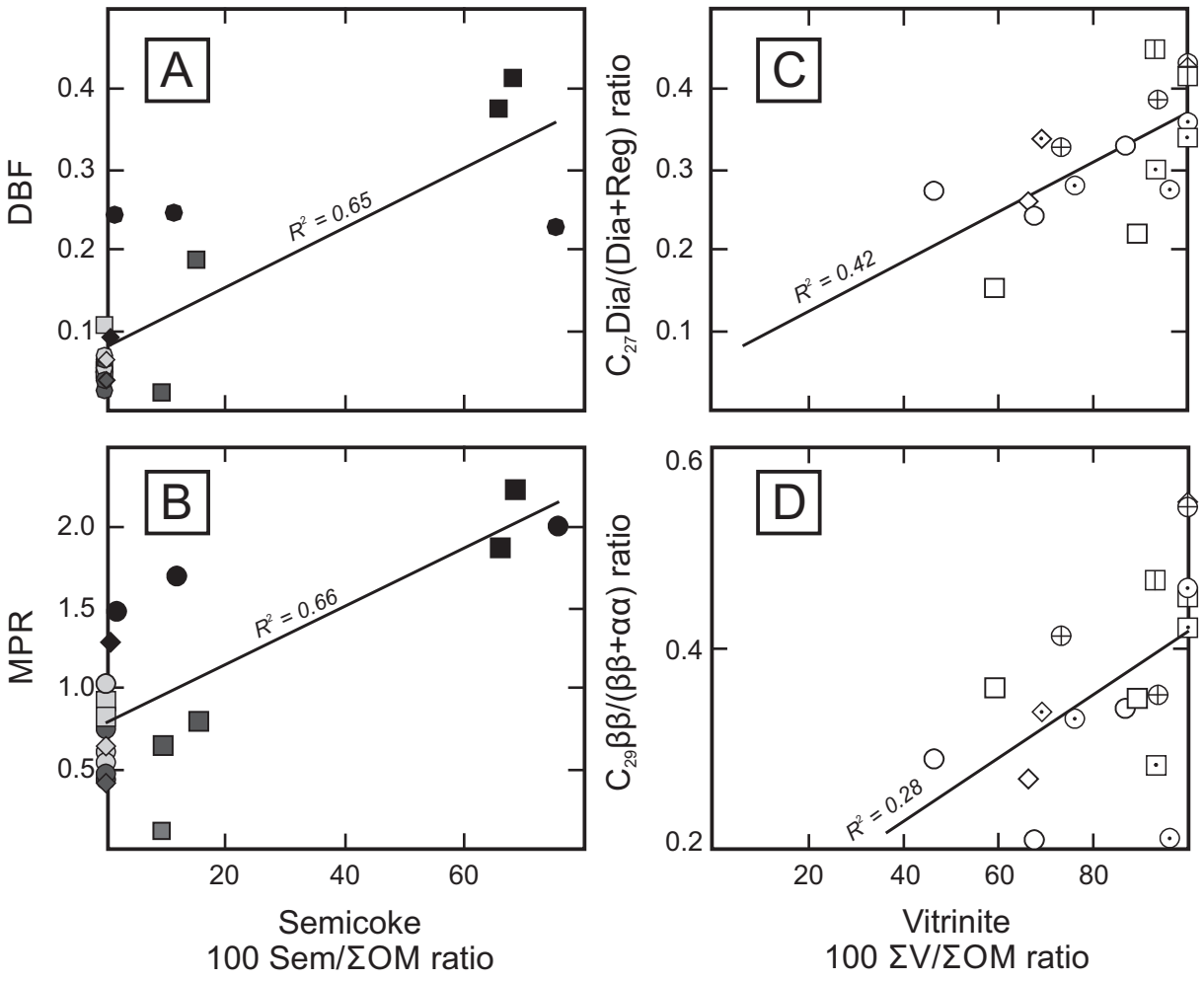

Fig. 18. (A) Dibenzofuran (DBF) and (B) MPR versus semicoke 100 Sem/ΣOM ratio, and (C) C_{27}Dia/(Dia + Reg) ratio and (D) C_{29}ββ/(ββ + αα) ratio versus 100 ΣV/ΣOM ratio of (A and B) coals and (C and D) carbonaceous shales of original samples and after HP at 330 °C and 360 °C for 72 h.
MPR = (2-MP)/(1-MP); MP – methylphenanthrene; C_{27} Dia/(Dia + Reg) = C_{27} βα 20(S + R) diasteranes/(C_{27} βα 20(S + R) diasteranes+Σ C_{27} regular steranes); C_{29}ββ/(ββ + αα) = ββ-epimers and sum ββ- and αα-epimers of C_{29} regular steranes ratio; ΣOM – sum of OM components = ΣV + ΣI + ΣL + Ch + Bit + Sem; ΣV – sum of vitrinite macerals; ΣI – sum of inertinite macerals; ΣL – sum of liptinite macerals; Ch – natural char; Bit – bitumen; Sem – semicoke.

and positively correlated with the C_{27} Dia/(Dia + Reg) in coals ($R^2 = 0.23$; Fig. 19D) and shales ($R^2 = 0.44$; Fig. 19F), respectively. Other maceral ratios (Table 3) did not show any correlations with biomarkers or PAHs in shales or coals.

It is clear that some biomarkers and PAHs are characteristic of specific macerals and that their ratios are controlled by lithology (i.e., OM type in coal or shale) and their thermal maturity related to the conditions of the HP experiment. Specifically, DBF correlated with semicoke only in coals (Fig. 18A), is a heterocyclic organic compound, suggested to be formed from phenols (Born et al., 1989), polysaccharides (Sephton et al., 1999) or even lichens (Radke et al., 2000) and which seems particularly abundant in coaly source rocks (Asif and Wenger, 2019). Thus, a good correlation between DBF and semicoke in coals (Fig. 18A) can be controlled by the source of OM and thermal maturity (Fig. 6A). The relative C_{27} diasteranes concentration seems to correlate better in shales with a sum of vitrinites ($R^2 = 0.42$; Fig. 18C) and with paler vitrinite contents in OM ($R^2 = 0.44$; Fig. 19F) than in coals (Tables 3 and 4), whereas DBF ($R^2 = 0.65$; Fig. 18A) and MPR ($R^2 = 0.66$; Fig. 18B) concentrations have much better correlations with semicoke in coals than in shales (Tables 3 and 4). This means that C_{27} diasteranes are also dependent on depositional environment and can be important in shale settings containing vitrinite. In fact, diasterenes, precursors of diasteranes, originate from sterols by catalysis of acidic clays (Kirk and Shaw, 1975; Rubinstein et al., 1975; Sieskind et al., 1979) can also be characteristic of redox (oxic) conditions (Brincat and Abbott, 2001; Moldowan et al., 1986) and elevated thermal maturity (Seifert and Moldowan, 1978). Goodarzi et al. (1989), for example, reported increases in the vitrinite reflectance and the C_{27} diasterane ratio during burial maturation.

The MPR parameter is a ratio involving two methylphenanthrene isomers (1-MP and 2-MP, Radke et al., 1982; Radke, 1988). In fact, Radke (1988) noted a gradual increase in the relative abundance with maturity of β- and β,β-type isomers of methyl- and dimethylphenanthrenes in various coals. Thus, the good correlation of MPR with the relative concentration of semicoke in coals suggests that the content of this component can be a useful palaeothermometer in thermal alterations of coal. Another thermal maturity parameter, C_{29} ββ/(ββ + αα) sterane (Seifert and Moldowan, 1986), has a low positive correlation with the sum of vitrinite concentration in OM of shales (Fig. 18D). However, values of this ratio during HP heating experiments may respond differently to different lithologies (Peters et al., 1990) and their abundance can be modulated by the kerogen type (Liang et al., 2015). Pr/Ph is the last parameter that has a low negative correlation with the concentration of vitrinite with pores in OM of coals (Fig. 19A) and paler vitrinite in coals and shales (Fig. 19C and E). Phytane and pristane derive from the phytyl side chain of chlorophyll contained in

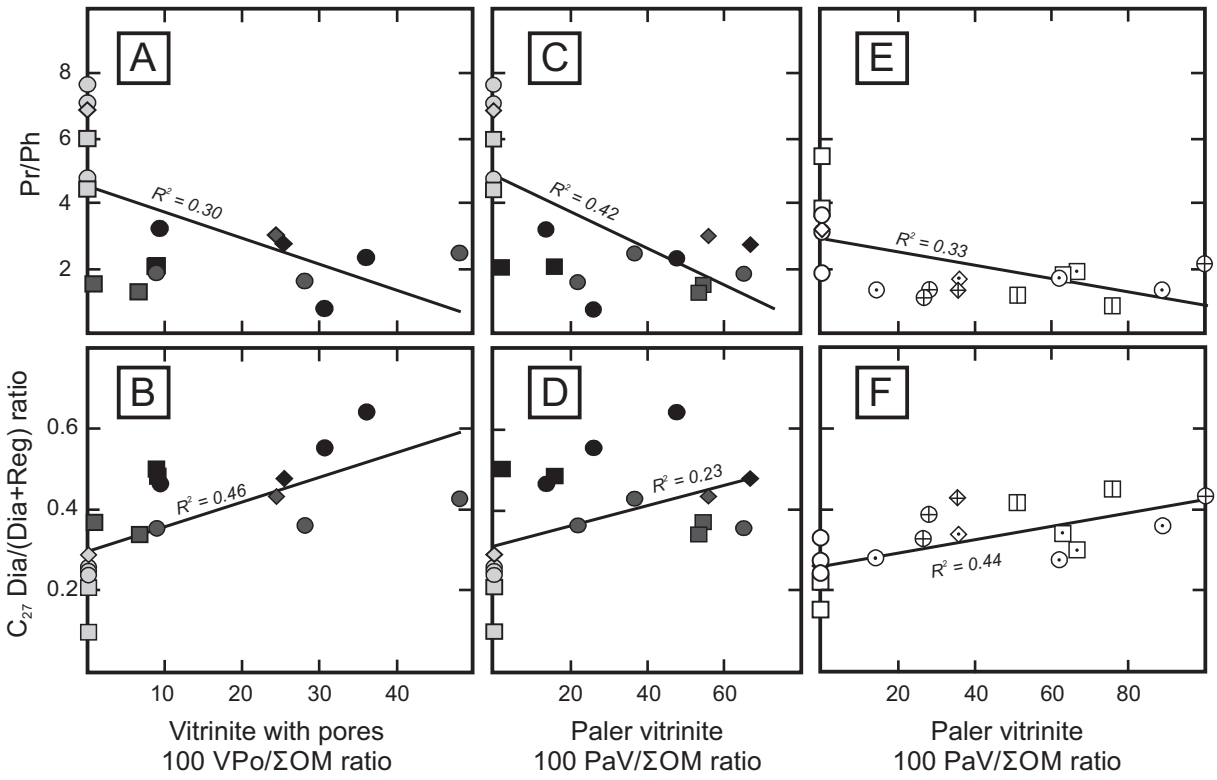

Fig. 19. (A, C and E) Pristane /phytane ratio and (B, D and F) C_{27} Dia/(Dia + Reg) ratio versus (A and B) 100 VPo/ΣOM ratio, and (C, D, E and F) 100 PaV/ΣOM ratio of (A, B, C and D) coals and (E and F) carbonaceous shales of original samples and after HP at 330 °C and 360 °C for 72 h.
C_{27} Dia/(Dia + Reg) = C_{27} βα 20(S + R) diasteranes/(C_{27} βα 20(S + R) diasteranes+ΣC_{27} regular steranes); VPo – vitrinite with pores; PaV – paler vitrinite; ΣV – sum of vitrinite macerals; ΣI – sum of inertinite macerals; ΣL – sum of liptinite macerals; Ch – natural char; Bit – bitumen; Sem – semicoke.

phototrophic organisms, most algae and higher plants (Brooks et al., 1969; Powell and McKirdy, 1973). Under oxidizing conditions, a significant portion of phytol can be oxidized to phytenic acid and subsequently through decarboxylation to pristene before final reduction to pristane. Thus, Pr/Ph is commonly used to estimate redox conditions during OM deposition (Didyk et al., 1978). Pr/Ph decreases with the increasing content of paler vitrinite and of vitrinite with pores which might be caused by aromatization processes and by heat-driven destruction of pristane (Amijaya et al., 2006; Dzou et al., 1995).

Geochemical- and petrographic genetic diversities between samples from the Serpukhovian- and Pennsylvanian coal-bearing strata of the USCB, and the Pennsylvanian coal-bearing strata of the LCB (Tables 3 to 6; Figs. 2, 18 and 19) have not been observed.

7. Conclusions

Hydrous pyrolysis (HP) experiments at 330 °C and 360 °C were performed on original bituminous coals (six samples) and carbonaceous shales (six samples) from the Serpukhovian (Mississippian) and Pennsylvanian coal-bearing strata of the USCB (ten samples) and the Pennsylvanian coal-bearing strata of the LCB (two samples). Interpretation of extracted bitumen fractions, biomarker indices, carbon isotope data and petrographic composition, augmenting HP simulation of OM maturation, constrain the origin, depositional environment, and OM maturity of the original coals and shales.

OM in the coals and shales is dominated by the vitrinite group macerals with subordinate liptinite- and inertinite group macerals are always derivatives of C3 plants. OM is of humic origin chiefly deposited in terrestrial-, paralic-terrestrial-, deltaic- and lacustrine environments under oxic conditions. The OM is rich in resins related to the presence of waxes derived from the coat of vascular plants. After heating at HP 330 °C and 360 °C, four vitrinite forms, i.e., vitrinite with pores, vitrinite with cracks, strongly reacted vitrinite and paler vitrinite, and semicoke, appeared in OM. The original coals and shales used for HP are of low thermal maturity. HP heated particles are paler in colour and contain devolatilisation pores and cracks. The prolonged HP heating results in the formation of semicoke in the coal and destruction of vitrinite particles in the shales.

The distribution of biomarkers and PAHs shows that all coals and shales have been deposited in a fluvio-deltaic and lacustrine environment, generally in sub-oxic or oxic conditions. Elevated concentrations of gammacerane suggest high salinity. A significant contribution of prokaryotes (bacteria and archaea) to the total OM is evident, especially in bottom shales. A high share of terrigenous vascular plants and microbially-reworked OM is also not excluded.

Shales are characterized by a much higher abundance of dibenzothiophene (DBT) than coals, suggesting a more brackish-lacustrine environment. The dominance of fluorene (F) suggests sedimentation in a freshwater lacustrine environment with algae and microbially reworked OM. Shales above coal seams were deposited in more dynamic conditions than shales below seams. No significant geochemical and petrographic OM differences between coal and shale from the Serpukhovian and Pennsylvanian coal-bearing strata of the USCB, and Pennsylvanian coal-bearing strata of the LCB have been identified.

The distributions of some biomarkers and PAHs are characteristic of specific macerals and their ratios are controlled by OM type in coal or shale and thermal maturity related to the conditions of the HP experiments. Distribution of biomarkers (steranes, diasteranes, terpanes, triaromatic steroids, *n*-alkanes and isoprenoids) and PAHs (dibenzothiophene and phenanthrene and their methyl derivatives) are routinely used in the evaluation of maturity. In coal and shale samples subjected to heating at HP 330 °C and 360 °C, typically change regularly, but not at the rate described by Radke (1988); the differences between our results and Radke's may reflect duration, temperature, and

rates of heating. Thus, our results may be useful for rocks (especially coals) subjected to fires or contact with magmatic intrusions. Only atypical vitrinite reflectance values (especially for shales) calculated from the methyldibenzothiopene ratio (MDR) question whether this ratio should be used to assess thermal maturity of terrigenous OM.

Some ratios, such as $C_{35}S/C_{34}S$ homohopane and Tri/Pen, commonly used as an indicator of sedimentary conditions and OM origin, increase with HP temperature; their use in diagenetic studies might not be appropriate. Other biomarker ratios ($C_{24}t/C_{23}t$, $C_{29}Ts/[C_{29}Ts + C_{29}H]$) and PAHs (DBT, DBF and F), change irregularly with increasing maturity. This behaviour can be related to type III of OM and chemical reactions at the maturation stage. As ever, some fluctuations may be due to inaccurate analysis of compounds at low concentrations.

Declaration of Competing Interest

The authors declare that they have no known competing financial interests or personal relationships that could have appeared to influence the work reported in this paper.

Acknowledgments

This research was sponsored by the National Science Centre, Poland (UMO-2016/22/M/ST10/00589) carried out in the AGH University of Science and Technology. We would like to express our gratitude to Dr. Padhraig Kennan, University College Dublin (Ireland) and two anonymous reviewers for their constructive comments and suggestions to an earlier version of this manuscript. Collection of samples, experimental, analytical and technical editorial works by M. Gardocki, J. Gawęda-Skrok, N. Kmiecik, A. Kowalski, T. Kowalski, T. Romanowski, J. Szumny and H. Zych are gratefully acknowledged.

References

Albrecht, P., Vandenbroucke, M., Mandengué, M., 1976. Geochemical studies on the organic matter from the Douala Basin (Cameroon)—I. Evolution of the extractable organic matter and the formation of petroleum. Geochim. Cosmochim. Acta 40, 791–799. https://doi.org/10.1016/0016-7037(76)90031-4.

Amijaya, H., Schwarzbauer, J., Littke, R., 2006. Organic geochemistry of the lower Suban coal seam, South Sumatra Basin, Indonesia: palaeoecological and thermal metamorphism implications. Org. Geochem. 37, 261–279. https://doi.org/10.1016/j.orggeochem.2005.10.012.

Aquino Neto, F.R., Restle, A., Connan, J., Albrecht, P., Ourisson, G., 1982. Novel tricyclic terpanes (C19, C20) in sediments and petroleums. Tetrahedron Lett. 23, 2027–2030. https://doi.org/10.1016/S0040-4039(00)87251-2.

Aquino Neto, F.R., Trendel, J.M., Restle, A., Connan, J., Albrecht, P.A., 1983. Occurrence and formation of tricyclic and tetracyclic terpanes in sediments and petroleums. In: Bjorøy, M., Albrecht, K., Cornford, K., de Groot, G., Eglinton, G., Galimov, E., Leythaeuser, D., Pelet, D., Rullkötter, J., Speers, G. (Eds.), Advances in Organic Geochemistry, 1981, Proceedings of the 10th International Meeting on Organic Geochemistry. John Wiley & Sons, New York, pp. 659–667.

Asif, M., Wenger, L.M., 2019. Heterocyclic aromatic hydrocarbon distributions in petroleum: a source facies assessment tool. Org. Geochem. 137, 103896. https://doi.org/10.1016/j.orggeochem.2019.07.005.

Asif, M., Alexander, R., Fazeelat, T., Grice, K., 2010. Sedimentary processes for the geosynthesis of heterocyclic aromatic hydrocarbons and fluorenes by surface reactions. Org. Geochem. 41, 522–530. https://doi.org/10.1016/j.orggeochem.2009.12.002.

Beach, F., Peakman, T.M., Abbott, G.D., Sleeman, R., Maxwell, J.R., 1989. Laboratory thermal alteration of triaromatic steroid hydrocarbons. Org. Geochem. 14, 109–111. https://doi.org/10.1016/0146-6380(89)90024-7.

Behar, F., Vandenbroucke, M., Tang, Y., Marquis, F., Espitalie, J., 1997. Thermal cracking of kerogen in open and closed systems: determination of kinetic parameters and stoichiometric coefficients for oil and gas generation. Org. Geochem. 26, 321–339. https://doi.org/10.1016/S0146-6380(97)00014-4.

Berner, U., Faber, E., 1996. Empirical carbon isotope/maturity relationships for gases from algal kerogens and terrigenous organic matter, based on dry, open-system pyrolysis. Org. Geochem. 24, 947–955.

Bertrand, P., Behar, F., Durand, B., 1986. Composition of potential oil from humic coals in relation to their petrographic nature. Org. Geochem. 10, 601–608. https://doi.org/10.1016/0146-6380(86)90056-2.

Bishop, A.N., Love, G.D., McAulay, A.D., Snape, C.E., Farrimond, P., 1998. Release of kerogen-bound hopanoids by hydropyrolysis. Org. Geochem. 29, 989–1001. https://doi.org/10.1016/S0146-6380(98)00140-5.

Born, J.G.P., Louw, R., Mulder, P., 1989. Formation of dibenzodioxins and dibenzofurans in homogenous gas-phase reactions of phenols. In: Chemosphere, Proceedings of the Eight International Symposium, 19, pp. 401–406. https://doi.org/10.1016/0045-6535(89)90342-1.

Brincat, D., Abbott, G.D., 2001. Some aspects of the molecular biogeochemistry of massive and laminated rocks from Naples Beach section (Santa Barbara-Ventura basin). In: The Monterey Formation: From Rocks to Molecules. Columbia University Press, New York.

Brooks, J.D., Gould, K., Smith, J.W., 1969. Isoprenoid hydrocarbons in coal and petroleum. Nature 222, 257. https://doi.org/10.1038/222257a0.

Buła, Z., Kotas, A. (Eds.), 1994. Geological Atlas of the Upper Silesian Coal Basin 1:100,000; Part III: Structural Geological Map of the Coal-Bearing Carboniferous. Państwowy Instytut Geologiczny, Warszawa.

Connan, J., 1974. Diagenese naturelle et diagenese artificielle de la matiere organique a element vegetaux predominants. In: Tissot, B.P., Bienner, F. (Eds.), Advances in Organic Geochemistry 1973. Editions Technip, Paris, pp. 73–95.

Connan, J., Bouroullec, J., Dessort, D., Albrecht, P., 1986. The microbial input in carbonate-anhydrite facies of a sabkha palaeoenvironment from Guatemala: a molecular approach. Org. Geochem. 10, 29–50. https://doi.org/10.1016/0146-6380(86)90007-0.

Coplen, T.B., 2011. Guidelines and recommended terms for expression of stable-isotope-ratio and gas-ratio measurement results. Rapid Commun. Mass Spectrom. 25, 2538–2560. https://doi.org/10.1002/rcm.5129.

Curiale, J.A., 2008. Oil–source rock correlations – limitations and recommendations. In: Organic Geochemistry, Advances in Organic Geochemistry 2007, 39, pp. 1150–1161. https://doi.org/10.1016/j.orggeochem.2008.02.001.

Curiale, J.A., Sperry, S.W., 2000. An isotope-based oil–source rock correlation in the Camamu Basin, offshore Brazil. Rev. Latino Am. Geoquimica Org. 4, 51–64.

Didyk, B.M., Simoneit, B.R.T., Brassell, S.C., Eglinton, G., 1978. Organic geochemical indicators of palaeoenvironmental conditions of sedimentation. Nature 272, 216–222. https://doi.org/10.1038/272216a0.

Duan, Y., Wu, B., He, J., Sun, T., 2011. Characterization of gases and solid residues from closed system pyrolysis of peat and coals at two heating rates. Fuel 90, 974–979. https://doi.org/10.1016/j.fuel.2010.10.039.

Dzou, L.I.P., Noble, R.A., Senftle, J.T., 1995. Maturation effects on absolute biomarker concentration in a suite of coals and associated vitrinite concentrates. Org. Geochem. 23, 681–697. https://doi.org/10.1016/0146-6380(95)00035-D.

Farrimond, P., Taylor, A., Telnæs, N., 1998. Biomarker maturity parameters: the role of generation and thermal degradation. Org. Geochem. 29, 1181–1197. https://doi.org/10.1016/S0146-6380(98)00079-5.

Franco, N., Filho, J.G.M., Silva, T.F., Stojanović, K., Fontana, L.F., Carvalhal-Gomes, S.B.V., Silva, F.S., Furukawa, G.G., 2016. Geochemical characterization of the hydrous pyrolysis products from a recent cyanobacteria-dominated microbial mat. Geol. Acta 14, 385–401.

Galimov, E.M., 1986. Isotope method of revealing oil-source deposits by the example of deposits from some regions of the USSR (in Russian). In: Izvestiya Akademii Nauk SSSR, Seriya Geologicheskaya, 4, pp. 3–21.

Galimov, E.M., 2006. Isotope organic geochemistry. In: Organic Geochemistry, Stable Isotopes in Biogeosciences, 37, pp. 1200–1262. https://doi.org/10.1016/j.orggeochem.2006.04.009.

Gmur, D., Kwiecińska, B.K., 2002. Facies analysis of coal seams from the Cracow Sandstone Series of the Upper Silesia Coal Basin, Poland. Int. J. Coal Geol. 52, 29–44. https://doi.org/10.1016/S0166-5162(02)00101-5.

Goodarzi, F., Brooks, P.W., Embry, A.F., 1989. Regional maturity as determined by organic petrography and geochemistry of the Schei Point Group (Triassic) in the western Sverdrup Basin, Canadian Arctic Archipelago. Mar. Pet. Geol. 6, 290–302. https://doi.org/10.1016/0264-8172(89)90026-3.

Higgs, M.D., 1986. Laboratory studies into the generation of natural gas from coals. Geol. Soc. Lond., Spec. Publ. 23, 113–120. https://doi.org/10.1144/GSL.SP.1986.023.01.08.

Huang, W.-Y., Meinschein, W.G., 1979. Sterols as ecological indicators. Geochim. Cosmochim. Acta 43, 739–745. https://doi.org/10.1016/0016-7037(79)90257-6.

Hughes, W.B., Holba, A.G., Dzou, L.I.P., 1995. The ratios of dibenzothiophene to phenanthrene and pristane to phytane as indicators of depositional environment and lithology of petroleum source rocks. Geochim. Cosmochim. Acta 59, 3581–3598. https://doi.org/10.1016/0016-7037(95)00225-O.

ICCP, 1993. International Handbook of Coal Petrography. Classification of Hydrogenation Residues. University of Newcastle upon Tyne.

ICCP, 1998. The new vitrinite classification (ICCP System 1994). Fuel 77, 349–358. https://doi.org/10.1016/S0016-2361(98)80024-0.

ICCP, 2001. The new inertinite classification (ICCP System 1994). Fuel 80, 459–471. https://doi.org/10.1016/S0016-2361(00)00102-2.

Isaksen, G.H., 1991. Molecular geochemistry assists exploration. Oil and Gas Journal 89, 127–131.

Jurczak-Drabek, A., 1996. Petrographic atlas of coal deposits of Upper Silesian Coal Basin. Państwowy Instytut Geologiczny. Warszawa.

Jureczka, J., Dopita, M., Gałka, M., Krieger, W., Kwarciński, J., Martinec, P., 2005. Geological Atlas of Coal Deposits of the Polish and Czech Parts of the Upper Silesian Coal Basin. Polish Geological Institute, Warsaw.

Kędzior, A., 2016. Reconstruction of an early Pennsylvanian fluvial system based on geometry of sandstone bodies and coal seams: the Zabrze Beds of the Upper Silesia Coal Basin, Poland. Ann. Soc. Geol. Pol. 86, 437–472. https://doi.org/10.14241/asgp.2016.020.

Kędzior, A., Gradziński, R., Doktor, M., Gmur, D., 2007. Sedimentary history of a Mississippian to Pennsylvanian coal-bearing succession: an example from the Upper Silesia Coal Basin, Poland. Geol. Mag. 144, 487–496. https://doi.org/10.1017/S001675680700341X.

Kirk, D.N., Shaw, P.M., 1975. Backbone rearrangements of steroidal 5-enes. J. Chem. Soc. Perkin Trans. 1 (22), 2284–2294. https://doi.org/10.1039/P19750002284.
Kodner, R.B., Pearson, A., Summons, R.E., Knoll, A.H., 2008. Sterols in red and green algae: quantification, phylogeny, and relevance for the interpretation of geologic steranes. Geobiology 6, 411–420. https://doi.org/10.1111/j.1472-4669.2008.00167.x.
Kohn, M.J., 2010. Carbon isotope compositions of terrestrial C3 plants as indicators of (paleo)ecology and (paleo)climate. PNAS 107, 19691–19695. https://doi.org/10.1073/pnas.1004933107.
Kotarba, M.J., Clayton, J.L., 2003. A stable carbon isotope and biological marker study of polish bituminous coals and carbonaceous shales. Int. J. Coal Geol. 55, 73–94. https://doi.org/10.1016/S0166-5162(03)00082-X.
Kotarba, M.J., Lewan, M.D., 2004. Characterizing thermogenic coalbed gas from polish coals of different ranks by hydrous pyrolysis. Org. Geochem. https://doi.org/10.1016/j.orggeochem.2003.12.001.
Kotarba, M.J., Clayton, J.L., Rice, D.D., Wagner, M., 2002. Assessment of hydrocarbon source rock potential of polish bituminous coals and carbonaceous shales. Chem. Geol. 184, 11–35. https://doi.org/10.1016/S0009-2541(01)00350-3.
Kotarba, M.J., Więcław, D., Dziadzio, P., Kowalski, A., Bilkiewicz, E., Kosakowski, P., 2013. Organic geochemical study of source rocks and natural gas and their genetic correlation in the central part of the Polish Outer Carpathians. Mar. Pet. Geol. 45, 106–120. https://doi.org/10.1016/j.marpetgeo.2013.04.018.
Kotarba, M.J., Więcław, D., Dziadzio, P., Kowalski, A., Kosakowski, P., Bilkiewicz, E., 2014. Organic geochemical study of source rocks and natural gas and their genetic correlation in the eastern part of the Polish Outer Carpathians and Palaeozoic–Mesozoic basement. Mar. Pet. Geol. 56, 97–122. https://doi.org/10.1016/j.marpetgeo.2014.03.014.
Kotarba, M.J., Bilkiewicz, E., Jurek, K., Waliczek, M., Więcław, D., Zych, H., 2021. Thermogenic gases generated from coals and shales of the Upper Silesian and Lublin basins: hydrous pyrolysis approach. Geol. Q. 65, 1–26.
Kotas, A., 1994. Coal bed methane potential of the Upper Silesian Coal Basin, Poland, 81 pp. Pr. Państw. Inst. Geol. 142, 1–81.
Kozłowska, A., Waksmundzka, M.I., 2020. Diagenesis, sequence stratigraphy and reservoir quality of the Carboniferous deposits of the southeastern Lublin Basin (SE Poland). Geol. Q. 64, 422–459. https://doi.org/10.7306/gq.1532.
Kufrasa, M., Stypa, A., Krzywiec, P., Słonka, Ł., 2019. Late Carboniferous thin-skinned deformation in the Lublin Basin, SE Poland: results of combined seismic data interpretation, structural restoration and subsidence analysis. Ann. Soc. Geol. Pol. 89, 175–194.
Kus, J., Misz-Kennan, M., ICCP, 2017. Coal weathering and laboratory (artificial) coal oxidation. Int. J. Coal Geol. 171, 12–36. https://doi.org/10.1016/j.coal.2016.11.016.
Kwiecińska, B., Petersen, H.I., 2004. Graphite, semi-graphite, natural coke, and natural char classification—ICCP system. Int. J. Coal Geol. 57, 99–116. https://doi.org/10.1016/j.coal.2003.09.003.
Lewan, M.D., 1993. Laboratory simulation of petroleum formation: hydrous pyrolysis. In: Engel, M., Macko, S. (Eds.), Organic Geochemistry. Plenum Publications Corp, New York, pp. 419–442.
Lewan, M.D., 1997. Experiments on the role of water in petroleum formation. Geochim. Cosmochim. Acta 61, 3691–3723. https://doi.org/10.1016/S0016-7037(97)00176-2.
Lewan, M.D., 1998. Reply to the comment by A. K. Burnham on "Experiments on the role of water in petroleum formation". Geochim. Cosmochim. Acta 62, 2211–2216. https://doi.org/10.1016/S0016-7037(98)00150-1.
Lewan, M.D., Kotarba, M.J., 2014. Thermal-maturity limit for primary thermogenic-gas generation from humic coals as determined by hydrous pyrolysis. AAPG Bull. 98, 2581–2610. https://doi.org/10.1306/06021413204.
Lewan, M.D., Ruble, T.E., 2002. Comparison of petroleum generation kinetics by isothermal hydrous and nonisothermal open-system pyrolysis. Org. Geochem. 33, 1457–1475. https://doi.org/10.1016/S0146-6380(02)00182-1.
Lewan, M.D., Kotarba, M.J., Więcław, D., Piestrzyński, A., 2008. Evaluating transition-metal catalysis in gas generation from the Permian Kupferschiefer by hydrous pyrolysis. Geochim. Cosmochim. Acta 72, 4069–4093. https://doi.org/10.1016/j.gca.2008.06.003.
Liang, M., Wang, Z., Zheng, J., Li, X., Wang, X., Gao, Z., Luo, H., Li, Z., Qian, Y., 2015. Hydrous pyrolysis of different kerogen types of source rock at high temperature-bulk results and biomarkers. J. Pet. Sci. Eng. 125, 209–217. https://doi.org/10.1016/j.petrol.2014.11.021.
Love, G.D., McAulay, A., Snape, C.E., Bishop, A.N., 1997. Effect of process variables in catalytic hydropyrolysis on the release of covalently bound aliphatic hydrocarbons from sedimentary organic matter. Energy Fuel 11, 522–531. https://doi.org/10.1021/ef960194x.
Marshall, D.M., Muhaidat, R., Brown, N.J., Liu, Z., Stanley, S., Griffiths, H., Sage, R.F., Hibberd, J.M., 2007. Cleome, a genus closely related to Arabidopsis, contains species spanning a developmental progression from C3 to C4 photosynthesis. Plant J. 51, 886–896. https://doi.org/10.1111/j.1365-313X.2007.03188.x.
McSween, H.Y., Richardson, S.M., Uhle, M.E., 2003. Geochemistry: Pathways and Processes, 2nd ed. Columbia University Press.
Moldowan, J.M., Seifert, W.K., Gallegos, E.J., 1985. Relationship between petroleum composition and depositional environment of petroleum source rocks. AAPG Bull. 69, 1255–1268.
Moldowan, J.M., Sundararaman, P., Schoell, M., 1986. Sensitivity of biomarker properties to depositional environment and/or source input in the lower Toarcian of SW-Germany. Org. Geochem. 10, 915–926. https://doi.org/10.1016/S0146-6380(86)80029-8.
Mouro, L.D., Rakociński, M., Marynowski, L., Pisarzowska, A., Musabelliu, S., Zatoń, M., Carvalho, M.A., Fernandes, A.C.S., Waichel, B.L., 2017. Benthic anoxia, intermittent photic zone euxinia and elevated productivity during deposition of the Lower Permian, post-glacial fossiliferous black shales of the Paraná Basin, Brazil. Glob. Planet. Chang. 158, 155–172. https://doi.org/10.1016/j.gloplacha.2017.09.017.
Narkiewicz, M., 2007. Development and inversion of Devonian and Carboniferous basins in the eastern part of the Variscan foreland (Poland). Geol. Q. 51, 231–256.
Narkiewicz, M., 2020. Variscan foreland in Poland revisited: new data and new concepts. Geol. Q. 64, 377–401.
Opluštil, S., Lojka, R., Rosenau, N., Strnad, L., Kędzior, A., 2019. Climatically-driven cyclicity and peat formation in fluvial setting of the Moscovian – early Kasimovian Cracow Sandstone Series, Upper Silesia (Poland). Int. J. Coal Geol. 212, 103234. https://doi.org/10.1016/j.coal.2019.103234.
Pan, C., Geng, A., Zhong, N., Liu, J., Yu, L., 2009. Kerogen pyrolysis in the presence and absence of water and minerals: amounts and compositions of bitumen and liquid hydrocarbons. Fuel 88, 909–919. https://doi.org/10.1016/j.fuel.2008.11.024.
Pepper, A.S., Corvi, P.J., 1995. Simple kinetic models of petroleum formation. Part I: oil and gas generation from kerogen. Mar. Pet. Geol. 12, 291–319. https://doi.org/10.1016/0264-8172(95)98381-E.
Peters, K.E., Moldowan, J.M., 1991. Effects of source, thermal maturity, and biodegradation on the distribution and isomerization of homohopanes in petroleum. Org. Geochem. 17, 47–61. https://doi.org/10.1016/0146-6380(91)90039-M.
Peters, K.E., Moldowan, J.M., 1993. The Biomarker Guide: Interpreting Molecular Fossils in Petroleum and Ancient Sediments, 363. Prentice Hall, New Jersey.
Peters, K.E., Moldowan, J.M., Sundararaman, P., 1990. Effects of hydrous pyrolysis on biomarker thermal maturity parameters: monterey Phosphatic and Siliceous members. Org. Geochem. 15, 249–265. https://doi.org/10.1016/0146-6380(90)90003-I.
Peters, K.E., Walters, C.C., Moldowan, J.M., 2005. The Biomarker Guide. Biomarkers and Isotopes in Petroleum Exploration and Earth History, 2. Cambridge University Press, Cambridge. https://doi.org/10.1017/CBO9781107326040, 1155 pp.
Petersen, H.I., 2017. The role of organic petrology in the exploration of conventional and unconventional hydrocarbon systems. In: Suárez-Ruiz, I., Mendonça Filho, J.G. (Eds.), Geology: Current and Future Developments. Bentham Books, Sharjah, pp. 104–130.
Philip, R.P., Gilbert, T.D., 1984. Characterization of petroleum source rocks and shales by pyrolysis-gas chromatography-mass spectrometry-multiple ion detection. Org. Geochem. 6, 489–501. https://doi.org/10.1016/0146-6380(84)90072-X.
Pickel, W., Kus, J., Flores, D., Kalaitzidis, S., Christanis, K., Cardott, B.J., Misz-Kennan, M., Rodrigues, S., Hentschel, A., Hamor-Vido, M., Crosdale, P., Wagner, N., 2017. Classification of liptinite – ICCP System 1994. Int. J. Coal Geol. 169, 40–61. https://doi.org/10.1016/j.coal.2016.11.004.
Porzycki, J., Zdanowski, A., 1995. The Carboniferous system in Poland. Pr. Państw. Inst. Geol. 168, 102–109.
Powell, T.G., McKirdy, D.M., 1973. Relationship between ratio of pristane to phytane, crude oil composition and geological environment in Australia. Nat. Phys. Sci. 243, 37–39. https://doi.org/10.1038/physci243037a0.
Radke, M., 1988. Application of aromatic compounds as maturity indicators in source rocks and crude oils. Mar. Pet. Geol. 5, 224–236. https://doi.org/10.1016/0264-8172(88)90003-7.
Radke, M., Welte, D.H., 1983. The methylphenanthrene index (MPI): a maturity parameter based on aromatic hydrocarbons. In: Bjoroy, M. (Ed.), Advances in organic geochemistry 1981. Wiley, Chichester, pp. 504–512.
Radke, M., Schaefer, R.G., Leythaeuser, D., Teichmüller, M., 1980. Composition of soluble organic matter in coals: relation to rank and liptinite fluorescence. Geochim. Cosmochim. Acta 44, 1787–1800. https://doi.org/10.1016/0016-7037(80)90228-8.
Radke, M., Welte, D.H., Willsch, H., 1982. Geochemical study on a well in the Western Canada Basin: relation of the aromatic distribution pattern to maturity of organic matter. Geochim. Cosmochim. Acta 46, 1–10. https://doi.org/10.1016/0016-7037(82)90285-X.
Radke, M., Leythaeuser, D., Teichmüller, M., 1984. Relationship between rank and composition of aromatic hydrocarbons for coal of different origins. Org. Geochem. 6, 423–430.
Radke, M., Welte, D.H., Willsch, H., 1986. Maturity parameters based on aromatic hydrocarbons: Influence of the organic matter type. Organic Geochemistry 10, 51–63.
Radke, M., Vriend, S.P., Ramanampisoa, L.R., 2000. Alkyldibenzofurans in terrestrial rocks: influence of organic facies and maturation. Geochim. Cosmochim. Acta 64, 275–286. https://doi.org/10.1016/S0016-7037(99)00287-2.
Rubinstein, I., Sieskind, O., Albrecht, P., 1975. Rearranged sterenes in a shale: occurrence and simulated formation. J. Chem. Soc. Perkin Trans. 1 (19), 1833–1836. https://doi.org/10.1039/P19750001833.
Schidlowski, M., 1988. A 3,800-million-year isotopic record of life from carbon in sedimentary rocks. Nature 333, 313–318. https://doi.org/10.1038/333313a0.
Seifert, W.K., Moldowan, J.M., 1978. Applications of steranes, terpanes and monoaromatics to the maturation, migration and source of crude oils. Geochim. Cosmochim. Acta 42, 77–95. https://doi.org/10.1016/0016-7037(78)90219-3.
Seifert, W.K., Moldowan, J.M., 1980. The effect of thermal stress on source-rock quality as measured by hopane stereochemistry. Phys. Chem. Earth 12, 229–237. https://doi.org/10.1016/0079-1946(79)90107-1.
Seifert, W.K., Moldowan, J.M., 1986. Use of biological markers in petroleum exploration. Meth. Geochem. Geophys. 24, 261–290.
Sephton, M.A., Looy, C.V., Veefkind, R.J., Visscher, H., Brinkhuis, H., de Leeuw, J.W., 1999. Cyclic diaryl ethers in a Late Permian sediment. Org. Geochem. 30, 267–273. https://doi.org/10.1016/S0146-6380(99)00002-9.

Shanmugam, G., 1985. Significance of coniferous rain forests and related organic matter in generating commercial quantities of oil, Gippsland Basin, Australia. AAPG Bull. 69, 1241–1254.

Sheldon, N.D., Tabor, N.J., 2009. Quantitative paleoenvironmental and paleoclimatic reconstruction using paleosols. Earth Sci. Rev. 95, 1–52. https://doi.org/10.1016/j.earscirev.2009.03.004.

Sieskind, O., Joly, G., Albrecht, P., 1979. Simulation of the geochemical transformations of sterols: superacid effect of clay minerals. Geochim. Cosmochim. Acta 43, 1675–1679. https://doi.org/10.1016/0016-7037(79)90186-8.

Sinninghe Damsté, J.S., Kenig, F., Koopmans, M.P., Köster, J., Schouten, S., Hayes, J.M., de Leeuw, J.W., 1995. Evidence for gammacerane as an indicator of water column stratification. Geochim. Cosmochim. Acta 59, 1895–1900. https://doi.org/10.1016/0016-7037(95)00073-9.

Sofer, Z., 1984. Stable carbon isotope compositions of crude oils; application to source depositional environments and petroleum alteration. AAPG Bull. 68, 31–49.

Spigolon, A.L.D., Lewan, M.D., de Barros Penteado, H.L., Coutinho, L.F.C., Mendonça Filho, J.G., 2015. Evaluation of the petroleum composition and quality with increasing thermal maturity as simulated by hydrous pyrolysis: a case study using a Brazilian source rock with Type I kerogen. Org. Geochem. 83–84, 27–53. https://doi.org/10.1016/j.orggeochem.2015.03.001.

Stasiuk, L.D., Burgess, J., Thompson-Rizer, C., Hutton, A., Cardott, B., 2002. Status Report on TSOP-ICCP Dispersed Organic Matter Classification Working Group, 19. The Society for Organic Petrology Newsletter, pp. 1–14.

Su, C., Qiu, J., Wu, Q., Weng, L., 2020. Effects of high temperature on the microstructure and mechanical behavior of hard coal. Int. J. Min. Sci. Technol. 30, 643–650. https://doi.org/10.1016/j.ijmst.2020.05.021.

Tabor, N.J., Myers, T.S., 2015. Paleosols as indicators of paleoenvironment and paleoclimate. Annu. Rev. Earth Planet. Sci. 43, 333–361. https://doi.org/10.1146/annurev-earth-060614-105355.

Taylor, G.H., Teichmüller, M., Davis, A., Diessel, C.F.K., Littke, R., Robert, P., 1998. Organic Petrology. Gerbrüder Borntraeger, Berlin, Stuttgart.

Tissot, B.P., Welte, D.H., 1984. Sedimentary processes and the accumulation of organic matter. In: Tissot, B.P., Welte, D.H. (Eds.), Petroleum Formation and Occurrence. Springer, Berlin, Heidelberg, pp. 55–62. https://doi.org/10.1007/978-3-642-87813-8_5.

Tomaszczyk, M., Jarosiński, M., 2017. The Kock Fault Zone as an indicator of tectonic stress regime changes at the margin of the East European Craton (Poland). Geol. Q. 61, 908–925. https://doi.org/10.7306/gq.1380.

Van Graas, G., 1986. Biomarker distributions in asphaltenes and kerogens analysed by flash pyrolysis-gas chromatography-mass spectrometry. Org. Geochem. 10, 1127–1135. https://doi.org/10.1016/S0146-6380(86)80054-7.

Waksmundzka, M.I., 2010. Sequence stratigraphy of Carboniferous paralic deposits in the Lublin Basin (SE Poland). Acta Geol. Pol. 60, 557–597.

Waksmundzka, M.I., 2013. Carboniferous coarsening-upward and non-gradational cyclothems in the Lublin Basin (SE Poland): palaeoclimatic implications. Geol. Soc. Lond., Spec. Publ. 376, 141–175. https://doi.org/10.1144/SP376.18.

Wei, Z., Moldowan, J.M., Zhang, S., Hill, R., Jarvie, D.M., Wang, H., Song, F., Fago, F., 2007. Diamondoid hydrocarbons as a molecular proxy for thermal maturity and oil cracking: geochemical models from hydrous pyrolysis. Org. Geochem. 38, 227–249. https://doi.org/10.1016/j.orggeochem.2006.09.011.

Zdanowski, A. (Ed.), 1999. Geological Atlas of the Lublin Coal Basin. Państwowy Instytut Geologiczny, Warszawa.

Zhusheng, J., Philp, R.P., Lewis, C.A., 1988. Fractionation of biological markers in crude oils during migration and the effects on correlation and maturation parameters. Org. Geochem. 13, 561–571. https://doi.org/10.1016/0146-6380(88)90076-9.